



TECHNISCHE UNIVERSITÄT MÜNCHEN

Lehrstuhl für Technische Chemie II

Insight into Catalytic Cracking of Hydrocarbons over MFI type Zeolites

Stefan Schallmoser

Vollständiger Abdruck der von der Fakultät für Chemie der Technischen Universität München zur Erlangung des akademischen Grades eines

Doktors der Naturwissenschaften (Dr. rer. nat.)

genehmigten Dissertation.

Vorsitzender: Univ.-Prof. Dr. K.-O. Hinrichsen

Prüfer der Dissertation:

1. Univ.-Prof. Dr. J. A. Lercher

2. Univ.-Prof. Dr. K. Köhler

Die Dissertation wurde am 16.10.2014 bei der Technischen Universität München eingereicht und durch die Fakultät für Chemie am 09.12.2014 angenommen.

*“There is no sadder sight in the
world than to see a beautiful theory
killed by a brutal fact.”*

Thomas Henry Huxley (1825 – 1895)

Für meine Eltern

Acknowledgements

Finally the day has come. Throughout the last years during which this thesis evolved, there may have been some ups and downs. Many people have supported me and also endured my moods during this chapter of my life. Before closing this chapter and moving to the next it's time to say thank you to all of them.

First of all I want to thank Prof. Johannes A. Lercher for offering me the position in his group. I enjoyed the freedom of research that you allowed me and the many lessons and anecdotes which you shared during our monthly meetings. In this environment I was able to develop as a scientist. Johannes, a special "Thank You" for believing in me in times when I didn't and for giving me a second chance.

I'm also grateful to my supervisors throughout this thesis. I owe special thanks to Maricruz Sanchez-Sanchez. It was my pleasure to work with you throughout the last 1.5 years of my thesis. Thank you for correcting my thesis and all of my papers in such an efficient way. Your input guided me always in the right direction. You're an excellent scientist! I wish you all the best for your future career in academia.

Thank you also to Prof. André C. van Veen who supervised me during the first 1.5 years of the MuniCat project. Thank you for helping me with the setup. Your constant scientific input always helped me to create new ideas. And thank you for enabling me to visit Singapore.

From the side of my project partner I want to thank CLARIANT SE for the financial support of my thesis. Dr. Markus Tonigold and Prof. Richard Fischer always provided helpful input throughout our monthly project meetings. Thank you also for the loose line with which I was allowed to conduct my research. Tassilo v. Aretin and Prof. Kai-Olaf Hinrichsen were persistent and helped me

thereby to improve my reactor setup and test conditions. Thank you Tassilo for the uncomplicated way of communication via the “kurzen Dienstweg”.

There are many more people that supported me throughout my thesis. Xaver Hecht helped me a lot with my setup and technical problems. But also thank you for organizing the “Ritteressen” and the “French Dinners”. Prof. Andreas Jentys always had an open ear for my questions on IR spectra or other issues. A big thank you goes to our secretary Steffi Seibold. Thanks for all the organizational work that you did but also thank you for the funny and cheering chats in between work. Thank you also for your support to Bettina Federmann, Karen Schulz, Martin Neumann and Andreas Marx.

My dear colleagues thank you for creating this nice atmosphere at TC2 and throughout conferences. Thank you to all of you. Special thanks go to my office mates Martina, Manuel, Moni, Jenny, Guoju, Robin, Steffi and John. I enjoyed our vivid and funny discussion which were mainly non-scientific and often gender related. Thank you also for keeping our “sweet secret”. Thank you to my lunch and coffee crew for making Mensa agreeable and waiting patiently for my “knock” since I became “Dienstältester” (Tobi, Kai, Peter, Ehrmi, Eva, Peter, Claudia, Sebastian F. Sebastian G., Stani, Christian, Linus, Sarah, Dani). I’m also obliged to Francisco, Anastasia, Jeongnam and Bo for sharing insight into their culture with me.

A special thanks to my former classmates Eva and Philip for sharing the ups and downs of life outside TC2. Thank you also to the members of the “Weißwurst Express” (Simon, Jan, Schorsch, Alex, Eva, Andy). In this context I want to mention my “Schafkopf Stammtisch” (Stefan, Stephan, Christoph, Simon, Lugge). Thank you for providing this weekly distraction from my thesis.

I want to thank the students Julia Tseglakova, Niko Krömer, Elena Popp, Simon Abendschein, Roland Drexel, Sarah Tschirner, Genoveva Reichl and Wolfgang Reitinger for their good work. Special thanks to Peter Hintermeier, Manuel

Wagenhofer and Takaaki Ikuno for their input to this thesis throughout their Master Thesis and internship. Keep up the good work.

Besonderer Dank gilt meiner Familie. Meinen Eltern Resi und Hans für die immerwährende Unterstützung. Meiner Frau Regina für die Geduld und Liebe mit der sie meine Stimmungsschwankungen während der Doktorarbeit aufgefangen hat. Meiner Schwester Angelika für ihr offenes Ohr und die Zeit die sich genommen hat wenn es in der Doktorarbeit wieder mal nicht so lief wie ich mir das vorstellte.

Stefan

Abbreviations

ΔS	Entropy change
°	degree
Å	Angstrom
θ	surface coverage
ads	adsorbed
BAS	Brønsted acid site
BEA	Framework type code for Zeolite Beta
cm^{-1}	wavenumber
DPE	Deprotonation energy
E_a	Activation energy
FAU	Framework type code for Faujasite
FER	Framework type code for Ferrierite
h	Planck's constant
H_{ads}	Heat of adsorption
int	intrinsic
IR	infrared
K	Kelvin / Adsorption constant
k	Boltzmann's constant
K_A	adsorption constant of reactant A
k_{int}	intrinsic rate constant
kJ	Kilojoule
k_{meas}	observed rate constant
LAS	Lewis acid site
LTA	Framework type code for Linde Type A
meas	measured (apparent)
MFI	Framework type code for ZSM-5
MOR	Framework type code for Mordenite
MR	membered ring
MTP	methanol to propylene
p_A	partial pressure of reactant A

PA	Proton affinity
R	universal gas constant
r_{meas}	observed rate
s	second
SBAS	Strong Brønsted acid site
SLAS	Strong lewis acid site
T	framework atom
T	temperature
TOF	turnover frequency
TON	Framework type code for Theta-1
TOS	time on stream
USY	Ultrastable Zeolite Y (FAU)
ZSM-5	Zeolite Socony Mobil-5

TABLE OF CONTENTS

1.	General Introduction.....	1
1.1.	Propene – increasing demand for a key raw material of chemical industry.....	1
1.2.	Structure and properties of zeolites.....	3
1.2.1.	Brief historic introduction.....	3
1.2.2.	Framework types and structure of zeolites.....	4
1.2.3.	Nature of acidity in zeolites.....	7
1.3.	Protolytic Alkane cracking.....	11
1.3.1.	Brief introduction into heterogeneous catalysis.....	11
1.3.2.	The Haag-Dessau mechanism of protolytic alkane cracking.....	12
1.3.3.	Analysis of the intrinsic kinetics of alkane cracking reactions.....	14
1.3.4.	The role of confinement and entropy in alkane cracking.....	16
1.3.5.	Adsorption of olefins.....	19
1.4.	Alkene cracking via carbenium ions.....	21
1.5.	Scope of the thesis.....	24
1.6.	References.....	26
2.	Impact of the local environment of Brønsted acid sites in ZSM-5 on the catalytic activity in n-pentane cracking.....	30
2.1.	Introduction.....	31
2.2.	Experimental.....	34
2.3.	Results and discussion.....	38
2.3.1.	Catalytic activity in n-pentane cracking as function of SBAS concentration.....	38
2.3.2.	Identification of the nature and location of the Al-OH sites.....	44
2.3.3.	Impact of SBAS-AlOH sites on the transition state in n-pentane cracking.....	50
2.4.	Deconvolution of rates.....	50
2.5.	Adsorption of n-pentane.....	51
2.6.	Analysis of the transition state in n-pentane cracking.....	53
2.7.	Conclusion.....	57
2.8.	References.....	59
2.9.	Supporting Information.....	61

3.	Study of adsorption and reaction of 1-pentene over MFI and FER at intermediate temperatures	65
3.1.	Introduction.....	66
3.2.	Experimental.....	68
3.3.	Results and discussion.....	71
3.3.1.	Characterization of the zeolites.....	71
3.3.2.	Adsorption of linear pentenes on silicalite.....	73
3.3.3.	Adsorption of linear pentenes on FER-25.....	74
3.3.4.	Study of adsorption and surface reaction of 1-pentene on MFI-90 ..	80
3.4.	Conclusions.....	88
3.5.	References	90
3.6.	Supporting Information	92
4.	Towards quantitative understanding of light alkene cracking on zeolites - case of 1-pentene on HZSM5	99
4.1.	Introduction.....	100
4.2.	Experimental.....	104
4.3.	Results and discussion.....	107
4.3.1.	Analysis of the reaction network of 1-pentene cracking.....	107
4.3.2.	Intrinsic barriers in alkene cracking.....	112
4.3.3.	Impact of Al content and presence of EFAl on 1-pentene cracking	115
4.4.	Conclusions.....	120
4.5.	References	122
4.6.	Supporting Information.....	124
5.	Summary and conclusions	132
6.	Zusammenfassung.....	135
7.	List of publications.....	139
8.	Lebenslauf.....	140

Chapter 1

1. General Introduction

1.1. Propene – increasing demand for a key raw material of chemical industry

Propene is one of the most important organic feedstock for chemical industry. A wide range of products, such as acrylonitrile, isopropanol, propylene oxide and cumene are produced on basis of this highly reactive chemical compound.^{2,3} Polypropylene is the product with the highest production volume by far (Figure 1.1) This polymer, which depending on the production conditions and additives can have very different properties, is found in a multitude of applications of daily life.⁴

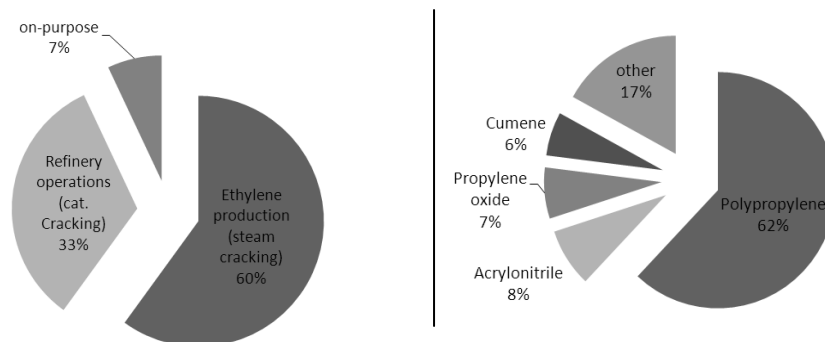


Figure 1.1: Distribution of (left) sources for propylene (Year 2009)⁵ and (right) propylene use for synthesis of industrial raw materials (Year 2008)².

It is surprising that propene is up today mainly produced as byproduct of ethylene. Considering the annual growth rate of propene demand (4 – 5 %)⁶ which outnumbers that of ethene, it is evident that in the future the focus will be shifted towards direct propene production. Traditional production pathways rely on steam cracking – with propene as a by-product of ethene production - and catalytic refinery operations such as e.g. Fluid Catalytic Cracking.⁵ In the light of the growing propene demand and the shift towards ethane rich

feedstocks in steam crackers, which results in less propylene output, on-purpose technologies for propene production will be more important in the near future.⁷

These on-purpose technologies are more selective to propene. The endothermic dehydrogenation of propane (PDH) over supported Pt catalysts is a well-established technology which is today already commercialized (e.g. UOP-Oleflex® and ABB-Catofin®).⁸

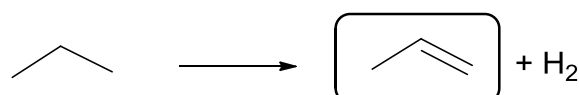


Figure 1.2: Simplified reaction scheme for propane dehydrogenation reaction and enthalpy of reaction at 298 K.

Another emerging technology is MTP® (methanol-to-propylene).⁸ The modern plant designs combine several steps, starting from coal and ending usually in polypropylene. In a first step, gasification of coal results in synthesis gas. This is catalytically converted to methanol which is followed by the actual methanol to propylene step. In a last step propylene is polymerized and polypropylene is obtained.⁹

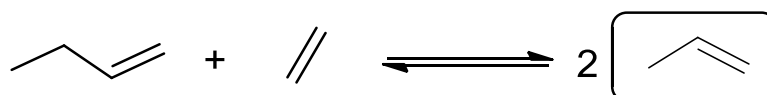


Figure 1.3: Illustration of metathesis reaction.

The third on-purpose technology is olefin metathesis, which is in principle the redistribution of olefin fragments.² It was first discovered and developed by *Philips Petroleum Company* and was initially designed to produce ethylene from butene.¹⁰ Today's application is the reverse reaction and consumes hence the valuable reactant ethene.² Therefore, profitability depends largely on relative costs of ethene and propene.

Another attractive possibility is reprocessing (most commonly catalytic cracking) of streams rich in low value higher olefins (typically C₄⁼ and C₅⁼).^{2,7} The zeolite ZSM-5 is used for this kind of interconversion and the feed might

be a raw C₄ stream coming from a steam cracker, a raffinate-1 and raffinate-2 stream.²

Most of the current and future technologies for production of propene rely on catalytic cracking of hydrocarbons (alkanes and alkenes) and the use of zeolites such as ZSM-5.

1.2. Structure and properties of zeolites

1.2.1. Brief historic introduction

The term zeolite is derived from the Greek and its meaning is “boiling stone”, which refers to the ability of zeolites to adsorb water and to release it upon heating.¹¹ Zeolites are generally speaking crystalline aluminosilicates which contain pores and cavities of molecular dimensions.¹²

Zeolites are not a pure synthetic product but are also commonly found in nature, especially in the alkaline environments of volcanic sediments and materials.^{12,13} The first zeolite discovered and identified is *stilbite*. Common and naturally abundant zeolites are *analcime*, *erionite* and *mordenite*.¹²

Development of hydrothermal synthesis started in the 1940s and 1950s by the pioneers *Richard Barrer* and *Robert Milton*.¹² The first synthetic zeolite was eventually developed at Linde’s laboratories and was named *zeolite A* and consists of eight membered rings forming sodalite cages.^{11,12} Linde’s template free approaches resulted also in synthesis of *faujasite* and *chabazite* structures.

The next leap in zeolite synthesis was initiated by introducing quaternary ammonium cations during hydrothermal synthesis.^{14,15} This resulted also in the first high-silica-zeolite (zeolite β) which is not found in nature.^{12,16} Upon this discovery, more systematic studies in the 1970’s resulted also in the discovery of ZSM-5 which was first patented in 1972.¹⁷ Later on (1978) a new polymorph material consisting of a tetrahedral framework enclosing a three dimensional structure was published in *Nature*, which was in fact Al free ZSM-5.^{12,17,18}

Today more than 200 different structure types of zeolites are known. The various structure types differ in channel and pore dimensions as well as geometry.¹⁹

1.2.2. Framework types and structure of zeolites

All zeolites have one thing in common - the primary building units are tetrahedral framework atoms (TO_4), with T being mostly Si and Al.²⁰ Despite of consisting of the same chemical elements, zeolites show a great complexity in terms of their three dimensional structure. The complexity is generated by formation of different primary building blocks out of the TO_4 units. The three-dimensional structure of the zeolite framework is obtained by linking those building blocks via their T-atoms.²⁰ In Figure 1.4 the pentasil building block characteristic for MFI is shown as well as the three dimensional channel structure obtained by combining these building blocks.²¹

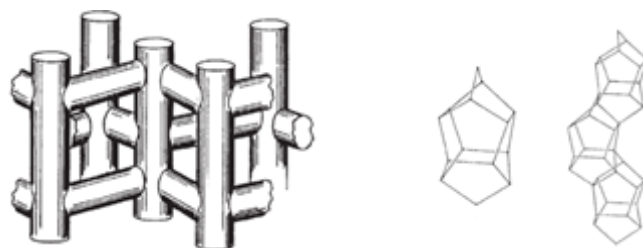


Figure 1.4: Left: Hollow tube representation of the channel structure of ZSM-5. Right: Characteristic building blocks in ZSM-5 (“Pentasil-unit”) and connection of this building blocks parallel to $[001]$ (Adapted from ref. ²¹).

Depending on the building block and the way of combining those building blocks, various three dimensional structures with differing pore dimensions can be obtained.^{11,19} Table 1.1 gives an overview over the commercially most important zeolite structures with differing pore geometries.¹¹

Zeolite A is constructed from sodalite cages which are connected by their 4-MR. This results in a cubic structure with three orthogonal 8-MR pores. Zeolite A is usually used for adsorption and separation applications.¹¹

Table 1.1: Examples for zeolites with differing structure and pore geometry.¹⁹

	small-pore zeolites	medium-pore zeolites	large-pore zeolites
Pore geometry	8-membered ring	10-membered ring	12-membered ring
Pore diameter	3.5 - 4.5 Å	4.5 - 6.0 Å	6.0 - 8.0 Å
Example	Zeolite A	ZSM-5	Zeolite Y
Structure code	LTA	MFI	FAU

Faujasite (FAU) is also based on sodalite cages, but these are connected via the 6-MR which results in a completely different framework structure with three orthogonal 12-MR pores. Faujasites (especially Zeolite Y) are used for catalytic cracking applications.^{11,20}

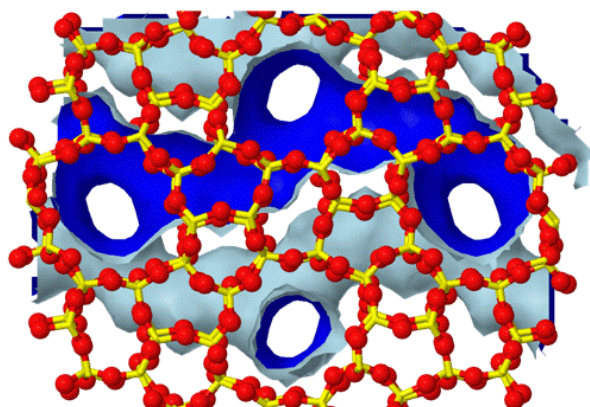


Figure 1.5: Framework structure of ZSM-5 highlighting the surface of the channel system viewed along [010]. Colors: silicon (yellow), oxygen (red), sinusoidal and straight channels (blue). (<http://www.iza-structure.org/databases/>).

ZSM-5 is another three dimensional aluminosilicate which consists of two types of elliptical channels (10-MR) constructed from the pentasil unit. The straight channels (Figure 1.5) run orthogonal to the sinusoidal channels resulting in spacious intersections. ZSM-5 shows a great flexibility in terms of Al content. Any Si:Al ratio between 10 and infinity (silicalite) can be easily

obtained. This makes it most useful in applications such as shape selective cracking and isomerization (e.g. xylene).^{11,20}

A commercially less relevant framework type is TON. It consists of a one dimensional pore system. This zeolite crystallizes in thin needles and the 10-MR pores run parallel to the needles.²²⁻²⁴ In contrast to MFI type zeolites there are no voluminous intersection as it is depicted in Figure 1.6 on the left. In Figure 1.6 (right) the naturally occurring zeolite FER is also represented.²⁵ This zeolite provides space for chemical reactions within a three dimensional structure consisting of 10 and 8 membered rings.²⁶

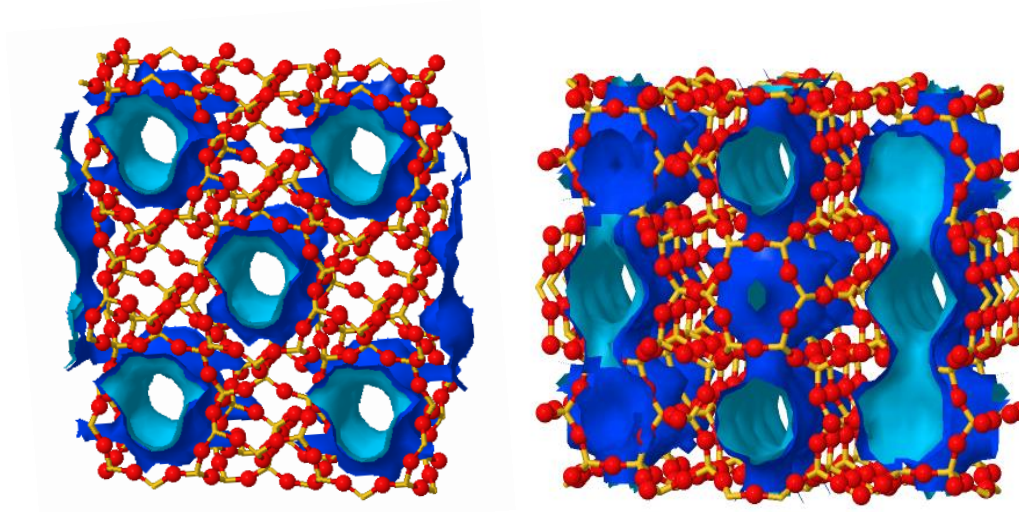


Figure 1.6: Framework structure of TON (left) viewed along [001] and FER (right) viewed along [100]. Colors: silicon (yellow), oxygen (red), channels (blue). (<http://www.iza-structure.org/databases/>)

The catalytically active sites are located within the micropores of the zeolites and can be described by an identical sequence of elements (Si, Al, O, H) for all zeolites.²⁷

1.2.3. Nature of acidity in zeolites

If zeolites contained only silicon and oxygen, all SiO_4 tetrahedra within the framework would be electrically neutral. The great industrial importance of zeolites is due to the isomorphous substitution of silicon by the trivalent element aluminum. This creates a negative charge in the lattice which can be balanced by the presence of a cation (e.g. Na^+) or a proton.^{20,27,28}



Figure 1.7: Illustration of nature of Brønsted acid sites (left) and Lewis acid sites (right) in zeolites (adapted from ref. ²⁸).

The structure of this so called bridged hydroxyl group was first proposed by Uytterhoeven et al. in 1965.²⁹ Their picture of a Si-OH group being strongly influenced by a neighboring tricoordinated Al provided a first description of the nature of acid sites in zeolites.^{27,29} Later on, it was discovered that there is actually a chemical bond between the OH group, the tetravalent Si and the trivalent Al as depicted in Figure 1.7.^{27,28,30} This interplay results in a strong Brønsted acidity.

The microporous confinement of these acid sites leads to further advantageous properties which are usually grouped under the term shape-selective catalysis.²⁰ These effects can be usually classified into three main categories:^{20,27,31}

- (i) *Reactant shape selectivity:* At least two different reactants with differing molecular dimensions compete for reaction at the internal acid sites. The less bulky molecule will preferentially diffuse to the active center and therefore will be more likely converted (Figure 1.8A).

(ii) *Product shape selectivity*: Different products could be formed (via consecutive or parallel pathways). Due to a difference in their molecular dimension, diffusion of one of the products is hindered. Therefore only the other products will be mainly observed (Figure 1.8B).

(iii) *Restricted transition state selectivity*: In this case, formation of a bulky transition state is disfavored over a different reaction pathway with a less voluminous transition state. As prerequisite for observation of this case, diffusion of products and reactants must not be hindered (Figure 1.8C).

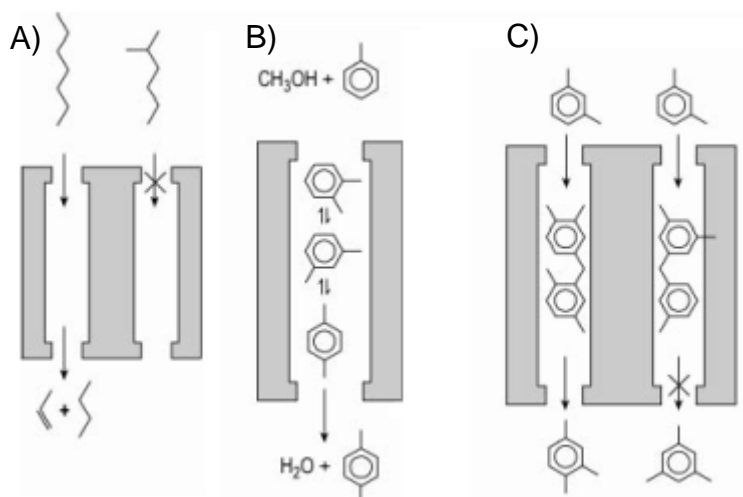


Figure 1.8: Illustration of the three categories of shape selectivity - A) reactant shape selectivity (cracking of n-heptane and 2-methyl-hexane), B) product shape selectivity (toluene methylation), C) restricted transition state selectivity (transalkylation of m-xylene). (Taken from ref. ³¹)

In addition to Brønsted acid sites there are also Lewis acid sites (LAS) commonly observed in zeolites.^{20,28} These sites can be either found at framework positions (Figure 1.7, dehydroxylated Brønsted acid site) or at extra-framework positions in the form of e.g. AlO^+ , $\text{Al}(\text{OH})_2$.^{28,32,33}

Besides the mere presence of the trivalent Al in the framework further factors influence the acidity and hence the catalytic activity of zeolites. Acid site

density has a large impact on the intrinsic acid strength.^{27,34,35} Figure 1.9 illustrates this relationship for USY zeolites.²⁷

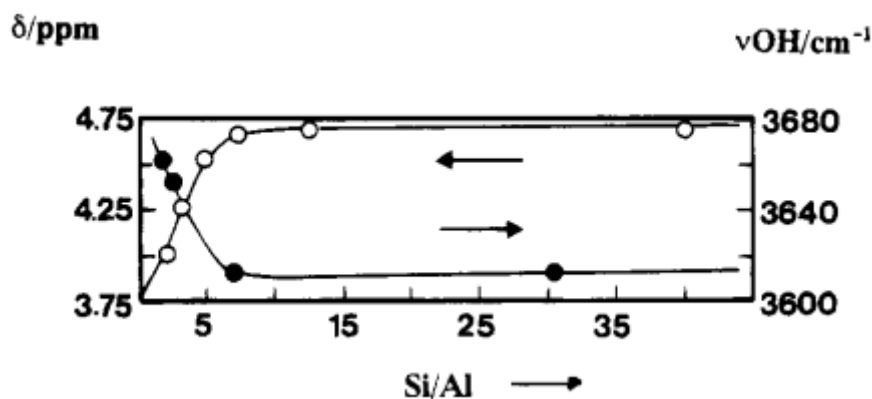


Figure 1.9: IR frequency of characteristic OH-stretching vibration (right axis, ●) and corresponding 1H MAS NMR shift (left axis, ○) as a function of Si/Al ratio of USY zeolites. (Taken from ref. ²⁷)

Below a molar Si/Al ratio of about 10, the characteristic stretching frequency of the bridged hydroxyl group shifts from about 3615 cm^{-1} to about 3660 cm^{-1} . This indicates a reduced acid strength. Above a Si/Al ratio of 10, intrinsic acid strength seems to be independent of the relative Al content.^{27,34}

The structure, e.g. the framework type, has an additional impact on the intrinsic acid strength of the Brønsted acid sites.²⁷ The T-O-T bond angles differ for different framework structures (e.g. MFI - $137 - 177^\circ$, MOR - $143 - 180^\circ$, FAU - $138 - 147^\circ$)²⁷. The angle crucially influences the acid strength,³⁶ and hence different OH stretching frequencies are observed for zeolites with a different framework. The same framework can provide in addition different environments (e.g. 12 MR, 10 MR and 8 MR pores) and therefore also within one framework acid sites with a differing intrinsic acidity can be observed (e.g. MFI - 3610 cm^{-1} , MOR - 3610 cm^{-1} and 3585 cm^{-1} , FAU - 3550 cm^{-1} and 3640 cm^{-1}).^{20,37}

In the last decade it was discovered that the distribution of BAS is not statistically random.³⁸⁻⁴¹ Synthesis conditions seem to have a large impact on the distribution of BAS in zeolites and Co^{2+} can be used as a probe for identification of paired BAS.³⁸⁻⁴⁰ Pairing means in this case that two BAS are

in spatial proximity within the three dimensional pore system of the zeolite. If the sodium form of a zeolite is exchanged with Co^{2+} , this bivalent cation will only bind to two BAS in spatial proximity. Consequently, each exchanged Co^{2+} cation represents one pair of BAS. ^{38,39}

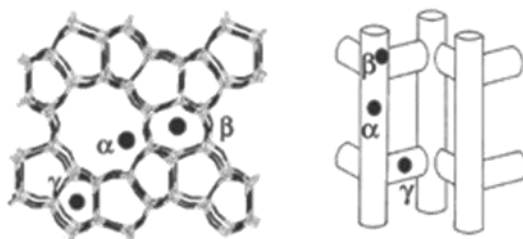


Figure 1.10: Location of acid site pairs within the pore system of MFI type zeolites as defined by Dědeček et al..(Taken from ref. ³⁹)

Careful deconvolution of the diffuse reflectance spectra of Co^{2+} exchanged zeolites enables even the discrimination between three different sites in MFI type zeolites (Figure 1.10).^{38,39}

α -sites: located within the straight channels

β -sites: intersections of the sinusoidal and straight channels

γ -sites: located within the sinusoidal channels

It was also discovered that the relative distribution of acid sites could have a huge impact on catalytic properties of zeolites. For cracking of 1-butene it was shown that isolated BAS preferentially enhance the cracking pathways whereas the presence of paired BAS seems to shift selectivity towards oligomerization and hydrogen transfer reactions.⁴⁰ Very recently, *Janda and Bell* concluded that butane cracking activity and pathway selectivity (dehydrogenation/cracking) depends crucially on the location of BAS. BAS located in β -sites exhibit in their opinion a higher catalytic activity by providing more space for the transition state.⁴²

In order to understand this argumentation, the fundamentals of alkane and alkene cracking will be briefly explained in the next sections.

1.3. Protolytic Alkane cracking

1.3.1. Brief introduction into heterogeneous catalysis

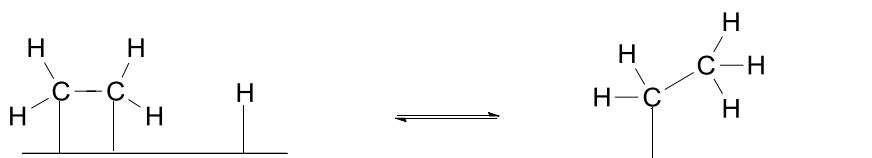
Over 80% of all industrially relevant chemical reactions are based on heterogeneous catalysis.³¹ The catalytic process can be classified as a cyclic process where the reactant(s) form a complex with the catalyst. This opens a pathway for transformation into the desired product(s).³¹ The catalyst is restored upon release of the product(s) and ready for another cycle.³¹ Numerous chemical bonds can be cleaved and new chemical bonds could form, whereas the catalyst itself shows no significant change after the cycle. In absence of a catalyst, the reaction itself would not take place in the desired efficiencies and rates.^{31,43}

In heterogeneous catalysis reactant and catalyst are in two different physical phases, usually the catalyst is solid and the reactant is in the gas phase. This allows one to run catalytic processes in a continuous mode, which is very desirable for chemical industry.³¹

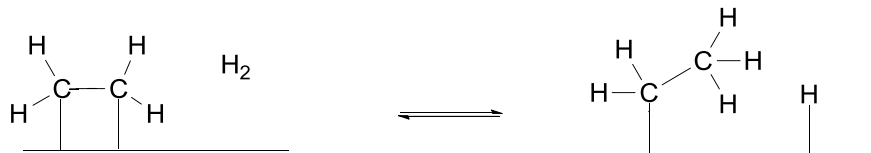
For heterogeneous surface reactions, three types of reaction modes are commonly defined in text books (Figure 1.11):^{31,44}

- i) *Langmuir-Hinshelwood mechanism*: All species are adsorbed on the catalyst surface (equilibrated with the gas phase). The surface species react and form the products.
- ii) *Eley-Rideal mechanism*: At least one of the reactants is adsorbed, whereas the other(s) reacts directly out of the gas phase (without intermediate adsorption on the catalyst surface).
- iii) *Mars-van-Krevelen mechanism*: An adsorbed reactant reacts with lattice oxygen of the catalyst. After desorption of the reactant, the catalyst is reoxidized by gas phase oxygen.

Langmuir-Hinshelwood mechanism



Eley-Rideal mechanism



Mars-van-Krevelen mechanism

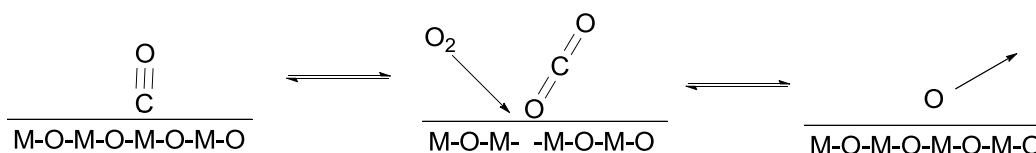


Figure 1.11: Illustration of possible reaction pathways for a heterogeneously catalyzed bimolecular surface reaction. (Adapted from ref. ⁴⁴)

Cracking of hydrocarbons (alkanes and alkenes) can be described by a modified Langmuir-Hinshelwood mechanism, where only one adsorbed reactant is considered.^{45,46} In the following section the mechanisms of alkane and alkene cracking will be discussed in more detail.

1.3.2. The Haag-Dessau mechanism of protolytic alkane cracking

The mechanism of protolytic alkane cracking is, even after more than 60 years of research, still discussed controversially.⁴⁶ In a first approach alkane cracking was explained via a carbenium ion mechanism.⁴⁶⁻⁴⁹ According to these suggestions, very strong aprotic Lewis centers present in the catalysts are responsible for the formation of a carbenium ion by abstracting a hydride from the saturated hydrocarbon. This carbenium ion cracks then via β -scission (see section 1.4), and forms one olefin and one alkane, the latter being formed by hydride addition to the remaining carbenium ion.⁴⁶⁻⁴⁹

This and similar models based on the carbenium ion as key intermediate had to be dropped, because of the inability to explain the product pattern typically

obtained for cracking of short chain hydrocarbons. For example, the presence of methane - which based on a mechanism involving a carbenium ion is very unlikely to be formed as it would involve a CH_3^+ fragment - disagrees with a carbenium ion type mechanism.⁴⁹⁻⁵²

Being aware of the shortcomings of the current model, it was soon realized that BAS of zeolites seem to be connected with the cracking activity.⁵³ It was then Haag and Dessau who proposed for the first time a penta-coordinated transition state (carbonium ion) for alkane cracking. This proposal initiated a paradigm shift in alkane cracking.^{46,54-56}

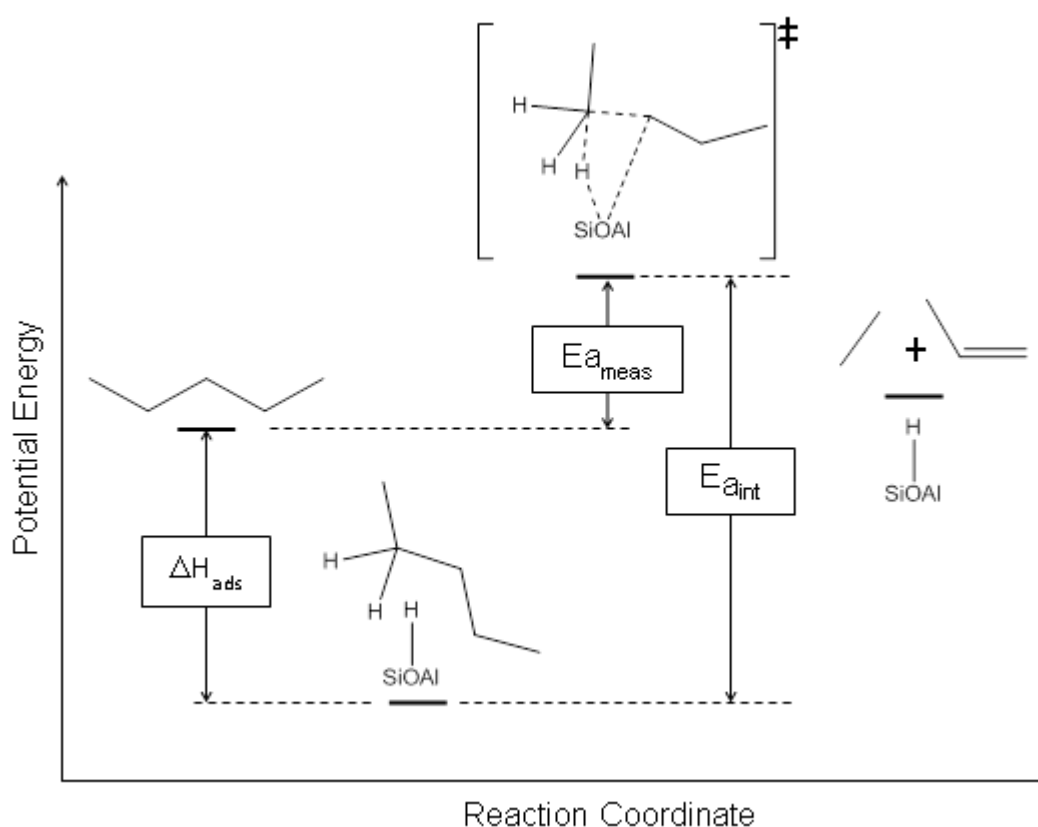


Figure 1.12: Simplified energy scheme for protolytic cracking of n-pentane.

The elementary steps involved in alkane cracking using zeolites are shown in a simplified scheme for n-pentane cracking in Figure 1.12. The first step is the adsorption of the alkane to the BAS. Starting from this ground state a penta-coordinated transition state is formed. This is a three center – two electron

complex which has almost covalent bonding character. As a consequence of formation of this non-classical complex, bonds in α -position of the C to which the proton has been transferred will be elongated, which will finally result in cracking of one of the bonds. As a result of this reaction one olefin and one alkane or one H_2 molecules are formed.^{46,53,54}

For n-pentane cracking four different reactions pathways can be deduced, when following the aforementioned mechanism.⁶⁰ Figure 1.13 summarizes these possibilities.

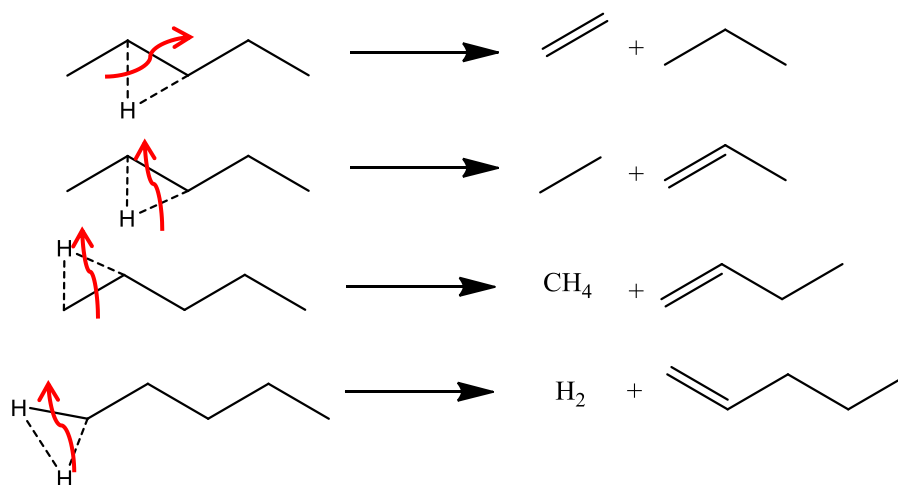


Figure 1.13. Possible pathways of protolytic cracking for n-pentane cracking.

1.3.3. Analysis of the intrinsic kinetics of alkane cracking reactions

The observed kinetics of alkane cracking can be described by a first order reaction.^{60,61} Cracking is usually conducted at temperatures above $400^{\circ}C$, therefore the coverage of the catalyst can be described by the linear correlation obtained in the Henry regime of the Langmuir adsorption isotherm ($\Theta = K_A p_A$).⁶¹ Hence, we obtain equation 1.1. which correlates the measured rate constant with intrinsic reaction parameters? In order to do so, several prerequisites must be fulfilled: 1) Adsorption of the alkane onto the BAS must be equilibrated via a non-activated step with the extra crystalline gas phase, 2) Low intrazeolite concentration of the alkane (most BAS are unoccupied), 3) Thermodynamic activity coefficients for the alkane in the transition state

(penta-coordinated carbonium ion) and in the adsorbed ground state must be identical.⁶¹

$$r_{meas} = k_{meas}P_A = k_{int}K_A P_A \quad (1.1.)$$

When using the Arrhenius expression for the rate constant and the adsorption constant equation 1.2. and 1.3. are obtained.⁶¹

$$k_{int}K_A = \frac{kT}{h} \left[\exp\left(\frac{\Delta S_{int}}{R}\right) \exp\left(\frac{-Ea_{int}}{RT}\right) \exp\left(\frac{\Delta S_{ads}}{R}\right) \exp\left(\frac{-\Delta H_{ads}}{RT}\right) \right] \quad (1.2.)$$

$$k_{meas} = \frac{kT}{h} \left[\exp\left(\frac{\Delta S_{meas}}{R}\right) \exp\left(\frac{-Ea_{meas}}{RT}\right) \right] \quad (1.3.)$$

Consequently, the measured activation entropies and activation energies reflect the sum of the entropies/energies of the intrinsic barrier (ground state → transition state) and the preceding adsorption step. This is also illustrated in equations 1.4 and 1.5.

$$\Delta S_{int} = \Delta S_{meas} - \Delta S_{ads} \quad (1.4)$$

$$Ea_{int} = Ea_{meas} - \Delta H_{ads} \quad (1.5)$$

For cracking of alkanes, Narbeshuber et al. showed that the intrinsic barrier is independent of the chain length of the alkane to be cracked (Figure 1.14) and it was found to lie around 200 kJ/mol for MFI.⁶⁰ For propane cracking, a comparable value (199 ± 11 kJ/mol) was observed for the intrinsic barrier for several different framework types (MFI, USY, MOR, BEA, FER).^{1,60}

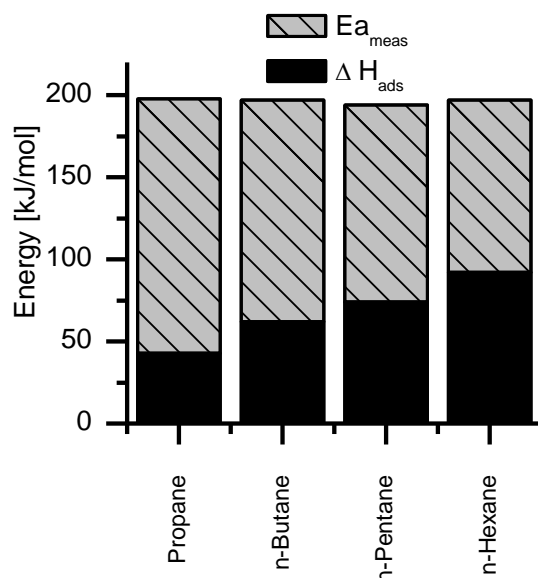


Figure 1.14: Intrinsic barriers for alkane cracking (Adapted from Ref ⁶⁰)

1.3.4. The role of confinement and entropy in alkane cracking

Zeolites provide voids for catalysis which have molecular dimensions. This confinement of the voids has therefore a huge impact on the transition state of cracking.⁶¹ In order to analyze and compare these stabilizing effects within the confinement of zeolites, a Born-Haber thermochemical cycle can be used (Figure 1.15).¹ This technique allows one to deconvolute the observed barriers into several independent elementary steps. These steps are the alkane adsorption (ΔH_{ads}), the deprotonation energy (DPE) of the BAS, the gas phase proton affinity (PA) of the alkane and the stabilization effect on the protonated alkane introduced by confinement within a zeolite pore (E_{stab}).^{1,61}

Values for the different elementary steps are accessible by experiments (ΔH_{ads} , $E_{a_{meas}}$) or can be estimated from theory, such as the proton affinity of the reactants or the deprotonation energy of acid sites.¹ This allows one to compare the stabilization effect introduced by different confinement (e.g. pore size).^{1,61}

It was for example shown for mordenite, a zeolite which contains BAS in an 8-MR environment (side pocket) as well as in 12 MR (main channel), that TOFs differ remarkably among different siting of the BAS.⁶¹ n-Butane

cracking is preferred in the 8 MR side pocket. The partial confinement of the transition state in this pocket results in a remarkable entropy gain, which is responsible for the enhanced activity at these sites.⁶¹

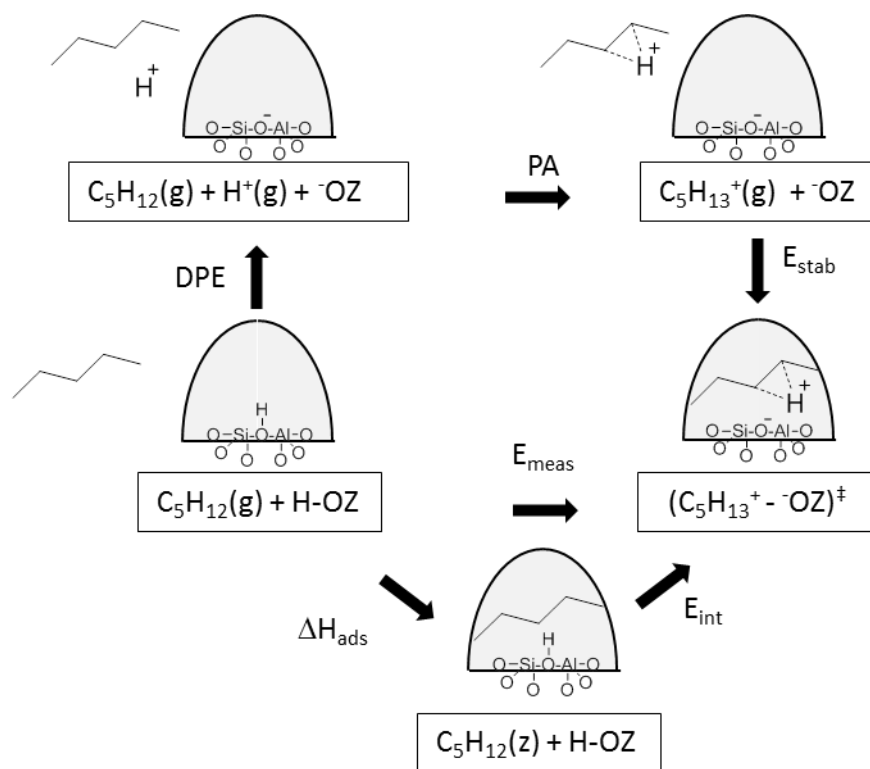


Figure 1.15: Thermochemical cycle for n-pentane cracking over zeolitic acid sites (H-OZ). The barrier of cracking can be analyzed as sum of elementary steps which involve adsorption of n-pentane (ΔH_{ads}), the acid site deprotonation energy (DPE), gas-phase proton affinity (PA) of n-pentane and stabilization upon confinement (E_{stab}). (Adapted from ¹).

A similar effect can be derived for cracking of alkanes with increasing chain length when using the same zeolite. As mentioned in the previous sections, the intrinsic barrier is independent of the hydrocarbon chain length.⁶⁰ Therefore differences in the rate must be correlated either with an increased adsorption or with a change in the preexponential factor. Table 1.2 gives an overview of reported cracking turnover frequencies (TOF) and corresponding adsorption values.^{60,62} Hexane cracking shows about 100x higher TOF than propane cracking. Conversely, the corresponding adsorption constant (K_{ads}) increases only by a factor of 5 (at reaction conditions). Hence, the increased rate cannot be solely attributed to an increased coverage of the reactant.⁶³

Table 1.2: Alkane cracking rates for C₃ – C₆ alkanes and corresponding adsorption values. (Taken from Ref^{60,62})

	TOF ^a ·x10 ³ [mol /(sites·s ·bar)]	ΔH _{ads} [kJ mol ⁻¹]	ΔS _{ads} [J mol ⁻¹ K ⁻¹]	K ^a _{ads} x1000
Propane	2.6	-41	-94	7.25
n-Butane	17.4	-52	-104	12.1
n-Pentane	89.3	-62.5	-118	23.6
n-Hexane	300	-72	-121	35.1

^a determined at 773 K

Adsorption of an alkane results in an entropy loss. The larger the alkane, the larger is the entropy loss. As the transition state complex is formed along the reaction coordinate, entropy of the complex increases when compared to the adsorbed ground state.⁶³ This additional entropy gain is consequently larger for higher alkanes. One has to recall, that monomolecular cracking reactions lead to an entropy gain as “six internal modes are incipiently converted into three translational and rotational degrees of freedom in the transition state”.⁶³

As can be seen from this short overview of recent insights into alkane cracking, complex models have been already established for alkane cracking. Adsorption of alkanes is experimentally easily accessible and hence intrinsic rate parameters can be derived and analyzed in great detail. The situation is more complex for olefins. Experimental values for adsorption and apparent rate parameters such as activation energies are, to the best of my knowledge, until today not reported. An overview over the state of the art in olefin adsorption and cracking will be presented in the upcoming chapters.

1.3.5. Adsorption of olefins

Generally speaking, it is difficult to experimentally study the adsorption of olefins at ambient conditions. The high reactivity of the double bond usually results in immediate reactions of the olefins under such conditions. Therefore experimental studies focus mainly on low temperature adsorption of olefins such as 1-butene.⁶⁴⁻⁶⁷

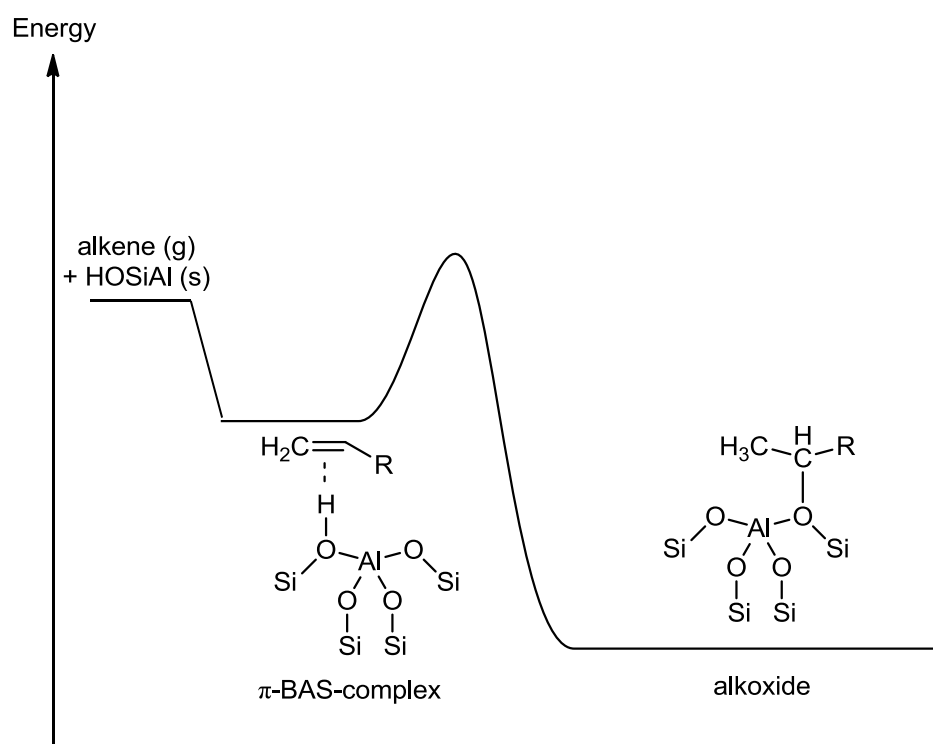


Figure 1.16: Illustration of activated transition from physisorbed π -BAS complex to chemisorbed alkene.

Adsorption of short chain alkenes on these acid sites is usually described by two steps (Figure 1.16): the weak interaction of the BAS with the double bond in the form of a π -complex which is followed by addition of the acidic proton to the double bond.⁶⁸⁻⁷⁰ The π -complex can be considered as a physisorbed state because, despite the clearly localized interaction between the π -electrons of the double bond and the BAS, bonds are neither formed nor broken in this interaction^{68,70} But one has to recall, that higher olefins such as 1-pentene could also coordinate via its aliphatic backbone to a BAS by van

der Waals interaction. Domen et al. showed for adsorption of 1-butene on ZSM-5 that first the alkyl-BAS complex is formed (at 166 K) followed by formation of the π -BAS complex upon heating above 170 K via an activated transition.⁶⁷ It is interesting to note, that double bond isomerization is already observed at 250 K – despite of the fact that only a π -interaction of the alkene with the BAS is observed.^{64,66} At these sub ambient temperatures, a concerted mechanism which does not involve a chemisorbed intermediate, is responsible for double bond isomerization.⁷¹

Upon warming to ambient temperatures reaction of the adsorbed olefins is observed. For short chain olefins such as butenes, dimerization seems to set in.^{64,72} This is an indication for the activated formation of a chemisorbed surface species. The nature of the resulting chemisorbed species is still under debate. It could exist as a covalently bound alkoxide or as an ion pair involving a free carbenium ion.^{66,68,72-74}

To date the adsorption of alkenes in zeolites has been mainly addressed by theoreticians.^{68,70,74,75} As alkenes undergo oligomerization and isomerization already at low temperatures, it is difficult to extract reliable data from adsorption-desorption experiments.^{68,70} Among the theoretical studies, calculated heats of adsorption (chemisorption and physisorption) depend largely on the selected zeolite cluster and the calculation methods.

Nieminen et al. found that for H-FER the heat of physisorption of alkenes was comparable to that of alkanes. The specific interaction of the double bond with the acidic OH is compensated by the overall reduced non-specific interaction (RCH_2-CH_2R' has two more C-H fragments than $RHC=CHR'$). The heat of chemisorption seems to depend largely on the geometry of the adsorbed alkene. For linear butenes, a chemisorption enthalpy of -190 kJ/mol was calculated whereas for 2-methyl-propene a value as low as -62 kJ/mol was obtained. It is believed that the steric repulsion within the confinement of a zeolite and the adsorbed olefin is strong enough to reverse the stability trends of gas phase carbocations.⁶⁸

Nguyen et al. presented a detailed study of the physisorption and chemisorption focusing on linear alkenes in zeolites.⁷⁰ They obtained for physisorption of e.g. 1-pentene in H-ZSM-5 a value of -84 kJ/mol and for chemisorption -168 kJ/mol.⁷⁰ This shows once again that, based on theory, chemisorption (at least for linear alkenes) is favored for enthalpic reasons over physisorption. It can be therefore presumed that the chemisorbed intermediate is the ground state from which olefin cracking proceeds.

1.4. Alkene cracking via carbenium ions

In analogy to alkane cracking, it is commonly accepted that BAS are the active sites in olefin cracking.⁴⁶ Hence, the weaker bond in β -position of the positive charge is cleaved. Figure 1.17 illustrates the elementary steps for the case of 1-pentene cracking. A gas phase pentene molecule is protonated by the BAS. After chemisorption of the alkene, the C-C bond in β -position is cleaved and ethene is released into the gas phase whereas the remaining propyl-cation is chemisorbed on the acid site. Upon desorption of propene the catalytic cycle is completed.⁴⁶ The observed empirical β -scission rule can be understood by the help of theory. Protonation of the alkene results in stabilization of the C-C bond in α -position and in a destabilization of that in β -position of the positive charge.⁴⁶ Hence, the weaker bond in β -position is cleaved.

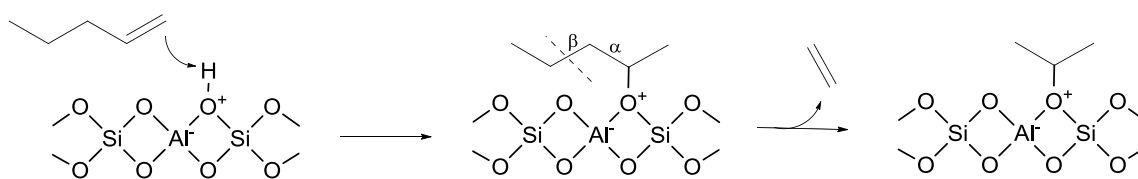


Figure 1.17: Illustration of elementary steps involved in cracking of 1-pentene over BAS of a zeolite.

Besides the cracking reaction, several other reactions of the highly reactive alkenes (isomerization, aromatization, H-transfer, dimerization/alkylation) are observed under typical reaction conditions.^{76,77}

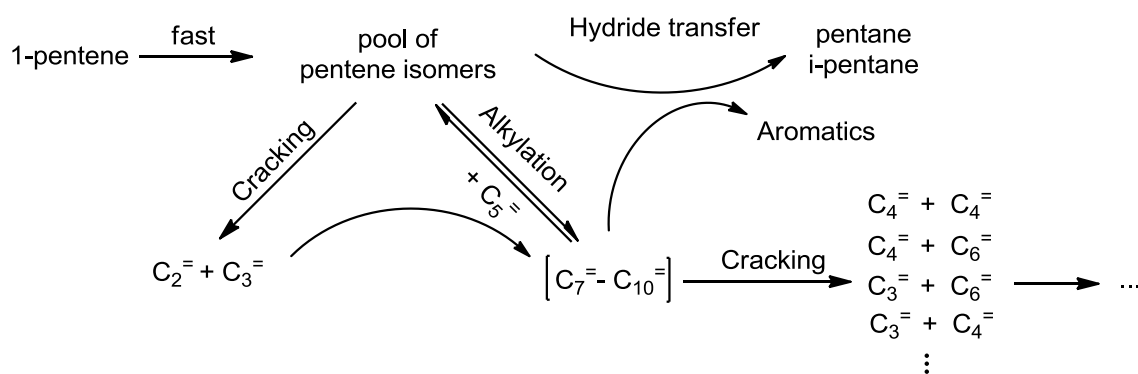


Figure 1.18: Reaction network for 1-pentene cracking over HZSM-5 at elevated temperatures. [Adapted from Ref.^{76,77}].

Figure 1.18 summarizes the most dominant reaction pathways which are commonly observed for 1-pentene cracking. If 1-pentene is employed as reactant at cracking conditions ($T > 400\text{ }^\circ\text{C}$) double bond and skeletal isomerization will be sufficiently fast over zeolites and will produce immediately all six pentene isomers. The relative concentration is defined by the thermodynamic equilibrium at these elevated temperatures.^{78,79}

Even though pentene isomers will be continuously withdrawn from this pentene pool by various reactions, fast re-isomerization will maintain a constant relative concentration of the pentene isomers. Hence, this pentene pool can be treated for a kinetic analysis as one species.

For cracking of the pentene isomers several pathways are available. First of all, pentene could crack directly and form ethene and propene as products. Besides this, dimerization and alkylation might precede the cracking step. For higher conversion levels also the initially formed products are available for alkylation reactions. Hence a broad spectrum of products is usually observed for olefin cracking reactions.^{79,80}

At this point it should be noted that shape selectivity induced by the microporous structure of the zeolites may inhibit certain pathways for the alkylation reactions by restricting reactions that require a large transition state. Hence bulky olefins are not expected to be observed within the product spectrum. Choosing zeolites with differing pore dimensions (FER, TON, MFI) allows one even to shift the product selectivity among the different short chain

olefins.⁸⁰ For zeolites with smaller pores, dimerization is disfavored due to steric reasons and hence less butenes and other higher olefins are observed.^{46,79,80}

According to this scheme a great number of different alkenes and hence carbenium ions can be formed, despite of feeding a single reactant. The rate of β -scission will be strongly influenced by the stability of the carbenium ions that are involved in the cracking reaction.⁷⁹

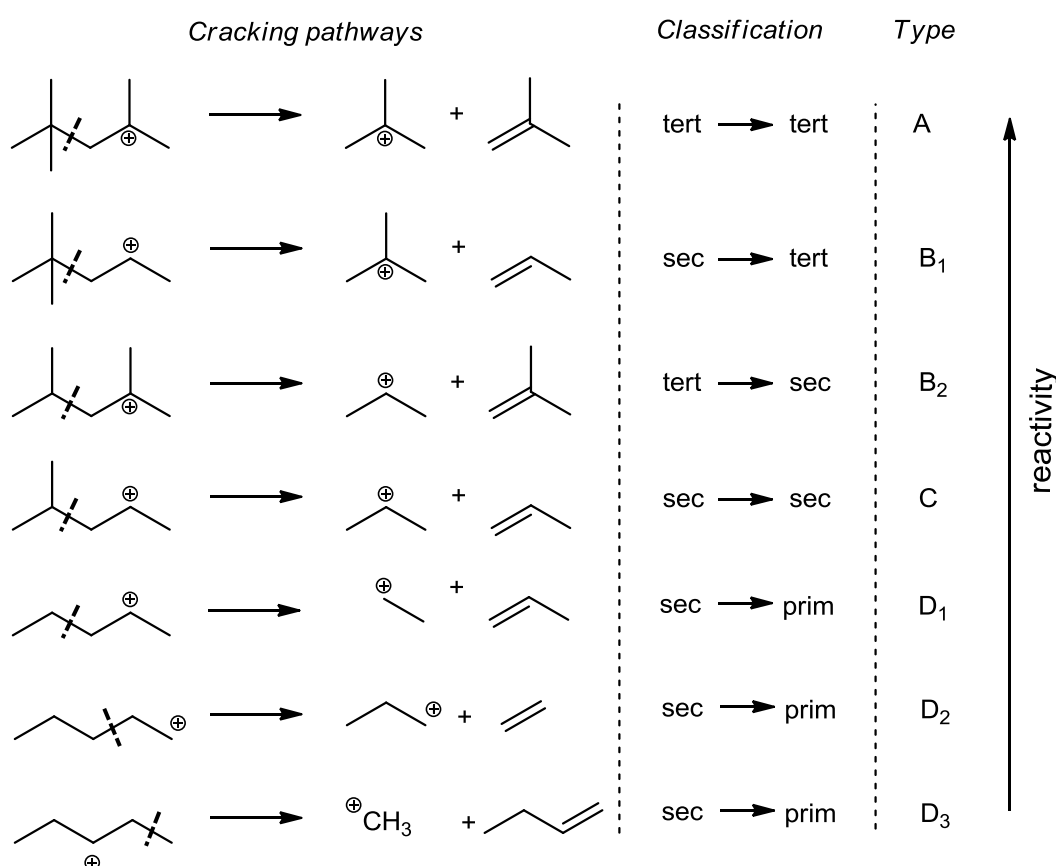


Figure 1.19: Relative reactivity of cracking pathways involving primary, secondary and tertiary carbenium ions. (Adapted from Ref. ⁷⁹)

Figure 1.19 gives a detailed overview over the different pathways and the relative reactivity in olefin cracking following the classification introduced by Buchanan et al.⁷⁹ The relative reactivity depends strongly on the participating carbenium ions. A cracking reaction that involves two tertiary carbenium ions will be the fastest (Type A). In contrast, any reaction which would result in formation of the highly unstable methyl cation will be very slow (Type D₃).⁷⁹

1.5. Scope of the thesis

The role of BAS in catalytic conversion of hydrocarbons is, as shown in the preceding section, well established. Nevertheless, the activities (normalized per BAS) reported in literature scatter quite remarkably.^{1,42,61} Several studies point to the fact that extraframework Al might be somehow connected with the enhanced activity observed for some zeolites. This work aims at elucidating the role of extraframework Al in catalytic conversion of alkanes and alkenes over industrially relevant MFI type zeolites.

In a first stage, n-pentane is selected as a model molecule and a set of seven different MFI type zeolites covering a broad range of acid site concentrations is used. The concentration of extraframework Al will be selectively tuned by chemical modifications and its impact on the catalytic activity and energetic barriers will be studied. In order to clarify the location and nature of these extraframework Al sites. Various characterization methods (IR, NMR, TPD, ...) will be used. The results obtained will enable us to get a better understanding of the role of EFAl in catalytic cracking of alkanes.

As a next step, it is desirable to extend this picture to alkene cracking. 1-Pentene is chosen as a model olefin. In contrast to alkane cracking, to date there is no detailed experimental description of the primary kinetics available nor has the adsorption of olefins on zeolites been addressed experimentally. Therefore, here firstly the adsorption and surface reaction of 1-pentene will be studied on two different zeolites (FER, MFI). FER, which contains small 8MR pores, was chosen as a reference zeolite in order to study the impact of pore confinement on the adsorption process. It is aimed to establish heats of physisorption and chemisorption. The experimentally determined values will be compared to those provided by theory.

Once the adsorption parameters are established, the complicated reaction network of 1-pentene will be investigated with a catalyst having a low acid site concentration. A broad temperature range (420 – 530 °C) will be studied and a kinetic analysis of the pathways leading to the main products is aimed. Activation energies will be determined. With the previously established

adsorption values, it will be possible to determine the intrinsic energetic barriers in olefin cracking.

In a last step, the role of EFAI in olefin cracking will be also studied and discussed, by using the same zeolite samples as employed for the study of n-pentane cracking.

1.6. References

- (1) Gounder, R.; Iglesia, E. *Chemical Communications* **2013**, *49*, 3491
- (2) Plotkin, J. S. *Catalysis Today* **2005**, *106*, 10.
- (3) Zimmermann, H. In *Ullmann's Encyclopedia of Industrial Chemistry*; Wiley-VCH Verlag GmbH & Co. KGaA: **2000**.
- (4) Heggs, T. G. In *Ullmann's Encyclopedia of Industrial Chemistry*; Wiley-VCH Verlag GmbH & Co. KGaA: **2000**.
- (5) Wittcoff, H. A.; Reuben, B. G.; Plotkin, J. S. In *Industrial Organic Chemicals*; John Wiley & Sons, Inc.: **2012**, p 211.
- (6) O'Connor, P. In *Studies in Surface Science and Catalysis*; Ocelli, M. L., Ed.; Elsevier: **2007**; Vol. Volume 166, p 227.
- (7) Tallman, M. J.; Eng, C.; Choi, S.; Park, D. S. *Petroleum Technology Quarterly* **2010**, *15*, 87
- (8) Diercks, R.; Arndt, J. D.; Freyer, S.; Geier, R.; Machhammer, O.; Schwartz, J.; Volland, M. *Chemical Engineering & Technology* **2008**, *31*, 631.
- (9) Traa, Y. *Chemical Communications* **2010**, *46*, 2175.
- (10) Banks, R. L.; Bailey, G. C. *I&EC Product Research and Development* **1964**, *3*, 170.
- (11) Chester, A. W.; Derouane, E. G. *Zeolite Characterization and Catalysis - A Tutorial*; Springer: Heidelberg, **2009**.
- (12) Cundy, C. S.; Cox, P. A. *Chemical Reviews* **2003**, *103*, 663.
- (13) Hay, R. L.; Sheppard, R. A. *Reviews in Mineralogy and Geochemistry* **2001**, *45*, 217.
- (14) Barrer, R. M.; Denny, P. J. *Journal of the Chemical Society (Resumed)* **1961**, 971.
- (15) Flanigen Edith, M. In *Molecular Sieves*; AMERICAN CHEMICAL SOCIETY: **1973**; Vol. 121, p 119.
- (16) Wadlinger, R. L.; Kerr, G. T.; Rosinski, E. J. **1967**; Vol. U.S. Patent 3.308.069.
- (17) Argauer, R. J.; Landolt, G. R. **1972**; Vol. U.S. Patent 3.702.886.
- (18) Flanigen, E. M.; Bennett, J. M.; Grose, R. W.; Cohen, J. P.; Patton, R. L.; Kirchner, R. M.; Smith, J. V. *Nature* **1978**, *271*, 512.
- (19) Weitkamp, J.; Puppe, L. *Catalysis and Zeolites - Fundamentals and Applications*; Springer, **1999**.
- (20) Weitkamp, J. *Solid State Ionics* **2000**, *131*, 175.
- (21) Kokotailo, G. T.; Lawton, S. L.; Olson, D. H.; Meier, W. M. *Nature* **1978**, *272*, 437.
- (22) Barri, S. A. I.; Smith, G. W.; White, D.; Young, D. *Nature* **1984**, *312*, 533
- (23) Hampson, J. A.; Rees, L. V. C. In *Studies in Surface Science and Catalysis*; Tadashi, H., Tatsuaki, Y., Eds.; Elsevier: **1994**; Vol. 83, p 197.
- (24) Parker, L. M.; Bibby, D. M. *Zeolites* **1983**, *3*, 8.
- (25) Vaughan, P. A. *Acta Crystallographica*, *21*, 983
- (26) Wichterlová, B.; Tvarůžková, Z.; Sobalík, Z.; Sarv, P. *Microporous and Mesoporous Materials* **1998**, *24*, 223.
- (27) Corma, A. *Chemical Reviews* **1995**, *95*, 559.

- (28) Woolery, G. L.; Kuehl, G. H.; Timken, H. C.; Chester, A. W.; Vartuli, J. C. *Zeolites* **1997**, *19*, 288.
- (29) Uytterhoeven, J. B.; Christner, L. G.; Hall, W. K. *The Journal of Physical Chemistry* **1965**, *69*, 2117.
- (30) Mortier, W. J.; Sauer, J.; Lercher, J. A.; Noller, H. *The Journal of Physical Chemistry* **1984**, *88*, 905.
- (31) Deutschmann, O.; Knözinger, H.; Kochloefl, K.; Turek, T. In *Ullmann's Encyclopedia of Industrial Chemistry*; Wiley-VCH Verlag GmbH & Co. KGaA: **2000**.
- (32) Crocker, M.; Herold, R. H. M.; Sonnemans, M. H. W.; Emeis, C. A.; Wilson, A. E.; Van der Moolen, J. N. *The Journal of Physical Chemistry* **1993**, *97*, 432.
- (33) Elanany, M.; Koyama, M.; Kubo, M.; Broclawik, E.; Miyamoto, A. *Applied Surface Science* **2005**, *246*, 96.
- (34) Freude, D.; Hunger, M.; Pfeifer, H.; Schwieger, W. *Chemical Physics Letters* **1986**, *128*, 62.
- (35) Kramer, G. J.; Van Santen, R. A. *Journal of the American Chemical Society* **1993**, *115*, 2887.
- (36) Sauer, J. *Chemical Reviews* **1989**, *89*, 199.
- (37) Sastre, G.; Katada, N.; Niwa, M. *The Journal of Physical Chemistry C* **2010**, *114*, 15424.
- (38) Dědeček, J.; Kaucký, D.; Wichterlová, B. *Microporous and Mesoporous Materials* **2000**, *35–36*, 483.
- (39) Dedecek, J.; Kaucky, D.; Wichterlova, B.; Gonsiorova, O. *Physical Chemistry Chemical Physics* **2002**, *4*, 5406.
- (40) Sazama, P.; Dědeček, J.; Gábová, V.; Wichterlová, B.; Spoto, G.; Bordiga, S. *Journal of Catalysis* **2008**, *254*, 180.
- (41) Sklenak, S.; Dedecek, J.; Li, C.; Wichterlova, B.; Gabova, V.; Sierka, M.; Sauer, J. *Physical Chemistry Chemical Physics* **2009**, *11*, 1237.
- (42) Janda, A.; Bell, A. T. *Journal of the American Chemical Society* **2013**, *135*, 19193.
- (43) George, S. M. *Chemical Reviews* **1995**, *95*, 475.
- (44) Chorkendorff, I.; Niemandsverdriet, J. W. *Concepts of modern catalysis and kinetics*; Wiley - VCH: Weinheim, **2003**.
- (45) van Bokhoven, J. A.; Williams, B. A.; Ji, W.; Koningsberger, D. C.; Kung, H. H.; Miller, J. T. *Journal of Catalysis* **2004**, *224*, 50.
- (46) Kissin, Y. V. *Catalysis Reviews* **2001**, *43*, 85.
- (47) Greensfelder, B. S.; Voge, H. H.; Good, G. M. *Industrial & Engineering Chemistry* **1949**, *41*, 2573.
- (48) Thomas, C. L. *Industrial & Engineering Chemistry* **1949**, *41*, 2564.
- (49) Abbot, J.; Wojciechowski, B. W. *Journal of Catalysis* **1988**, *113*, 353.
- (50) Bizreh, Y. W.; Gates, B. C. *Journal of Catalysis* **1984**, *88*, 240.
- (51) Engelhardt, J.; Hall, W. K. *Journal of Catalysis* **1995**, *151*, 1.
- (52) Lombardo, E. A.; Hall, W. K. *Journal of Catalysis* **1988**, *112*, 565.
- (53) Haag, W. O.; Lago, R. M.; Weisz, P. B. *Nature* **1984**, *309*, 589.
- (54) Haag, W. O.; Dessau, R. M. *Proceedings of 8th International Congress on Catalysis*; Verlag Chemie, **1984**; Vol. 2.
- (55) Engelhardt, J.; Hall, W. K. *Journal of Catalysis* **1990**, *125*, 472.

- (56) Shertukde, P. V.; Marcelin, G.; Sill, G. A.; Keith Hall, W. *Journal of Catalysis* **1992**, *136*, 446.
- (57) Olah, G. A.; Halpern, Y.; Shen, J.; Mo, Y. K. *Journal of the American Chemical Society* **1971**, *93*, 1251.
- (58) Olah, G. A.; Halpern, Y.; Shen, J.; Mo, Y. K. *Journal of the American Chemical Society* **1973**, *95*, 4960.
- (59) Richter, W. J.; Schwarz, H. *Angewandte Chemie* **1978**, *90*, 449.
- (60) Narbeshuber, T. F.; Vinek, H.; Lercher, J. A. *Journal of Catalysis* **1995**, *157*, 388.
- (61) Gounder, R.; Iglesia, E. *Journal of the American Chemical Society* **2009**, *131*, 1958.
- (62) De Moor, B. A.; Reyniers, M.-F. o.; Gobin, O. C.; Lercher, J. A.; Marin, G. B. *The Journal of Physical Chemistry C* **2010**, *115*, 1204.
- (63) Bhan, A.; Gounder, R.; Macht, J.; Iglesia, E. *Journal of Catalysis* **2008**, *253*, 221.
- (64) Kondo, J. N.; Liqun, S.; Wakabayashi, F.; Domen, K. *Catalysis Letters* **1997**, *47*, 129.
- (65) Kondo, J. N.; Domen, K.; Wakabayashi, F. *Microporous and Mesoporous Materials* **1998**, *21*, 429.
- (66) Kondo, J. N.; Wakabayashi, F.; Domen, K. *The Journal of Physical Chemistry B* **1998**, *102*, 2259.
- (67) Yoda, E.; Kondo, J. N.; Domen, K. *The Journal of Physical Chemistry B* **2005**, *109*, 1464.
- (68) Nieminen, V.; Sierka, M.; Murzin, D. Y.; Sauer, J. *Journal of Catalysis* **2005**, *231*, 393.
- (69) Sauer, J.; Ugliengo, P.; Garrone, E.; Saunders, V. R. *Chemical Reviews* **1994**, *94*, 2095.
- (70) Nguyen, C. M.; De Moor, B. A.; Reyniers, M.-F.; Marin, G. B. *The Journal of Physical Chemistry C* **2011**, *115*, 23831.
- (71) Boronat, M.; Viruela, P.; Corma, A. *The Journal of Physical Chemistry A* **1998**, *102*, 982.
- (72) Ishikawa, H.; Yoda, E.; Kondo, J. N.; Wakabayashi, F.; Domen, K. *The Journal of Physical Chemistry B* **1999**, *103*, 5681.
- (73) Boronat, M.; Viruela, P. M.; Corma, A. *Journal of the American Chemical Society* **2004**, *126*, 3300.
- (74) Bhan, A.; Joshi, Y. V.; Delgass, W. N.; Thomson, K. T. *The Journal of Physical Chemistry B* **2003**, *107*, 10476.
- (75) Pascual, P.; Ungerer, P.; Tavitian, B.; Pernot, P.; Boutin, A. *Physical Chemistry Chemical Physics* **2003**, *5*, 3684.
- (76) Höchtl, M.; Jentys, A.; Vinek, H. *Applied Catalysis A: General* **2001**, *207*, 397.
- (77) Bortnovsky, O.; Sazama, P.; Wichterlova, B. *Applied Catalysis A: General* **2005**, *287*, 203.
- (78) Mäurer, T.; Kraushaar-Czarnetzki, B. *Journal of Catalysis* **1999**, *187*, 202.
- (79) Buchanan, J. S.; Santiesteban, J. G.; Haag, W. O. *Journal of Catalysis* **1996**, *158*, 279.
- (80) Miyaji, A.; Sakamoto, Y.; Iwase, Y.; Yashima, T.; Koide, R.; Motokura, K.; Baba, T. *Journal of Catalysis* **2013**, *302*, 101.

CHAPTER 2

2. Impact of the local environment of Brønsted acid sites in ZSM-5 on the catalytic activity in n-pentane cracking

This chapter is based on:

S. Schallmoser, T. Ikuno, M.F. Wagenhofer, R. Kolvenbach, M. Sanchez-Sanchez, J.A. Lercher, „Impact of the local environment of BAS in ZSM-5 on the catalytic activity in n-pentane cracking” *J. Catal* (2014), 316 93 – 102.

Reprinted with permission from Elsevier.

ABSTRACT: The impact of the zeolite Brønsted and Lewis acid site concentration on the catalytic cracking of alkanes was explored using n-pentane and H-ZSM-5 as examples. Rates normalized to strong Brønsted acid sites (i.e., the turnover frequencies, TOF) showed that the two samples with the highest Al content had much higher TOF than all other samples. This difference has been unequivocally linked to the presence of extra-lattice alumina. Post-treatment of the zeolites with ammonium hexafluorosilicate and static calcination was used to vary the concentration of extra-lattice alumina. After extraction of extra-lattice alumina from the samples with high TOF, all TOFs were identical. IR spectra of adsorbed pyridine and NH₃, coupled with ²⁷Al MAS NMR, showed that the overall enhanced activity is associated with tetrahedral coordinated extra-lattice alumina in close proximity to strong Brønsted acid sites. The TOF of these sites is approximately 40-times higher than the TOF on normal Brønsted acid sites.

2.1. Introduction

Zeolites, such as ZSM-5, are commonly employed as solid acid catalysts in petroleum and petrochemical industry for reactions such as isomerization, alkylation and cracking.^{1,2} It is generally accepted that strong Brønsted acid sites (SBAS), the bridging OH groups (SiOHAl), are the active sites for these reactions.¹⁻⁵ The importance of the zeolite catalyzed conversions for industry and the seeming simplicity of the reaction have led to a wide range of fundamental and applied studies using alkanes and alkenes as reactants and as probes to understand the catalytic properties of Brønsted acid sites.^{3,6-13} For protolytic cracking of alkanes, the reaction path involving a penta-coordinated carbonium ion as a transition state is now widely accepted.^{1,4}

While cracking activity can be attributed to SBAS, the intrinsic activity per SBAS has been found to depend markedly on the local environment of these sites.^{2,5,14} Mild steaming, which removes some of the SBAS and creates extra framework Al (EFAl), enhances the catalytic activity per H⁺.^{5,15-17} Because the specific activity of SBAS sites is crucial for the overall performance of industrial catalysts, significant attention has been paid to understand potential design parameters, which would enhance the specific activity of Brønsted acid sites.

The strong variation of zeolite specific activity has been the subject of a large number of studies and, in consequence, a substantial variety of explanations have been proposed in the literature. Lago et al. were the first to describe that very mild steaming enhances catalytic activity in hexane cracking. They attributed this to a partial hydrolysis of a tetrahedral framework Al which is in proximity of a second tetrahedral framework site. They concluded that this should increase acidity of the second SBAS and increases therefore the catalytic activity.¹³ Following this rationale, the enhancement of specific catalytic activity is most commonly attributed to a cooperative interaction between a SBAS and an adjacent EFAl as depicted in Figure 2.1.^{14,16-18} The

direct interaction would involve a partial electron transfer from the OH bond to the EFAl species which has been proposed to increase its acid strength.¹⁶ Surprisingly, the corresponding downfield shift of the ¹H NMR signal and the red-shift of the characteristic OH stretching vibration in the IR spectrum have not been observed.^{16,18} Based on NMR experiments and DFT calculations, Li et al. have developed a modified picture of this interaction between the SBAS and EFAl,¹⁶ suggesting that the proton affinity of the SBAS substantially decreases even when the EFAl species are coordinated to a neighboring oxygen atom (Figure 2.1).¹⁶

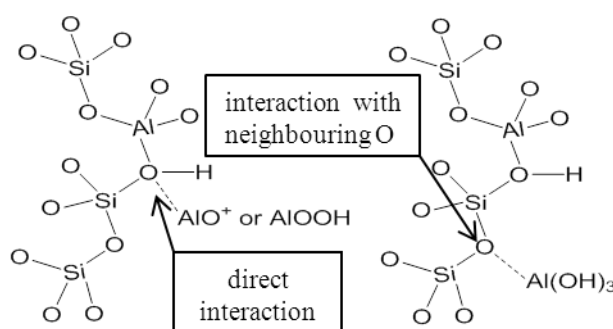


Figure 2.1: Possible modes for interaction of extra framework Al with SBAS.

Gounder *et al.* argued against that interpretation.¹⁰ Evidence is provided in ref. ¹⁰ that space-occluding EFAl reduces the effective void size in FAU and increases therefore interaction of the hydrocarbon via dispersion forces.¹⁰ Gounder et al. noted also recently that the cracking and dehydrogenation rate constants (normalized to BAS) published in the open literature differ by a factor of 10 for different MFI type zeolites (propane cracking).⁹ The rate differences are stated to reflect the Al distribution on different T-sites in the zeolite. While it is concluded that the acid strength is identical for these unique T-sites, the geometry of the surrounding space varies as a function of the location in the zeolite lattice. Due to the variation in the stabilization of hydrocarbons and surface species at the different T-sites, the rates per SBAS are expected to differ, if the Al distribution among these T-sites changes.^{9,19} Interestingly, a similar argument has been recently used by Janda and Bell to rationalize that for n-butane cracking the rate depends crucially on the presence of SBAS in the intersections of the zeolite, i.e., at a location for

which the constraints are the least in H-ZSM5.¹¹ Van Bokhoven *et al.* argue, in contrast, that the rate enhancement is related to an increased heat of adsorption of alkanes after mild steaming. The consequently higher coverage of the reactant is seen as the cause for the overall enhanced rate.⁵

Recently, it was shown that chemical vapor deposition of trimethylaluminum in FAU and subsequent decomposition in H₂ resulted in a very active catalyst for propane cracking.²⁰ Also in this case differences in the intrinsic proton acidity were not observed, when comparing modified and unmodified samples. Nevertheless, the rate enhancement was attributed to proximity of strong Lewis acid sites (SLAS) to SBAS.

These reports show unequivocally that the presence of EFAl is associated with the rate enhancement in cracking. The specific role of the EFAl is described, however, by two models, i.e., (a) the increased acid strength of the SBAS caused by the interaction of EFAl with SBAS and (b) the increased interaction with the alkane via dispersion forces (“solvation”) enhanced by the presence of EFAl. The term EFAl is used here to describe several chemically different Al species, which are present in zeolites besides the framework Al.²⁰⁻²² The nature of EFAl species could be that of a charged aluminum oxide or neutral species such as monomeric AlOOH, Al(OH)₃ as well as aluminum-oxo and hydroxyl clusters and bulk aluminum oxide aggregates.²⁰⁻²² Non-framework Al still partially connected to the framework (O₃Si-O-Al-OH), also referred to as partially dealuminated framework Al, has also been considered.^{6,22-25}

The present contribution resolves the discrepancies of the various assignments of the specific catalytic activity by systematically exploring the impact of the local environment of SBAS on activity and selectivity in alkane cracking, using n-pentane as a model substrate and H-ZSM-5 as model zeolite.

2.2. Experimental

Zeolite samples and modification

Five commercial H-ZSM-5 samples provided by *Zeolyst International* (MFI-15 = CBV3024E, MFI-25 = CBV5524G and MFI-40 = CBV8014) and *Clariant AG* (MFI-60 and MFI-90) were used. Two additional H-ZSM-5 catalysts were synthesized to extend the investigation to higher Si/Al ratios. Depending on their composition, the samples were designated as MFI-X, with “X” relating to their overall Si/Al ratio (atom/atom).

Zeolite synthesis

The samples with the highest Si/Al ratios (MFI-240 and MFI-470) were prepared by hydrothermal synthesis according to the following procedure. For H-MFI-240, 0.42 g (1.1 mmol) of $\text{Al}(\text{NO}_3)_3 \cdot 9\text{H}_2\text{O}$ (purity $\geq 98\%$, *Sigma-Aldrich*) were dissolved in 30 ml of deionized water and slowly added to a solution of 3.0 g (75 mmol) NaOH (purity $\geq 98\%$, *Fluka-Analytical*) dissolved in 30 ml of deionized water. The corresponding amount of $\text{Al}(\text{NO}_3)_3 \cdot 9\text{H}_2\text{O}$ for H-MFI-470 was 0.21 g. The resulting solution was clear (solution A). Then, another solution, containing 14.8 g (55 mmol) tetrapropyl ammonium bromide (TPABr, purity $\geq 98\%$, *Sigma-Aldrich*) and 1.51 g (38 mmol) NaOH dissolved in 70 ml of deionized water, was added to solution A. To the resulting, clear solution, 20 g of a fumed silica nano-powder (*Cabosil M-5*, *Supelco-Analytical*) were added gradually under vigorous stirring. The resulting viscous mixture was then stirred for 20 h at room temperature to yield an opaque gel. The subsequent hydrothermal synthesis was carried out in an autoclave with a PTFE liner for 24 h at 423 K. The resulting material was separated from the mother liquor, washed twice with deionized water, and calcined for 5 h in a stream of synthetic air (100 ml min^{-1} , heating rate 10 K min^{-1} , 823 K) to oxidatively remove the organic template. The crystallographic purity of the Na-ZSM-5 samples was verified by X-ray diffraction (not shown).

Subsequently, the as-synthesized samples were ion-exchanged three times at 353 K for 2 h, each time using 150 ml of a 1 M NH_4NO_3 -solution

(corresponding to 25 ml per 1 g of sample), to produce NH₄-ZSM-5 zeolites. The resulting samples were dried at 393 K for 2 h and calcined for 5 h in a stream of synthetic air (100 ml min⁻¹, heating rate 10 K min⁻¹, 823 K) to yield the catalytically active H-forms.

AHFS-Treatment

NH₄-ZSM-5 (approx. 2 g of sample per 80 ml of solution) was added to a solution of (NH₄)₂SiF₆ (AHFS) at 353 K and then stirred vigorously for 5 h. The synthesis was done in a PTFE-liner with a volume of 100 ml. The solution contained a 4-fold excess of AHFS with respect to the Al-content of the sample. This was 1.42 g (8.0 mmol) AHFS for 1.92 g of MFI-15 (2.9 wt-% Al corresponding to 2 mmol) and 0.88 g (5.0 mmol) AHFS for 1.92 g of MFI-25 (1.7 wt-% Al corresponding to 1.3 mmol). After the AHFS treatment, the samples were washed six times in hot deionized water (353 K) and calcined for 5 h in a stream of synthetic air (100 ml min⁻¹, heating rate 10 K min⁻¹, 823 K). The samples modified by AHFS treatment were designated as MFI-X-AHFS, where “X” stands for the overall Si/Al ratio (atom/atom) as determined by atomic absorption spectroscopy.

Static calcination

The H form of MFI-15 was placed as shallow bed (approx. 2 g, layer thickness ≈ 2 – 3 mm) into a quartz boat and was then heated under static atmospheric conditions (no flow of gas, ambient air present) with a temperature ramp of 10 K min⁻¹ to 823 K and kept there for 30 minutes, before it was allowed to cool to room temperature. This sample was designated as MFI-15-ST.

Kinetic measurements of n-pentane cracking

The protolytic cracking of n-pentane was investigated in a plug flow reactor (length = 350 mm; inner diameter = 6 mm, quartz) which was operated at atmospheric pressure. The catalysts (pellet size: 250 – 325 μm) were activated in situ with a heating ramp of 2 K min⁻¹ for 2 h in synthetic air (flow

rate: 20 ml min⁻¹) at 803 K before introducing the reactant via a saturator (2 vol.% n-pentane in He), the reactor was flushed for 30 minutes with pure He. n-Pentane cracking was studied in the temperature range between 753 and 793 K. Reactant and products were separated and analyzed by on-line chromatographic measurements (HP 5890, capillary column: HP-Al₂O₃/KCl, 50 m × 0.32 mm × 8.0 μm) using an FID detector.

Characterization of acid sites

The nature and concentration of acid sites were analyzed by IR spectroscopy of adsorbed pyridine following the procedure described earlier.²⁶ Briefly, the concentrations of BAS and Lewis acid sites (LAS) were determined by adsorption of pyridine at 423 K and subsequent outgassing for 1 h. Subsequently, the concentrations of strong Brønsted acid sites (SBAS) and strong Lewis acid sites (SLAS) were determined by heating to 723 K (10 K min⁻¹) for 30 minutes. After subsequent cooling to 423 K another IR spectrum is collected for quantification. Deconvolution of the difference spectra of pyridine adsorbed onto MFI-15 and MFI-15-ST (after having heated to 723 K) was done by using two Gaussian functions centered at 3656 cm⁻¹ and 3606 cm⁻¹.

Adsorption of NH₃ was studied by means of IR spectroscopy using a similar procedure. After activation of the samples in vacuum at 723 K for 1 hour and cooling to 423 K, approximately 0.1 mbar of NH₃ was introduced. After equilibration for 30 minutes the sample was evacuated for another 30 minutes before spectra were recorded.

As a complementary technique for quantitative acid site characterization, temperature programmed desorption experiments (TPD) of adsorbed NH₃ were performed. The pelletized sample (0.5 – 0.71 mm) was activated at 723 K for 1 h prior to adsorption of 1 mbar of NH₃ at 423 K. After equilibration for 1 h and subsequent outgassing for 2 h, the temperature was increased to 1043 K at 10 K min⁻¹. Desorption of NH₃ was monitored by mass spectrometry (m/z = 16).

Elemental analysis

The elemental composition of the samples was determined by atomic absorption spectroscopy in a Unicam M Series Flame-AAS equipped with an FS 95 autosampler and a GF 95 graphite furnace.

Adsorption of n-pentane

The gravimetric sorption isotherms of n-pentane on either the parent or the two modified ZSM-5 zeolites were measured in a Setaram TG-DSC 111 thermoanalyzer connected to a high vacuum system. About 20 mg of the corresponding sample was placed in a quartz sample holder and activated at 723 K for 1 h under vacuum ($p < 10^{-4}$ mbar) with an incremental heating rate of 10 K min^{-1} . The equilibration with the sorbate was performed in small pressure steps from $3 \cdot 10^{-2}$ to 1 mbar. Both the sample mass and the thermal flux were monitored. The heat of adsorption was directly obtained by integration of the observed heat flux signal.

The adsorption isotherms were analyzed in terms of a dual site Langmuir model (Equ. 2.1):

$$n(p) = \frac{K_1 \cdot p \cdot n_{\max,1}}{1 + K_1 \cdot p} + \frac{K_2 \cdot p \cdot n_{\max,2}}{1 + K_2 \cdot p} \quad (\text{Equ. 2.1})$$

Where K denotes the equilibrium constant of adsorption, n is the amount of sorbate on the sample, n_{\max} is the maximum surface coverage of the individual adsorption site and p is the normalized (referred to $p^0 = 1013$ mbar) pressure.

MAS NMR spectroscopy

Magic angle spinning spectra were recorded on a Bruker Avance AMX-500 spectrometer. Samples were packed after hydration (48 h) at 42 mbar H_2O into ZrO_2 rotors, which were spun at 10 kHz. $\text{Al}(\text{NO}_3)_3 \cdot 9\text{H}_2\text{O}$ was used as reference. For measuring the 1D spectrum an excitation pulse with power level of 7 dB and a length of $0.7 \mu\text{s}$ was applied. Relaxation time was set to 250ms and 2400 scans were recorded. MQMAS spectra were recorded using a sequence of three pulses as described earlier.²⁷ The power level was 7 dB

for the first two pulses and 35 dB for the third one. The corresponding pulse lengths were $p_1 = 8\mu\text{s}$, $p_2 = 3.2\mu\text{s}$, $p_3 = 52\mu\text{s}$. The data were processed and sheared after Fourier transformation using Bruker's software Topspin. The orthogonal projection on an isotropic axis of the likewise obtained 2D spectra gave the 1D spectra free of anisotropic broadening.²⁷

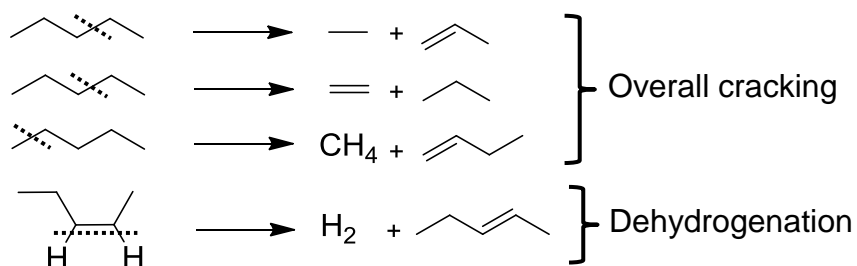
Texture

Specific surface area and porosity were determined from N_2 adsorption/desorption isotherms recorded on an automated *PMI Sorptomatic 1990* instrument at liquid N_2 temperature (77 K). The samples were outgassed in vacuum ($p = 1 \times 10^{-3}$ mbar) for 2 h at 523 K prior to adsorption.

2.3. Results and discussion

2.3.1. Catalytic activity in n-pentane cracking as function of SBAS concentration

Figure 2.2. shows the rate for cracking and dehydrogenation normalized to the weight of the zeolite as a function of the SBAS concentration at 733 K (see Table S1 for details). As expected the catalytic activity increased with increasing concentration of aluminum in the samples leading to an increasing concentration of strong Brønsted acid sites (see below for details of the characterization). The rates of cracking and dehydrogenation of these parent samples increase monotonically but nonlinearly. Especially for SBAS concentrations higher than 400 $\mu\text{mol/g}$, the activity per SBAS was significantly higher compared to the samples with a lower concentration of aluminum in the zeolite lattice, suggesting a higher intrinsic activity of these SBAS sites (Figure 2.2.).



Scheme 2.1: Illustration of pathways observed in protolytic cracking of n-pentane. Dotted line indicates location of the scission.

This implies, however, that a certain fraction of the Brønsted acid sites is highly active, while others, especially those in samples with a very low aluminum concentration in the lattice, possess a much lower catalytic activity. Per se this is surprising, because it is generally accepted that the acid strength in samples with low aluminum concentration is higher than in samples in which aluminum is abundant in the lattice.²⁸

In protolytic n-pentane cracking, three cracking pathways are identified (methane + butene, ethane + propene, propane + ethene), while pentene is formed by protolytic dehydrogenation (see Scheme 2.1.). Analysis showed, that the pathway selectivity is subtly shifted towards methane at the expense of propane and ethane for the samples with higher Al content, i.e., terminal cracking seems to be slightly more favorable in the presence of a higher concentration of acid sites (Figure 2.2.). With increasing concentration of Brønsted acid sites the difference in rates between cracking and dehydrogenation increased suggesting that the transition state for dehydrogenation, which resembles the direct interaction between the zeolite OH group and the hydrogen at a -CH₂- group of the alkane, is more favored at lower concentrations of OH groups.

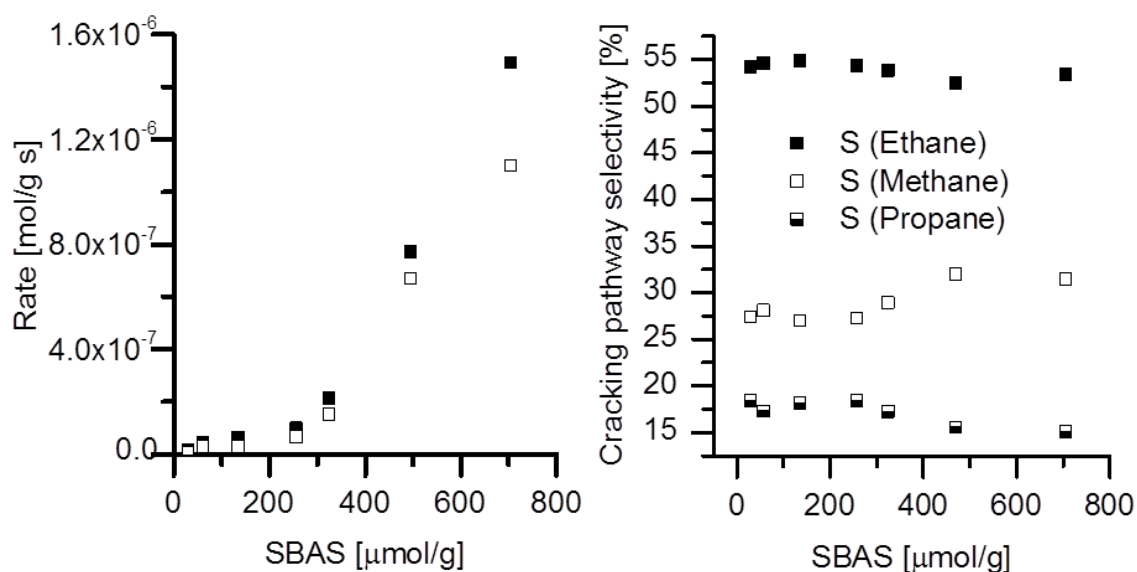


Figure 2.2: Rate normalized to catalyst mass for overall cracking (closed symbols) and dehydrogenation (open symbols) plotted as function of SBAS ($T = 763$ K). (Left) Corresponding cracking pathway selectivities plotted as function of SBAS (Right).

Because the reaction rate of protolytic cracking increased with the concentration of Brønsted acid sites let us discuss the nature and properties of the acid sites in this series of zeolites. The overall determination of Brønsted and Lewis acid sites by adsorption of pyridine and ammonia is compiled in Table S1. A perfect correlation has been observed between the concentrations of Brønsted acid sites determined by both bases (see Figure S.1) underlining the consistency of the method. A more faceted information about the nature of acid sites is derived from the IR spectra of the OH groups of the activated zeolites (Figure 2.3.).

All parent samples show the characteristic band of a bridging hydroxyl groups acting as SBAS at 3610 cm^{-1} .²⁴ This indicates that the intrinsic sites are identical for all samples. In addition, a band at around 3740 cm^{-1} was observed, which is attributed to surface silanols groups terminating the exterior of the crystal.²⁴ A third distinct band at 3780 cm^{-1} was observed only for MFI-15 and is attributed to the presence of OH groups associated with octahedral EFAI.^{24,25} For the samples MFI-15 and MFI-25, however, an additional band was observed at 3656 cm^{-1} . Because the variation of its

intensity did not parallel that of the band at 3780 cm^{-1} , the band at 3656 cm^{-1} is attributed to an OH group on a different EFAI species.^{6,24,25} As the samples exhibiting this band showed a remarkable higher TOF for cracking and dehydrogenation than other samples tested, its presence was empirically associated with the high catalytic activity.

With the aim of proving this hypothesis, the highly active samples were treated with AHFS in order to remove the EFAI. For the AHFS treated samples (MFI-15-AHFS and MFI-25-AHFS) the band at 3656 cm^{-1} and the band at 3780 cm^{-1} were no longer observed (Figure 2.3) indicating that the extra lattice alumina has been removed from both zeolites, which is also reflected in the increasing Si/Al ratio (Table S1) after AHFS modification, and it is in good agreement to results published in the literature.²⁹

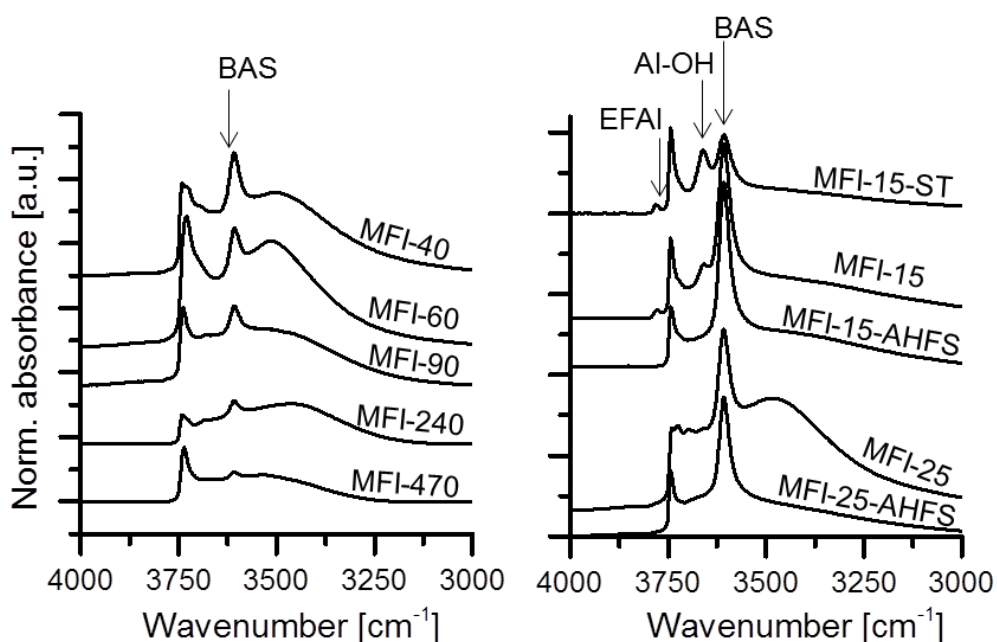


Figure 2.3: Spectra of OH stretching vibrations region of activated zeolite samples (normalized to the overtone and combination region of ZSM-5 lattice vibrations between 2095 and 1735 cm^{-1}).

It is interesting to note that, for the parent samples, there is a linear correlation between the SBAS and SLAS (Figure 2.4). The fact that the samples were of three different origins (homemade synthesis and two different commercial suppliers) let us conclude that this correlation is

independent of the synthesis conditions and reflects the probability of an Al atom to be fully tetrahedrally coordinated into the framework versus to form a coordinately unsaturated SLAS. Upon AHFS treatment, the samples MFI-15-AHFS and MFI-25-AHFS do not fall on this correlation, because this treatment removes preferentially SLAS.

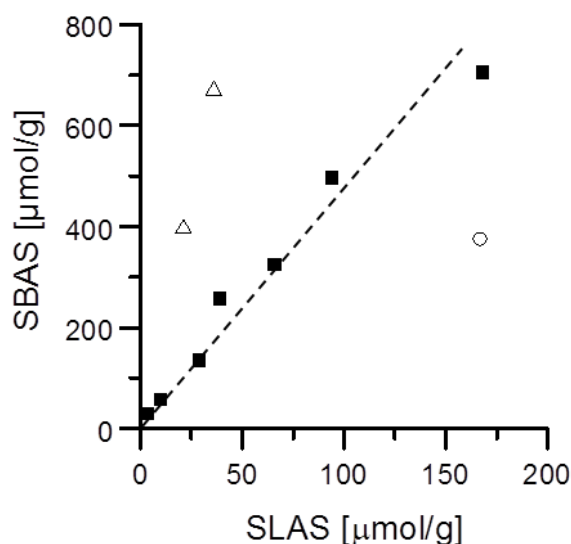


Figure 2.4: Correlation of SBAS and SLAS for parent zeolites (full squares), AHFS modified samples (open triangles) and MFI-15-ST (open circle). A line is added as guidance of the eye.

The AHFS modification had a huge impact on the catalytic performance. It is remarkable, that after this treatment, all catalysts show a linear increase of activity with increasing concentration of Brønsted acid sites with the origin at the intercept (Figure 2.5). None of these samples contains detectable concentrations of EFAl characterized by Al-OH groups (band at 3656 cm^{-1}). The catalytic activity decreased markedly and the TOF became comparable to that of the parent zeolites with a SBAS concentration below $400\text{ }\mu\text{mol/g}$, supporting further the conclusion that all SBAS were equally active.

Hence, we conclude that for MFI-15 and MFI-25 the higher activity is related to the presence of EFAl. It is interesting to note that despite of its huge impact on cracking activity, AHFS modification hardly influenced the pathway selectivity (Figure 2.5). Another characteristic of the zeolite and its acid

centers must therefore be responsible for the observed selectivity shift for high SBAS concentrations. This shift towards terminal cracking with increasing Al content agrees with the observations for n-butane cracking.¹¹

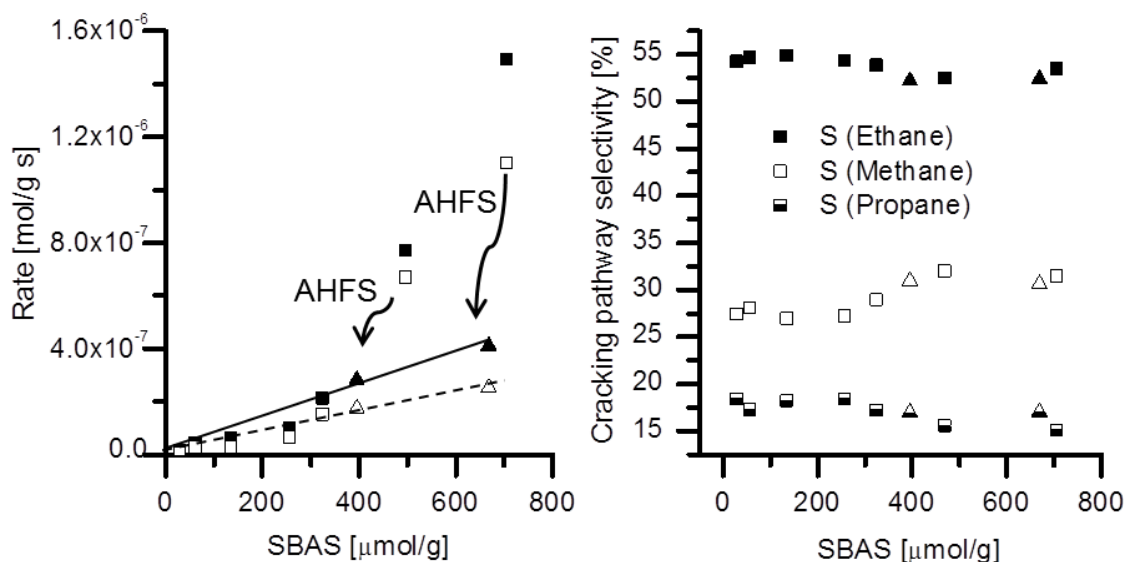


Figure 2.5: Impact of AHFS modification on rates (left) and cracking pathway selectivity (right). Left side: Closed symbols signify overall cracking and open symbols dehydrogenation. Arrows indicate impact of AHFS treatment on catalytic performance. Lines are added as guide for the eye. (T = 763 K). Right side: Corresponding cracking pathway selectivities plotted as function of SBAS. Parent samples are generally symbolized by squares and AHFS modified samples by triangles.

Having shown that the concentration of the highly active sites can be reduced by eliminating extra-framework aluminum, the question arises whether the concentration of these sites can be enhanced by mild steaming. Static calcination of the fresh sample MFI-15 in a muffle furnace (MFI-15-ST) decreased the concentration of strong Brønsted acid sites and increased the concentration of extra lattice alumina species (Figure 2.3.). The catalytic activity per SBAS in cracking as well as in dehydrogenation was more than doubled (Figure 2.6.) through mild steaming.

Having established that the extra-lattice alumina species characterized by the band at 3656 cm^{-1} is responsible for the rate enhancement and that the series of the zeolites MFI-15-ST, MFI-15 and MFI-15-AHFS showed remarkable differences in the turnover frequencies (Figure 2.6.), we explore in the next step the nature of the catalytically enhanced sites and their environment as well as the kinetic details of cracking and dehydrogenation on such sites.

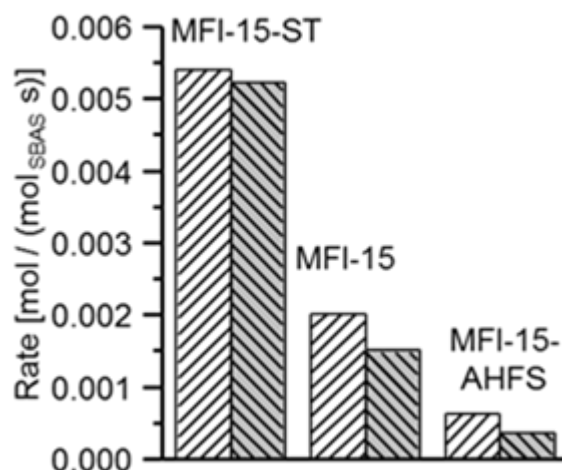


Figure 2.6: Rate of overall cracking (white) and dehydrogenation (grey) normalized to SBAS for the MFI-15 series.

2.3.2. Identification of the nature and location of the Al-OH sites

In exploring the nature of the extra-lattice alumina, let us focus now on the parent zeolite MFI-15 and modified variants generated by calcination (MFI-15-ST) and AHFS modification (MFI-15-AHFS). While for the former one only a relatively small concentration of aluminum was removed from the lattice (the Si/Al ratio increased slightly from 15 to 17 (Table S1), significantly more Al was removed by the AHFS treatment (Si/Al = 27). It is important to note that for the latter sample the SBAS concentration decreased only by about 5%, whereas almost 80% of all SLAS were removed. In the case of the static calcination (MFI-15-ST), the concentration of SBAS was reduced approximately by 50%, while the concentration of SLAS remained almost unchanged (Table S1). We conclude that dealumination of the framework took place during the thermal treatment as a result of mild steaming, caused by the humidity present in the zeolite. Figure 2.3. shows the correlation of the

decrease of the bridging OH group at 3610 cm^{-1} and the absorbance of the Al-OH vibration at 3656 cm^{-1} . This correlation suggests that a fraction of sites are converted from tetrahedrally coordinated lattice Al^{3+} to extra-framework $\text{Al}(\text{OH})_x$ species.

IR spectra recorded after adsorption of pyridine showed that not only the OH group of SBAS disappeared, but also the band at 3656 cm^{-1} (negative peak in difference spectrum, Figure 2.7A). Pyridine interacting with this OH group remained stable even after heating to 723 K in vacuum and it was, therefore, classified as a strong interaction. This is surprising, as the OH groups with bands in this region (almost 50 cm^{-1} higher wavenumber than SBAS) are usually associated to very weak Brønsted acid sites. The strength of this interaction is, therefore, tentatively attributed to a lateral interaction of pyridine adsorbed on a strong Brønsted acid with the OH groups on the extra-lattice alumina. In turn, this suggests that these sites are in close proximity to a strong Brønsted acid site and interact with the aromatic ring of pyridine. In order to test this hypothesis, it must be probed if the OH groups themselves are able to interact with a basic molecule.

The comparison between the adsorption of pyridine ($\text{pK}_B \sim 9$)³⁰ and the adsorption of the more basic, but smaller NH_3 ($\text{pK}_B \sim 5$)³⁰ should help to characterize the nature of the interaction between pyridine and the extra-lattice alumina OH groups (3656 cm^{-1}). Figure 2.7B shows these difference spectra after adsorption at 423 K, equilibration and subsequent outgassing for 30 minutes. Compared to pyridine, only a small fraction of the extra-lattice Al-OH groups interacted with ammonia (Figure 2.7B). This lack of interaction points to the fact that the OH group indeed does not possess high acid strength and confirms the assignment to a lateral interaction between pyridinium ions and the Al-OH group causing the shift of the O-H vibration at 3656 cm^{-1} to lower wavenumbers (Figure 2.7A).

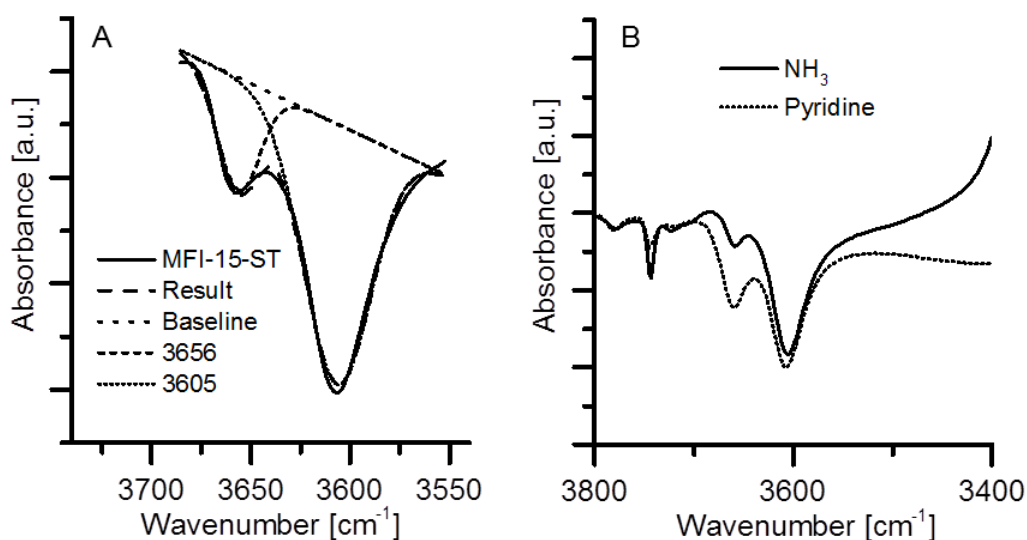


Figure 2.7: Difference spectrum of OH stretching vibration region for sample MFI-15-ST measured at 423 K with (A) pyridine being adsorbed and after having heated to 723 K including the result of the deconvolution and (B) after adsorbing and outgassing of pyridine and ammonia at 423 K. Note the difference in scale for the y-axis.

Considering the fact that the sample has been outgassed at 723 K, only lateral interaction of pyridinium ions are expected to contribute to the negative band at 3656 cm⁻¹ in Figure 2.7A. This allows one to determine the concentrations of SBAS being in close proximity of extra lattice Al-OH. For this calculation, comparable molar extinction coefficients for the two OH stretching vibrations (bands at 3656 and 3606 cm⁻¹) have been assumed, as well as a stoichiometric ratio of 1:1 for the SBAS-Al-OH site interaction. The results are presented in Table 2.1. SBAS-AIOH denotes those acid sites which have an Al-OH site in close proximity, whereas the term bare SBAS reflects isolated Brønsted acid sites (without Al-OH in close proximity).

Figure S.2 shows the normalized 1D ²⁷Al MAS NMR spectrum for the MFI-15 series. At -0.55 ppm octahedral Al ²¹ is observed for all samples. A broad shoulder with a maximum at 30 ppm was observed for MFI-15-ST, which is tentatively assigned to penta-coordinated Al. ³¹ The integral intensity of the signal at -0.5 ppm, characteristic for octahedral aluminum was the highest for

MFI-15-ST, followed by MFI-15 and MFI-15-AHFS. However, while we were able to remove most of these species in MFI-15-AHFS the increase in concentration for MFI-15-ST compared to MFI-15 was too modest to explain the marked increase in activity. It is speculated that the alumina clusters causing the signal at -0.5 ppm are located at the outer surface of the zeolite crystals.

For all samples the signal at 55 ppm indicates the presence of tetrahedral coordinated framework Al.²⁷ The peak shape is narrow and symmetric for MFI-15-AHFS, whereas a significant broadening is observed for MFI-15-ST and MFI-15. The intensities for MFI-15 and MFI-15-AHFS are comparable, whereas for MFI-15-ST the intensity is significantly lower. This is as well in good agreement with the significantly lower concentration of SBAS sites determined by pyridine IR spectroscopy for this sample.

Table 2.1. Results of deconvolution of difference spectra (adsorbed pyridine, heated to 723 K).

Sample	Area G1 (3656 cm⁻¹) [a.u.]	Area G2 (3606 cm⁻¹) [a.u.]	Bare SBAS [μmol/g]	SBAS-AIOH [μmol/g]
MFI-15-ST	1.41	6.09	289	87
MFI-15	0.43	8.90	671	34
MFI-15-AHFS	not visible	n.d	669	0

The NMR signal in the region 40-70 ppm can be deconvoluted by using two Gaussian functions (Figure 2.8). One broad function at 55.1 ± 0.5 ppm (Gaussian 1) and one narrow function at 54.6 ± 0.3 ppm (Gaussian 2) are obtained. The latter one corresponds to the tetrahedral framework Al.²⁷ The Al species connected with Gaussian 1 must also be of tetrahedral nature, given the peak position, but in view of the large broadening of the signal, this species is concluded to be slightly distorted.²¹

Further information can be derived from 2D ^{27}Al MQMAS spectra. Two types of line broadening can be generally differentiated by MQMAS experiments: a) horizontal broadening due to quadrupolar coupling because of local electric field gradients around the Al atoms, caused by nearby cationic species or coordination-symmetry distortions, and b) broadening along the diagonal of the MQMAS spectrum because of chemical heterogeneity.^{20,21}

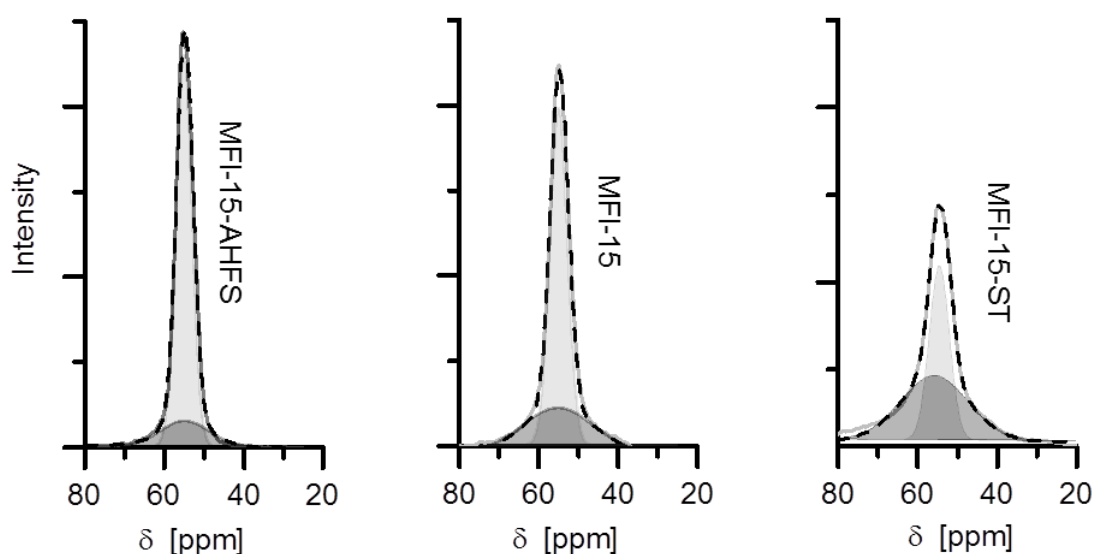


Figure 2.8: 1D ^{27}Al MAS NMR spectra for the MFI-15 series. -- experimental spectrum, - - fitting result; dark grey area, Gaussian 1; light grey area, Gaussian 2.

The isotropic F1 projection (Figure 2.9) provides high resolution Al NMR spectra without quadrupolar second order broadening. Results indicated that for the MFI-15 series there are at least two different framework Al species (P-IV1 = 56.3 ± 0.5 ppm and P-IV2 = 53.1 ± 0.5 ppm) in different T-positions with differing T-O-T angles. In the 1D spectrum these two signals are convoluted and give rise to the peak Gaussian 2.

Figure 2.9 shows that the horizontal broadening in the F2 projection is comparable for the MFI-15 series (F2 projection). However, a closer look at the 2D spectra shows clearly an increased broadening orthogonal to the

diagonal for the sample MFI-15-ST. This type of broadening of the 2D spectra is attributed to the existence of a third type of tetrahedral Al, which corresponds to the growth of Gaussian 1 contribution in 1D for this sample. This Al species, denoted as P-IV3, would have a distorted environment, as can be derived from the extensive broadening of the contour lines for lower intensities. Species P-IV3 shows a larger quadrupolar broadening in the 1D spectra due to the interaction of the distorted local environment with the external magnetic field.²⁷ The peak position as determined from the 1D spectra lies between P-IV1 and P-IV2, and therefore P-IV3 might not be easily discernible from the F1 projection. Given the relatively strong decrease in Brønsted acidity caused by ST treatment of MFI-15 and the small changes observed in LAS concentration and in octahedral and penta-coordinated EFAI signals in NMR, we attribute this Al species (P-IV3, Gaussian 1) to extra-framework tetrahedral Al species generated by dealumination during static calcination (although naturally existing at lower concentration in MFI-15).

For the sample MFI-15-AHFS the broad peak at 55.1 ppm in ²⁷Al MAS NMR spectra is almost invisible and there is no band at 3656 cm⁻¹ in the IR spectra. For samples MFI-15 and MFI-15-ST, these features gradually increase in the NMR spectra and IR spectra respectively, while other EFAI signals as octahedral Al at -0.5 ppm undergo only slight changes. Consequently, we identify the Al species associated with the Al-OH vibration at 3656 cm⁻¹ as distorted tetrahedral Al, which is speculated to be in the form of (quite symmetric) Al(OH)_x clusters in the zeolite pore. However, from our ²⁷Al MAS NMR it cannot be ruled out that the coexistence of other Al(OH)_x species with different coordination, partially or totally extracted from the framework, would contribute to narrowing the accessible space for reaction and, thus, to the rate enhancement.

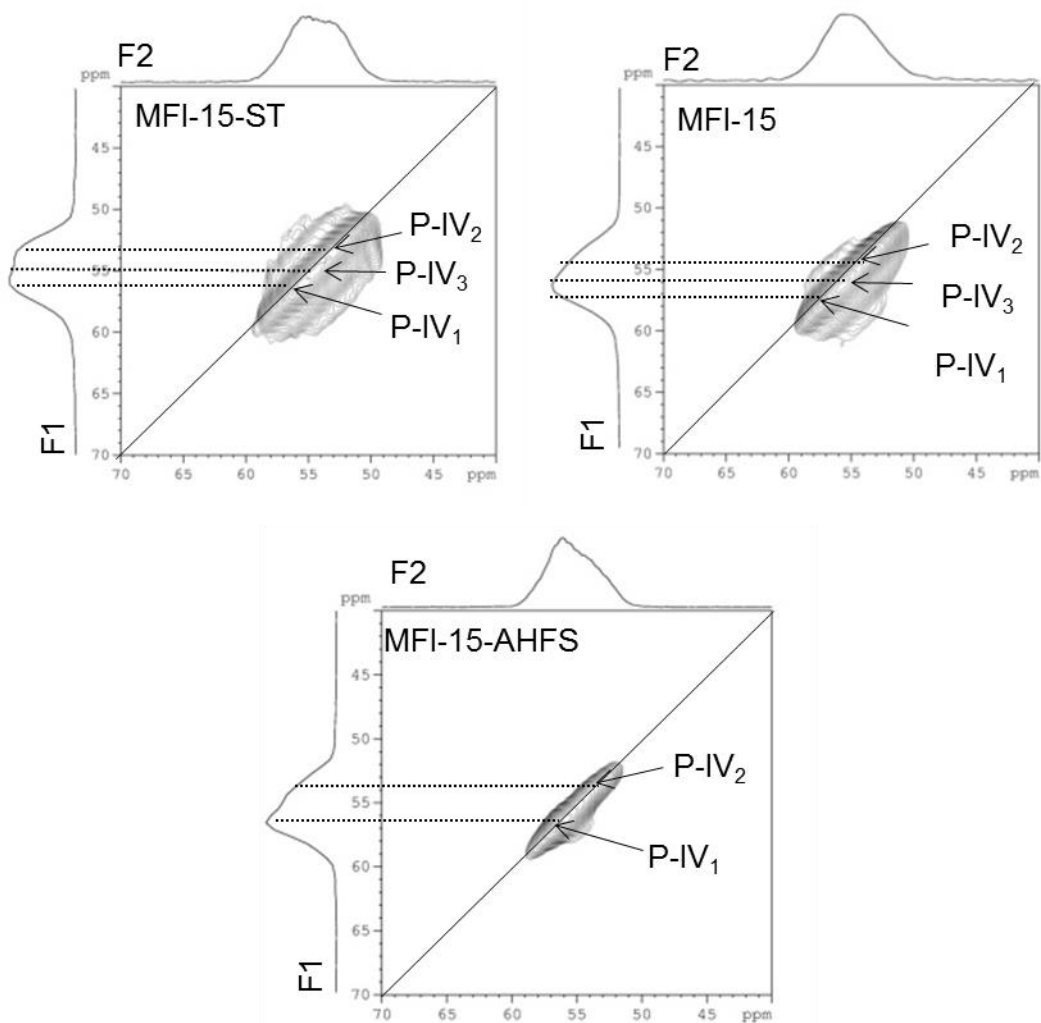


Figure 2.9: ^{27}Al 2D MQMAS for samples MFI-15-ST, MFI-15 and MFI-15-AHFS. Arrows indicated presence of different Al species.

2.3.3. Impact of SBAS-AIOH sites on the transition state in n-pentane cracking

2.4. Deconvolution of rates

So far we have shown that MFI-15-ST and MFI-15 contain SBAS, which are in close proximity of EFAl. These sites are been associated with high cracking activity. Thus, for these samples one has to discriminate between two active sites, the isolated SBAS, and the SBAS in proximity of EFAl (SBAS-AIOH). It can be then assumed that the overall measured rate (r_{overall}) normalized to the weight of catalyst results from a linear combination of the rate stemming from

isolated SBAS ($r_{\text{SBAS(iso)}}$) and the rate on SBAS-AIOH ($r_{\text{SBAS-AIOH}}$) as shown in equation 2.2.

$$r_{\text{overall}} = r_{\text{SBAS(iso)}} + r_{\text{SBAS-AIOH}} \quad (\text{Equ. 2.2})$$

$r_{\text{SBAS(iso)}}$ can be deduced from the sample MFI-15-AHFS and the zeolite samples with low concentration of aluminum in the lattice. The rate per isolated SBAS has been determined for overall cracking (dehydrogenation) as $6.1 \cdot 10^{-4} \text{ mol} \cdot \text{mol}_{\text{SBAS}}^{-1} \cdot \text{s}^{-1}$ ($3.7 \cdot 10^{-4} \text{ mol} \cdot \text{mol}_{\text{SBAS}}^{-1} \cdot \text{s}^{-1}$) and these values can be now used to calculate the rate originating from isolated sites on a weight basis for MFI-15 and MFI-15-ST. The difference between the rate of isolated SBAS and the actual measured weight normalized rate must, hence, be caused by SBAS-AIOH sites.

Table 2.2 summarizes the results of this estimate for the cracking and dehydrogenation pathways for the two samples containing SBAS-AIOH. Both samples gave comparable values for $r_{\text{SBAS-AIOH}}$ (normalized to SBAS-AIOH). Therefore, it can be concluded that these sites are approximately 40 (60) times more active in n-pentane cracking (and n-pentane dehydrogenation) than the isolated SBAS.

2.5. Adsorption of n-pentane

In order to understand whether or not the high activity is related to a higher concentration of the alkane the adsorption of n-pentane was studied at 343 K for the MFI-15 series (Figure 2.8). The adsorption isotherm (Figure 2.10A) showed an increasing slope with increasing SBAS concentration in the Henry regime. The adsorption enthalpy was identical for all three samples (Figure 2.10B). It should be noted that the cooperative sites SBAS-AIOH are present only in a small number (e.g. $87 \mu\text{mol/g}$ for MFI-15-ST). However, if there were SBAS with a different heat of adsorption, a deviation should be visible in the differential heats of adsorption when $n_{\text{ads}} < 0.1 \text{ mmol/g}$ (Figure 2.10B).

A dual Langmuir approach was used to fit the experimentally obtained isotherms (Equation 1). For $n_{\text{max},1}$ the concentration of SBAS in the zeolite was used, whereas $n_{\text{max},2}$ was calculated by the difference between the

maximum coverage of n-pentane for MFI (1.28 mmol/g)⁷ and $n_{\max,1}$. The results are summarized in (Table 2.3.). Determination of the adsorption constants enables calculation of the adsorption entropy (ΔS_{ads}) using Equation 2.3.³²

$$\Delta S_{\text{ads}} = \frac{\Delta H_{\text{ads}}}{T} + R \cdot \ln(K_1) \quad (\text{Equ. 2.3})$$

Table 2.2. Cracking and dehydrogenation activity per SBAS-AIOH calculated according to Eq. (2) (T = 763 K).

Sample	$r_{\text{crack_SBAS-AIOH}}$ [mol mol _{SBAS} ⁻¹ s ⁻¹]	$r_{\text{dehydro_SBAS-AIOH}}$ [mol mol _{SBAS} ⁻¹ s ⁻¹]
MFI-15	0.030	0.023
MFI-15-ST	0.021	0.021

For the MFI-15 series, the calculated K values as well as adsorption entropies and enthalpies were comparable for the three samples (Table 2.3.). The obtained values for ΔH_{ads} (-62 to -63 kJ/mol) agree well with the values reported earlier for ZSM-5, whereas the values for ΔS_{ads} were about 7 J/mol K more positive.

It is therefore concluded that extra-lattice Al in close proximity to SBAS have little impact on the adsorption of n-pentane. This suggests that the ground state for pentane cracking (adsorbed n-pentane) is energetically identical for all catalysts tested in the MFI-15 series. Consequently, any change in enthalpic and entropic barriers are concluded to reflect a change in the transition state.

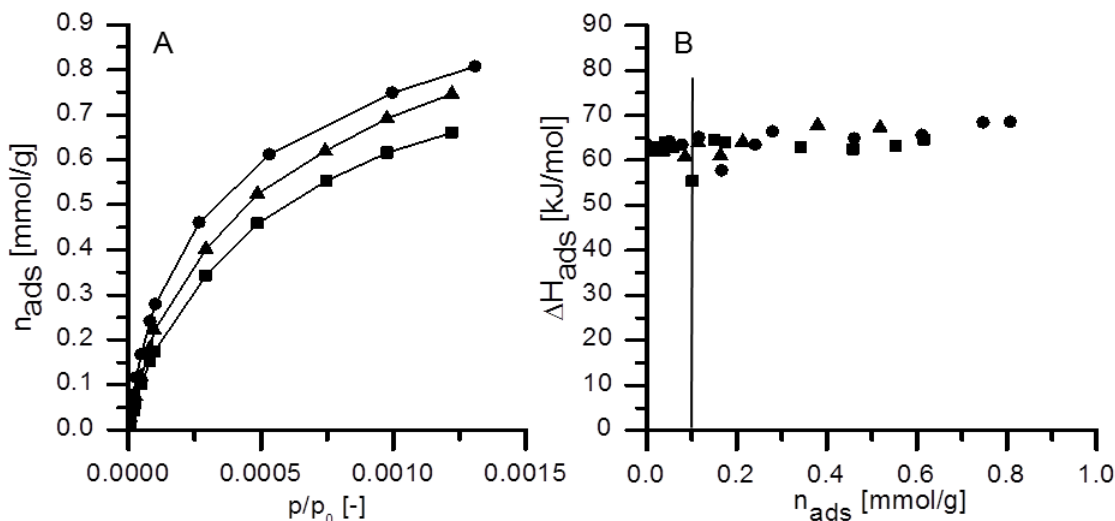


Figure 2.10: (A) Adsorption isotherm of n-pentane and (B) heat of adsorption as function of number of adsorbed n-pentane molecules for samples (■) MFI-15-ST, (●) MFI-15 and (▲) MFI-15-AHFS measured at 343 K.

2.6. Analysis of the transition state in n-pentane cracking

As shown above, the adsorbed ground state is identical for all three samples. Therefore, intrinsic barriers (enthalpy and entropy) allow one to deduce differences in the transition state for the MFI-15 series. Table 2.4 summarizes the intrinsic activation energy and entropy for the overall cracking as well as for the dehydrogenation pathway. The values were obtained by analysis of experimentally determined rates using transition state theory in analogy to a recent contribution.⁸ For both MFI-15 and MFI-15-ST, comparable values for the activation energy and activation entropy were obtained.

The values obtained for sample MFI-15-AHFS clearly deviate by about 14 kJ/mol (E_a) and 27 J/mol K (ΔS) for cracking and 13 kJ/mol (E_a) and 32 J/mol K (ΔS) for dehydrogenation. The intrinsic activation energy of the overall cracking pathway calculated for MFI-15-AHFS is in good agreement with the experimentally observed $E_{a,\text{int}}$ values (195 – 200 kJ/mol) reported for HZSM-5^{8,33}, which is a value independent of the size of the alkane. The situation is less clear for the intrinsic dehydrogenation barrier of alkanes. Reported values scatter widely.⁹ The experimentally determined barrier for

dehydrogenation here was about 15- 20 kJ/mol higher than the barrier for cracking, in good agreement with the values reported by Gounder et al.⁸

In order to understand the enthalpic and entropic differences between the samples as shown in Table 2.4, we use the approach of a thermochemical cycle, which expresses the measured activation barriers in terms of elementary steps, i.e., adsorption, deprotonation of the SBAS, protonation of n-pentane and stabilization of the transition state.⁹ We have seen before that the adsorption enthalpy (ΔH_{ads}) is identical for all three samples. The deprotonation energy of SBAS is also expected to be identical for all samples in the MFI-15 series, as indication for differences in the polarizability or polar dissociation, such as a difference in the wavenumber or in the shift after adsorption of pentane (not reported here) have not been detected in the IR spectra. With regard to the proton affinity of the n-pentane molecule, it is referenced to the gas phase and is therefore independent of the zeolite.

This leads to the conclusion that enthalpic destabilization of the transition state causes the about 10 kJ/mol higher intrinsic barriers at the SBAS-AIOH sites compared to a Brønsted acid site without the presence of extra lattice alumina. The rate enhancement despite the increase in the true energy of activation points, therefore, to a marked overcompensation by a significantly increased transition entropy. Two models can be invoked to rationalize this. The first option is that the presence of AIOH in close proximity to SBAS stabilizes a later and hence looser transition state in comparison to the case of bare SBAS (Figure 2.11). This means that the C-C bond to be cleaved (C-H in the case of dehydrogenation) is more elongated in the looser transition state, which explains the higher enthalpic barrier.

Concomitantly, this configuration increases the degrees of freedom (vibrational and rotational) of the transition state complex, which resemble more the products. In some contrast to the interpretation in the recent paper of Janda and Bell¹¹ the current results demonstrate that the higher activity is

a result of a higher constraint around the Brønsted acid site and not related to a larger volume available to the transition state. This higher constraint appears to better stabilize the transition state entropically.

Table 2.3. Adsorption parameters as determined from fitting a dual Langmuir model to experimentally obtained isotherm at 343 K.

Sample	K_1	$n_{\max,1}$ [mmol/g]	K_2	$n_{\max,2}$ [mmol/g]	ΔH_{ads} [kJ/mol]	ΔS_{ads} [J/mol K]
MFI-15-ST	5365	0.376	505	0.904	- 62	-110
MFI-15	5558	0.705	334	0.575	- 63	-110
MFI-15-AHFS	4131	0.669	344	0.611	- 62	-111

In good agreement with the observations in ref ¹¹, we find a comparable shift of cracking selectivity towards terminal cracking, which seems to be not correlated with the presence of SBAS-AIOH sites. On the basis of our analysis of this new site, SBAS-AIOH, that has enhanced activity that is intrinsic, location of the site at intersections cannot be ruled out, but this is not a fundamental property. Our analysis does not provide at present information about which T site it occupies. However, wherever it is sited, our analysis reveals that the activity is directly correlated with the site structure of SBAS-AIOH, as described herein, not necessarily with its location in the framework.

The increased (more positive) transition state entropy becomes even more evident if transition state theory is applied to the rate constants derived from Equation 2.2. Normalization to SBAS-AIOH sites, which are present in lower number compared to bare SBAS, does not change the enthalpic barrier which is obtained by an Arrhenius type plot. But, by taking into account only the very active SBAS-AIOH sites, the value of the preexponential factor increases drastically for overall cracking and dehydrogenation. Actual intrinsic entropic barriers for the reaction proceeding via SBAS-AIOH sites are found to lie between 52 – 58 J/(mol K) for cracking (62 - 64 J/ (mol K) for dehydrogenation) for the sample MFI-15 and MFI-15-ST.

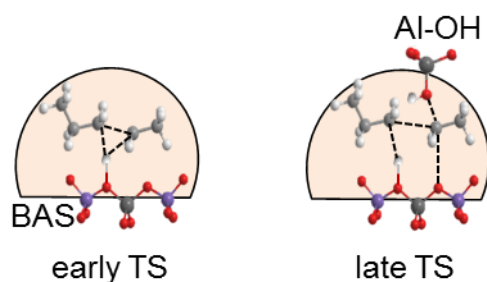


Figure 2.11: Schematic illustration of effect of presence of tetrahedral Al-OH in proximity of SBAS on transition state (TS) in cracking of n-pentane.

In the light of this remarkable increase of the preexponential factor, we would like also to put forward an alternative to the model that proposes that high activity is related to a late transition state. The model assumes that not the nature of the transition state is changed, but rather that the synergistic action of Brønsted and Lewis acid site (SBAS-ALOH sites) allows a better charge delocalization in the zeolite lattice resulting in a more delocalized proton which together with a pre-orientation of the reacting n-pentane increases the probability for a successful protonation of the molecule. This would also better explain why the observed pathway selectivity was independent of the presence of SBAS-AIOH sites.

Table 2.4. Intrinsic enthalpic and entropic barriers for overall cracking and dehydrogenation for MFI-15 series (based on normalization to all SBAS).

Name	Overall cracking		Dehydrogenation	
	$E_{a,int}^a$	$\Delta S_{,int}^b$	$E_{a,int}^a$	$\Delta S_{,int}^c$
	[kJ/mol]	[J/(mol K)]	[kJ/mol]	[J/(mol K)]
MFI-15	214	28	229	40
MFI-15-ST	216	37	234	49
MFI-15-AHFS	202	10	221	17

The increased (more positive) transition state entropy becomes even more evident if transition state theory is applied to the rate constants derived from Equation 2. Normalization to SBAS-AIOH sites, which are present in lower number compared to bare SBAS, does not change the enthalpic barrier which is obtained by an Arrhenius type plot. But, by taking into account only the very

active SBAS-AIOH sites, the value of the preexponential factor increases drastically for overall cracking and dehydrogenation. Actual intrinsic entropic barriers for the reaction proceeding via SBAS-AIOH sites are found to lie between 52 – 58 J/(mol K) for cracking (62 - 64 J/ (mol K) for dehydrogenation) for the sample MFI-15 and MFI-15-ST.

2.7. Conclusion

While HZSM-5 samples with low concentrations of aluminum in the lattice showed - as expected - identical turnover frequencies for protolytic cracking and dehydrogenation of n-pentane independently of the chemical composition of the samples, HZSM-5 samples with high concentrations of aluminum in the lattice ($\text{Si/Al} < 25$) were significantly more active. Their unusually high TOF has been systematically explored combining detailed kinetic measurements and the quantitative characterization of the Brønsted and Lewis acid sites. The high specific activity has been related to an active site consisting of a Brønsted acidic bridging hydroxyl group (SBAS) and an extra-lattice Al site in close proximity.

This extra-lattice Al is postulated to be tetrahedrally coordinated and to have at least one -OH group with an IR vibration at 3656 cm^{-1} . Selective removal of the extra-lattice alumina by treatment with AHFS reduced the TOF to the level of zeolites with low acid site concentrations for which all sites contribute equally to the catalytic activity. The concentration of these highly active sites, which always appear in parallel to the Brønsted acid sites generated by bridging OH groups without extra-lattice alumina, was increased via static calcination, producing a material with enhanced catalytic activity. An increase in acid strength of the SBAS was not observed for these highly active samples. Separating the contributions of the two sites, i.e., isolated SBAS and SBAS-AIOH showed, that the SBAS-AIOH sites are about 40 (60) times more active in catalytic cracking (dehydrogenation) of n-pentane compared to isolated SBAS.

Adsorption of n-pentane varied only subtly with the concentration of Brønsted acid sites, but did not show significant differences in terms of adsorption enthalpy and entropy on samples containing such highly active sites, which allows us to conclude that the high specific activity is not related to a higher coverage of reactants. Note in passing that the concentration of the sites would be by far above the threshold of changes to be quantitatively analyzed by the gravimetry and calorimetry used. Analysis of intrinsic activation energies and entropies suggest, that protolytic cracking has a higher energy of activation, which is, however, overcompensated by a significantly higher transition entropy. This higher transition entropy is speculated to be associated either with a later (and looser) transition state or with a higher mobility of the proton of the acid sites (without changing its intrinsic strength though), which would entropically facilitate protonation. While further investigations are under way, we currently favor the latter hypothesis, because cracking and dehydrogenation possessing different transition states are equally drastically enhanced.

The new site proposed here and its genesis allows not only a quantitative explanation of the frequent drastic variations in activities of zeolites in dependence of the activation and pretreatment procedures, it also opens new pathways to generate highly active zeolite catalysts. Current investigations explore the thermal and hydrothermal stability of these sites and options to maximize their generation in catalytic practice.

ACKNOWLEDGMENTS

The authors thank Franz X. Hecht for N₂ physisorption measurements, Martin Neukamm for conducting elemental analysis, Dr. MuthusamyVishnuvarthan for help with measuring 2D 3Q MAS NMR spectra and Prof. Andreas Jentys for helpful discussions concerning the IR spectra. We also thank BU Catalysts, Clariant Produkte (Deutschland) GmbH (former Sued-Chemie AG) for the financial support and fruitful discussions in the framework of MuniCat.

2.8. References

- (1) Kissin, Y. V. *Catalysis Reviews* **2001**, *43*, 85.
- (2) Xu, B.; Sievers, C.; Hong, S. B.; Prins, R.; van Bokhoven, J. A. *Journal of Catalysis* **2006**, *244*, 163.
- (3) Bhan, A.; Gounder, R.; Macht, J.; Iglesia, E. *Journal of Catalysis* **2008**, *253*, 221.
- (4) Kotrel, S.; Knözinger, H.; Gates, B. C. *Microporous and Mesoporous Materials* **2000**, *35–36*, 11.
- (5) van Bokhoven, J. A.; Tromp, M.; Koningsberger, D. C.; Miller, J. T.; Pieterse, J. A. Z.; Lercher, J. A.; Williams, B. A.; Kung, H. H. *Journal of Catalysis* **2001**, *202*, 129.
- (6) Datka, J.; Marschmeyer, S.; Neubauer, T.; Meusinger, J.; Papp, H.; Schütze, F. W.; Szpyt, I. *The Journal of Physical Chemistry* **1996**, *100*, 14451.
- (7) Eder, F.; Stockenhuber, M.; Lercher, J. A. *The Journal of Physical Chemistry B* **1997**, *101*, 5414.
- (8) Gounder, R.; Iglesia, E. *J. Am. Chem. Soc.* **2009**, *131*, 1958.
- (9) Gounder, R.; Iglesia, E. *Chemical Communications* **2013**, *49*, 3491.
- (10) Gounder, R.; Jones, A. J.; Carr, R. T.; Iglesia, E. *Journal of Catalysis* **2012**, *286*, 214.
- (11) Janda, A.; Bell, A. T. *J. Am. Chem. Soc.* **2013**, *135*, 19193.
- (12) Miyaji, A.; Sakamoto, Y.; Iwase, Y.; Yashima, T.; Koide, R.; Motokura, K.; Baba, T. *Journal of Catalysis* **2013**, *302*, 101.
- (13) Lago, R. M.; Haag, W. O.; Mikovsky, R. J.; Olson, D. H.; Hellring, S. D.; Schmitt, K. D.; Kerr, G. T. In *Studies in Surface Science and Catalysis*; Y. Murakami, A. I., Ward, J. W., Eds.; Elsevier: 1986; Vol. Volume 28, p 677.
- (14) Yu, Z. W.; Li, S. H.; Wang, Q.; Zheng, A. M.; Jun, X.; Chen, L.; Deng, F. *J. Phys. Chem. C* **2011**, *115*, 22320.
- (15) DeCanio, S. J.; Sohn, J. R.; Fritz, P. O.; Lunsford, J. H. *Journal of Catalysis* **1986**, *101*, 132.
- (16) Li, S. H.; Zheng, A. M.; Su, Y. C.; Zhang, H. L.; Chen, L.; Yang, J.; Ye, C. H.; Deng, F. *Journal of the American Chemical Society* **2007**, *129*, 11161.
- (17) Niwa, M.; Sota, S.; Katada, N. *Catalysis Today* **2012**, *185*, 17.
- (18) Mirodatos, C.; Barthomeuf, D. *Journal of the Chemical Society, Chemical Communications* **1981**, *0*, 39.
- (19) Jones, A. J.; Carr, R. T.; Zones, S. I.; Iglesia, E. *Journal of Catalysis* **2014**, *312*, 58.
- (20) Pidko, E. A.; Almutairi, S. M. T.; Mezari, B.; Magusin, P. C. M. M.; Hensen, E. J. M. *ACS Catalysis* **2013**, *3*, 1504.
- (21) Almutairi, S. M. T.; Mezari, B.; Filonenko, G. A.; Magusin, P. C. M. M.; Rigutto, M. S.; Pidko, E. A.; Hensen, E. J. M. *ChemCatChem* **2013**, *5*, 452.
- (22) Kanellopoulos, J.; Unger, A.; Schwieger, W.; Freude, D. *Journal of Catalysis* **2006**, *237*, 416.
- (23) Sazama, P.; Wichterlova, B.; Dedeczek, J.; Tvaruzkova, Z.; Musilova, Z.; Palumbo, L.; Sklenak, S.; Gonsiorova, O. *Microporous and Mesoporous Materials* **2011**, *143*, 87.
- (24) Holm, M. S.; Svelle, S.; Joensen, F.; Beato, P.; Christensen, C. H.; Bordiga, S.; Bjorgen, M. *Appl. Catal. A-Gen.* **2009**, *356*, 23.

- (25) Sommer, L.; Krivokapić, A.; Svelle, S.; Lillerud, K. P.; Stöcker, M.; Olsbye, U. *The Journal of Physical Chemistry C* **2011**, *115*, 6521.
- (26) Maier, S. M.; Jentys, A.; Lercher, J. A. *The Journal of Physical Chemistry C* **2011**, *115*, 8005.
- (27) Ong, L. H.; Dömök, M.; Olindo, R.; van Veen, A. C.; Lercher, J. A. *Microporous and Mesoporous Materials* **2012**, *164*, 9.
- (28) Corma, A. *Chemical Reviews* **1995**, *95*, 559.
- (29) Triantafillidis, C. S.; Vlessidis, A. G.; Nalbandian, L.; Evmiridis, N. P. *Microporous and Mesoporous Materials* **2001**, *47*, 369.
- (30) Parry, E. P. *Journal of Catalysis* **1963**, *2*, 371.
- (31) Gilson, J.-P.; Edwards, G. C.; Peters, A. W.; Rajagopalan, K.; Wormsbecher, R. F.; Roberie, T. G.; Shatlock, M. P. *Journal of the Chemical Society, Chemical Communications* **1987**, 91.
- (32) De Moor, B. A.; Reyniers, M.-F. o.; Gobin, O. C.; Lercher, J. A.; Marin, G. B. *The Journal of Physical Chemistry C* **2010**, *115*, 1204.
- (33) Narbeshuber, T. F.; Vinek, H.; Lercher, J. A. *Journal of Catalysis* **1995**, *157*, 388.

2.9. Supporting Information

S1. Physicochemical characterization of the zeolite samples

N₂ physisorption results confirm the microporous character of all samples. SEM micrographs of the unmodified samples demonstrates that the diameter of primary crystallites is smaller than 1 μm in all cases (not shown). This allows meaningful comparison of all samples in catalytic cracking of alkanes and all criteria used points to the absence of diffusion limitations.

Table S1: Physiochemical properties of investigated catalysts.

Name ^a	S _{BET} [m ² /g]	Si:Al ^a [-]	BAS ^b	SBAS ^b	LAS ^b [μmol/g]	SLAS ^b	BAS ^c
MFI-15	405	15	843	705	213	168	820
MFI-15-AHFS	409	27	717	669	51	36	691
MFI-15-ST	415	17	444	376	234	167	398
MFI-25	425	25	564	496	137	94	538
MFI-25-AHFS	446	26	425	396	31	21	449
MFI-40	425	39	374	324	78	66	353
MFI-60	512	58	286	257	59	39	238
MFI-90	454	88	141	135	33	29	158
MFI-240	431	240	62	57	11	10	68
MFI-470	400	470	30	29	7	3	36

^a Molar ratio of Si and Al determined with AAS.

^b Determined by IR spectroscopy of adsorbed pyridine.

^c Determined by NH₃ TPD.

Table S2: Intrinsic enthalpic and entropic barriers for overall cracking and dehydrogenation for MFI type zeolites (based on normalization to all SBAS).

Sample	Overall cracking		Dehydrogenation	
	$E_{a,int}^a$	$\Delta S_{,int}^b$	$E_{a,int}^c$	$\Delta S_{,int}^d$
	[kJ/mol]	[J/mol K]	[kJ/mol]	[kJ/mol]
MFI-25-AHFS	204	6	228	19
MFI-40	195	-9	215	0
MFI-60	189	-17	185	-39
MFI-90	191	-11	200	-21
MFI-240	189	-9	194	-22
MFI-470	190	-14	179	-49

^aErrors are ± 3 kJ/mol, ^b Errors are ± 4 J/molK, ^cErrors are ± 6 kJ/mol, Errors are ± 9 J/mol K.

S2. Analysis of catalytic rates according to transition state theory

We follow the analysis which was introduced earlier by *Gounder* and *Iglesia*.

Starting from an irreversible reaction $A+B \rightarrow P$, the rate of the reaction can be described as:

$$r = \vec{r} = \gamma C_z \quad (\text{S.1})$$

Assuming that the system is in equilibrium, the transition state Z with the concentration C_z is also in equilibrium with the reactants A and B:

$$K_c^\ddagger = \frac{C_z}{C_A C_B} \quad (\text{S.2})$$

With the thermodynamic correlation:

$$RT \ln K_c^\ddagger = -\Delta G^{0\ddagger} = -\Delta H^{0\ddagger} + T \Delta S^{0\ddagger} \quad (\text{S.3})$$

Where R is the gas constant, $\Delta G^{0\ddagger}$ is the change in standard Gibbs free energy for the reaction while $\Delta H^{0\ddagger}$ and $\Delta S^{0\ddagger}$ are the change in standard

enthalpy and entropy respectively. In the expression the superscript ‡ denotes the species formed at the transition state.

Combining (S.2) and (S.3), (S.1) is transformed into:

$$r = \gamma \exp\left(\frac{\Delta S^{\ddagger}}{R}\right) \exp\left(\frac{-\Delta H^{\ddagger}}{RT}\right) C_A C_B \quad (\text{S.4})$$

By making further assumptions and simplifications (see Ref ¹ for more details) we obtain:

$$r = k_{\text{int}} K_A P_A = \frac{kT}{h} \exp\left(\frac{\Delta S^{\ddagger}}{R}\right) \exp\left(\frac{-\Delta H^{\ddagger}}{RT}\right) \times K_A P_A \quad (\text{S.5})$$

h is Planck's constant, k is Boltzmann's constant, P_A denotes the partial pressure of alkanes in the gas phase and K_A the adsorption constant of the alkanes. Therefore, the corresponding activation energies and entropies determined experimentally can be directly related to intrinsic terms by using the adsorption parameters of alkane molecules on Brønsted acid sites:

$$E_{a_{\text{meas}}} = E_{a_{\text{int}}} + \Delta H_{\text{ads}} \quad (\text{S.6})$$

$$\Delta S_{\text{meas}} = \Delta S_{\text{int}} + \Delta S_{\text{ads}} \quad (\text{S.7})$$

$$\ln(A_{\text{meas}}) = \ln(A_{\text{int}}) + (\Delta S_{\text{ads}}/R) \quad (\text{S.8})$$

$E_{a_{\text{meas}}}$ and A_{meas} (ΔS_{meas}) refer to the measured activation barriers and pre-exponential factors, while E_{int} and A_{int} (ΔS_{int}) are their corresponding intrinsic terms. If these equations are combined (S.5) to (S.8) the measured entropy of activation can be defined as:

$$\Delta S_{\text{meas}} = R[\ln(A_{\text{meas}}) - \ln(k_B T/h)] \quad (\text{S.9})$$

Figures

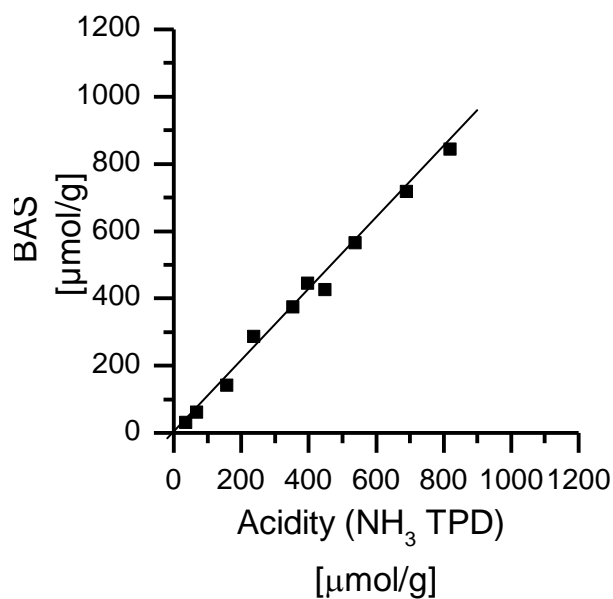


Figure S.1: Correlation of acidity determined by IR spectroscopy of adsorbed pyridine and TPD of NH₃.

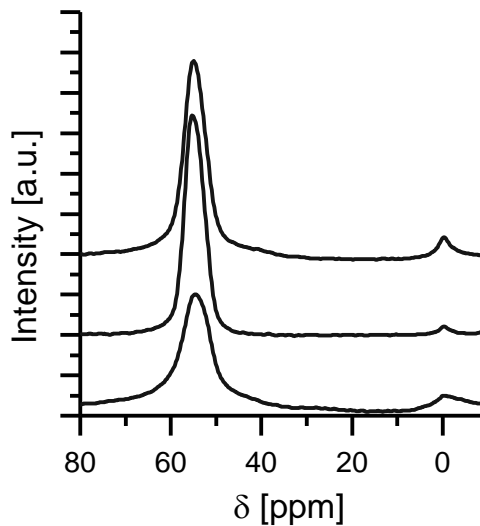


Figure S.2: 1D ²⁷Al MAS NMR spectra of MFI-15 (top), MFI-15-AHFS and MFI-15-ST (bottom).

References

- (1) Gounder, R.; Iglesia, E. *J. Am. Chem. Soc.* **2009**, *131*, 1958.

Chapter 3

3. Study of adsorption and reaction of 1-pentene over MFI and FER at intermediate temperatures

This chapter is based on:

S. Schallmoser, J. Van der Mynsbrugge, K. De Wispelaere, M. Sanchez-Sanchez, M. Waroquier, V. Van Speybroeck, J.A. Lercher, “*Study of adsorption and reaction of 1-pentene over MFI and FER at intermediate temperatures*”, paper in preparation.

Abstract: Adsorption of linear pentene molecules was studied on silicalite, MFI and FER by infrared spectroscopy and calorimetric measurements at 323 K. During adsorption of highly reactive 1-pentene and 2-pentene on silicalite, the absence of any reaction was confirmed. For the zeolite FER rapid double bond isomerization was observed. Pentene interacts with the Brønsted acid sites (BAS) via reversible formation of a π -complex which is evidenced in the IR spectra by a bathochromic shift of the OH group by about 500 cm^{-1} . The heat of adsorption in the easily accessible 10 and 8 membered pores was determined to be -92 kJ/mol which enables estimation of the enthalpic contribution from π -complex formation (-33 kJ/mol).

Adsorption of 1-pentene on a MFI type zeolite showed a completely different behavior. Dimerization is observed and the chemisorbed dimer is formed readily. By following the dimerization reaction at different temperatures it was possible to extract an activation energy (35 kJ/mol) which corresponds most likely to the carbenium ion formation in the transition state. Moreover, by a careful analysis of the individual reactions involved in dimerization an estimate for the enthalpic contribution from chemisorption to form an alkoxide (-44 kJ/mol in comparison to the π -bonded alkene) was obtained.

3.1. Introduction

Solid acids such as zeolites are routinely applied in chemical industry for conversion of hydrocarbons in reactions such as catalytic cracking, hydrocracking and alkylation of aromatics.¹⁻⁴ These reactions commonly involve alkanes and alkenes as reactants and products which interact with the zeolite and its Brønsted acid sites (BAS).¹ The understanding of adsorption of alkanes on various zeolites is today quite advanced whereas, in comparison, only little is known about adsorption of alkenes on zeolites.⁵⁻⁷ As alkenes undergo oligomerization and isomerization already at low temperatures, it is difficult to extract reliable data from adsorption-desorption experiments.^{1,8}

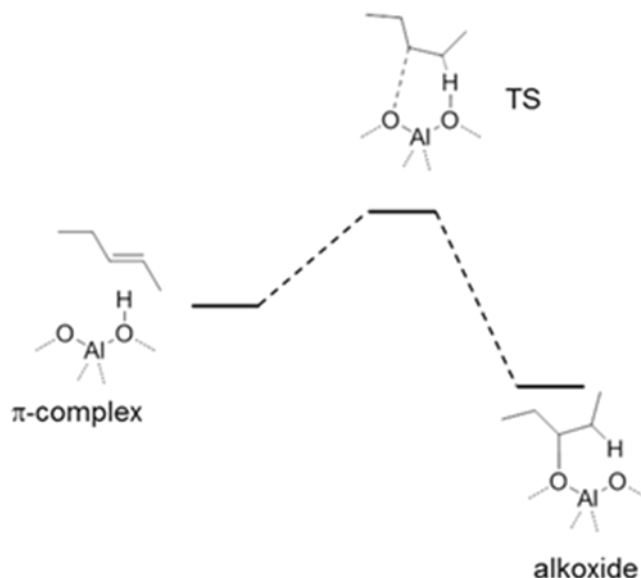


Figure 3.1: Illustration of activated transition from physisorbed π -BAS complex to chemisorbed alkene.

It is commonly agreed that the interaction of an alkene with the BAS of a zeolite proceeds via two different states (Figure 3.1).^{1,9-11} First a π -complex is formed, which can be considered as a physisorbed state, because despite the clearly localized interaction between the π -electrons of the double bond and the Brønsted acid site, bonds are neither formed nor broken in this interaction.^{1,8} π -Complex formation is followed by chemisorption via an activated transformation.^{1,11}

The nature of the resulting chemisorbed species is still under debate. It could exist as a covalently bound alkoxide or as an ion pair involving a free carbenium ion.^{8,9,11-13} To date the adsorption and especially the chemisorption of alkenes in zeolites has been mainly theoretically addressed, with the exception of a series of NMR studies.^{1,8,11,14,15}

In order to avoid confusion of the different possible adsorption states of an alkene in a zeolite we use strictly the following expressions: physisorbed signifies non-selective adsorption on the zeolite wall, π -complex represents a H-bonded (double bond and BAS) alkene and chemisorption describes the alkoxide.

Among the theoretical studies, calculated heats of adsorption (chemisorption and π -complex formation) depend largely on the selected zeolite cluster and the calculation methods applied. Nieminen et al. found that for H-FER the heat of π -complex formation of alkenes was comparable to that of alkanes. The specific interaction of the double bond with the acidic OH is compensated by the overall reduced non-specific interaction ($\text{RCH}_2\text{-CH}_2\text{R}'$ has two more C-H fragments than $\text{RHC=CHR}'$).⁸ Nguyen *et al.* presented a detailed study of the physisorption and chemisorption of linear alkenes in zeolites.¹ They obtained for physisorption of e.g. 1-pentene in H-ZSM-5 a value of -84 kJ/mol and for chemisorption -168 kJ/mol.¹

Domen et al. studied the adsorption and reaction of butenes on H-ZSM-5 and mordenite in great detail.^{9,10,13,16,17} They observed that at sub-ambient temperatures a stable π -complex of butene is formed on H-ZSM-5 and that double bond isomerization occurs already at temperatures of 230 K.^{10,16,18} A concerted mechanism was suggested in order to explain the rapid double bond isomerization despite the absence of a classical carbenium ion, as evidenced from isotope experiments, at these temperatures.¹⁸⁻²⁰

Stepanov et al. studied the kinetics of the double-bond shift reaction, H/D exchange and ¹³C scrambling for linear butenes on FER by means of ¹H, ²H

and ^{13}C MAS NMR.^{19,21} They determined the activation energy for the double bond shift reaction (41 kJ/mol) and showed convincingly that carbenium ions are formed but no alkoxide species were observed within the temperature range studied.^{19,21} Isotope experiments evidenced in addition the high mobility of alkenes at these low temperatures.^{16,18,19} Hence, the π -bonded alkenes cannot be considered static. Alkenes are moving with a low barrier, mediated by the zeolite wall, from BAS to BAS.¹⁰

At room temperature the π -complex is no longer stable and linear butenes are gradually transformed to a dimer, which in the opinion of Domen et al. is for steric reasons mainly physisorbed via its aliphatic backbone.¹⁰ Interestingly, they observed for the analogous reaction of 2-methyl-propene on mordenite formation of a dimerized alkoxy species.⁹

This contribution examines the adsorption and reaction of 1-pentene at intermediate temperatures (323 – 423 K) on two zeolites with differing pore structures, namely FER and MFI. It is attempted to derive, based on experimentally determined values, estimates for the enthalpy of the π -interaction and chemisorption of alkenes.

3.2. Experimental

Zeolites

The samples MFI-90 and silicalite were provided by Clariant Produkte (Deutschland) GmbH in the H-form, NH_4 -FER was obtained from Zeolyst (CP 914C). The sample was calcined for 5 h in a stream of synthetic air (100 ml min^{-1} , heating rate 10 K min^{-1} , 823 K) to yield the H-form.

Zeolite characterization

In order to determine the acid site concentration, temperature programmed desorption experiments (TPD) of adsorbed NH_3 were used. The samples were pelletized (0.5 – 0.71 mm) and activated at 723 K for 1 h prior to equilibration with 1 mbar of NH_3 at 423 K for 1 h. After subsequent outgassing

for 2 h, the temperature was increased to 1043 K at 0.17 K s^{-1} . Desorption of NH_3 was monitored by mass spectrometry following the fragment $m/z = 16$. An MFI-45 of known acid site concentration was used as internal standard in order to quantify the acid sites.

The elemental composition of the samples was determined by atomic absorption spectroscopy in a Unicam M Series Flame-AAS equipped with an FS 95 autosampler and a GF 95 graphite furnace.

Specific surface area and porosity were determined from N_2 adsorption/desorption isotherms recorded on an automated *PMI Sorptomatic 1990* instrument at liquid N_2 temperature (77 K). The samples were outgassed in vacuum ($p = 1 \times 10^{-3}$ mbar) for 2 h at 475 K prior to adsorption.

X-Ray powder diffraction was used to determine the crystal structure of all samples. Measurements were performed with a Philips X'Pert Pro System using Cu-K_α radiation of 0.154056 nm (45 kV and 40 mA). Patterns were recorded in a 2θ range of 5° to 70° with a step size of $0.019^\circ / \text{s}$ employing a rotating powder sample holder.

IR Spectroscopy

Infrared spectra were measured on a BRUKER Vertex 70 spectrometer at a resolution of 4 cm^{-1} . Samples were prepared as self-supporting wafers (density approximately 10 mg cm^{-2}) and activated in vacuum ($p = 10^{-6}$ mbar) for 1 h at 723 K (heating rate = 10 K/min). After this pretreatment, the sample was allowed to cool to the desired temperature ($50 - 150 \text{ }^\circ\text{C}$) and 1-pentene (Fluka, 99.5% purity) and 2-pentene (mixture of cis and trans, Fluka >98.5% purity) was introduced via a needle valve. Pentene pressures between 0 and 5 mbar were studied.

Pulse Experiments

In order to follow dimerization on MFI-90 at different temperatures (303 K – 333 K), about 0.03 mbar of 1-pentene was introduced into the cell via a

needle valve (1-pentene pulse). The cell was evacuated as soon as pressure had dropped to about 0.015 mbar (about 30 s after the 1-pentene pulse). The surface reaction was followed by taking spectra in regular intervals (usually one or two minutes).

TGA-DSC

The gravimetric and calorimetric measurements were performed in a modified SETARAM TG DSC 111 instrument with a BARATRON 122A pressure transducer. In a typical procedure the samples (about 20 mg) was activated for 1 h at 723 K (10 K min^{-1}). After cooling to the desired temperature (323 – 423 K) the adsorption studies were performed.

For H-FER, equilibration with 2-pentene was performed in small pressure steps from $1 \cdot 10^{-3}$ to 3 mbar. The thermal flux and the sample mass were followed.

For MFI, dimerization was followed at 323 K following the procedure (pulse experiments) explained for IR spectroscopy. The overall heat flux during dimerization was monitored and normalized to the mass uptake.

3.3. Results and discussion

3.3.1. Characterization of the zeolites

Table 3.1 summarizes the results of the physicochemical characterization. All samples were of microporous nature and the framework identity was confirmed by XRD (Figure S.1). Elemental analysis showed the absence of Al for silicalite.

Table 3.1: Physicochemical properties of the investigated samples

	$S_{\text{BET}}^{\text{a}}$ [m ² /g]	NH_3 Acidity ^b [mol/g]	Si:Al ^c [-]
MFI-90	423	158	88
FER-25	397	560	25
Silicalite	365	n.d.	>1800

^a Determined by N₂ physisorption.

^b Determined by NH₃ TPD.

^c Molar ratio of Si and Al determined with AAS.

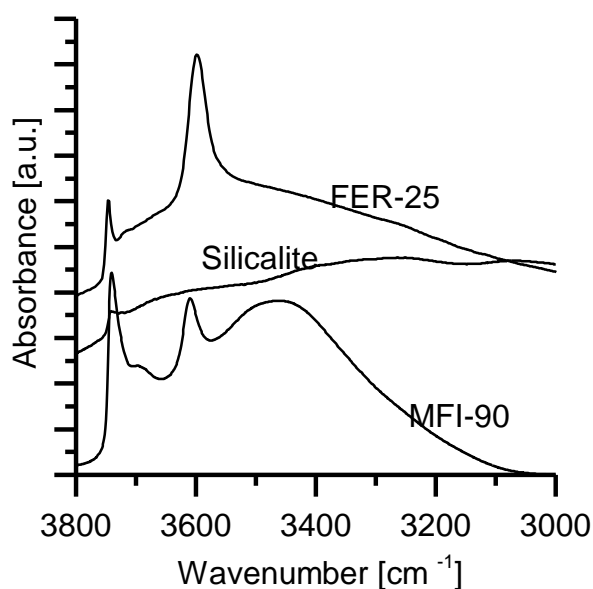


Figure 3.2: IR spectra of OH stretching region of samples MFI-90, silicalite and FER-25.

IR spectra of the OH stretching frequency region are shown in Figure 3.2 for all samples. If Brønsted acid sites (BAS) are present, a characteristic stretching vibration of the bridging hydroxyl groups around 3600 cm^{-1} is expected to be observed. This is absent for silicalite. For MFI-90 the band is located at 3610 cm^{-1} , which is characteristic for BAS in 10 membered rings (MR).²² For FER, BAS are located at different positions within the framework. Therefore, deconvolution was performed following the analysis of Zholoblenko et al.²³, using four Gaussian functions centered at 3609 cm^{-1} , 3600 cm^{-1} , 3587 cm^{-1} and 3563 cm^{-1} (Figure 3.3, details of deconvolution can be found in Supporting Information S.1). These optimized peak positions are in good agreement with peak positions described by Zholoblenko et al. (3609 cm^{-1} , 3601 cm^{-1} , 3587 cm^{-1} , 3567 cm^{-1}).²³ Hence, BAS are located here at four different positions in the framework of FER. The assignment is according to literature as follows:^{22,23} 3609 cm^{-1} – BAS in 10 MR ring channel, 3600 cm^{-1} - BAS in the 8 MR cage vibrating in the extended intersection of 8 and 6 MR, 3587 cm^{-1} - BAS in the 8 MR ring channel and 3563 cm^{-1} – BAS in the 6 MR ring channels.^{22,23}

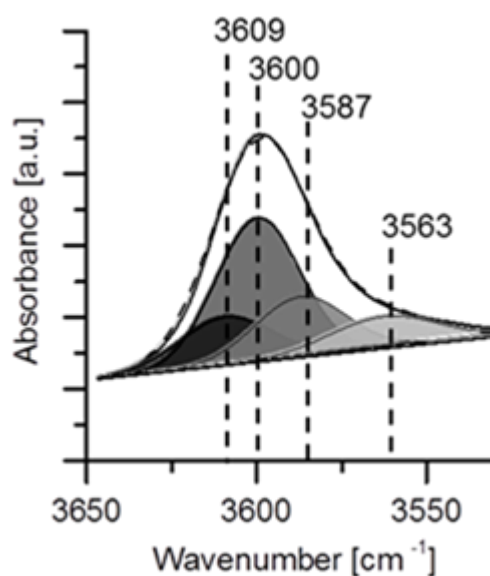


Figure 3.3: Deconvolution of OH stretching region for sample FER. Four Gaussian functions were used. - - - = Experimental, ----- = Fitting Result.

3.3.2. Adsorption of linear pentenes on silicalite

In a first set of experiments, adsorption of linear pentenes was studied at 323 K over non-acidic silicalite (Figure S.2 and S.3.). Pressures of 0.1 to 0.6 mbar had to be applied in order to result in a detectable coverage of the linear pentenes on silicalite. It is interesting to note, that for 1-pentene the C=C stretching vibration is clearly visible at 1642 cm^{-1} , whereas for the more symmetric 2-pentene molecules this vibration mode of an internal C=C group seems to be IR inactive on silicalite (Figure S.2). These two double bond isomers can be further differentiated by the positions of the characteristic H-C=C stretching vibration.²⁴ For 1-pentene (2-pentene) this is observed at a frequency of 3077 cm^{-1} (3023 cm^{-1}). Further differentiation is possible by comparison of H-C stretching vibrations of the two samples in the region of $3000 - 2800\text{ cm}^{-1}$ (Figure S.3). For 1-pentene there are three characteristic bands observed (2962 cm^{-1} , 2934 cm^{-1} and 2878 cm^{-1}) and for 2-pentene there are clearly five peaks discernible (2964 cm^{-1} , 2936 cm^{-1} , 2920 cm^{-1} , 2876 cm^{-1} and 2859 cm^{-1}). On silicalite adsorption was completely reversible and no reaction (especially double bond isomerization) was observed.

Adsorption of 2-pentene on silicalite was studied by TGA-DSC and the differential heat of adsorption is shown in Figure 3.4. A maximum coverage of 1.29 mmol/g was observed. Up to coverages of 0.6 mmol/g a constant value of 56 kJ/mol is observed. As reasoned before, no surface reactions are observed for 2-pentene on silicalite. Therefore the value of 56 kJ/mol corresponds to the mere interaction of the olefin with the zeolite wall via van-der-Waals forces. For higher loadings the heat of adsorption increases most likely due to additional interaction between adjacent n-pentene molecules.

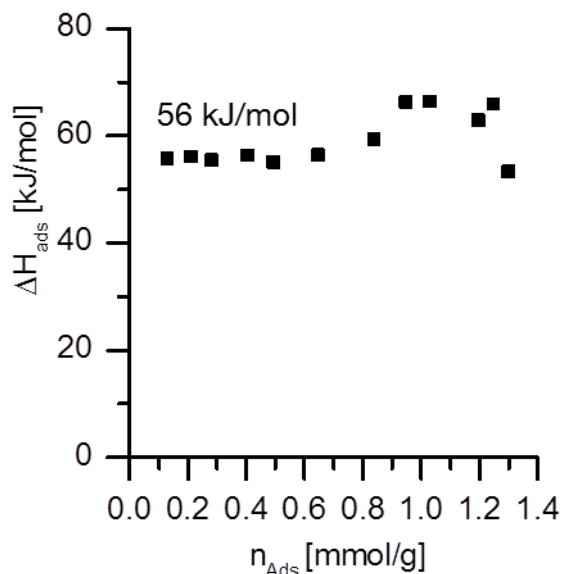


Figure 3.4: Differential heat of adsorption determined at 323 K (2-pentene on silicalite).

3.3.3. Adsorption of linear pentenes on FER-25

FER is in contrast to silicalite more reactive with respect to olefins. Within one minute upon adsorption of 1-pentene mainly 2-pentenes are observed on FER-25 (Figure 3.5). This is evidenced from the characteristic H-C=C stretching vibration which is slightly shifted by 5 cm^{-1} (3018 cm^{-1}) to lower frequencies when compared to 2-pentene on silicalite. The intensities and the positions of the five characteristic peaks, although shifted to higher frequencies by about $6 - 13 \text{ cm}^{-1}$, indicate also clearly the fast formation of 2-pentene. It is interesting to note, that on FER-25 the band associated with C=C stretching vibrations is visible at 1654 cm^{-1} .¹³ Hence, the double bond in 2-pentene is distorted upon adsorption in a way that the dipole moment changes now during this vibrational mode. A selective interaction of the double bond with the BAS might explain this. This π -bonded alkene is further evidenced by the shift of the OH (BAS) stretching vibration. A negative peak is observed in the difference spectrum at 3600 cm^{-1} and a broad contribution centered around 3100 cm^{-1} is clearly visible. This implies a shift of 500 cm^{-1} of the OH stretching vibration induced upon adsorption of 2-pentene. This shift

is in good agreement with observations of butene adsorption at sub-ambient temperatures.^{10,17,18}

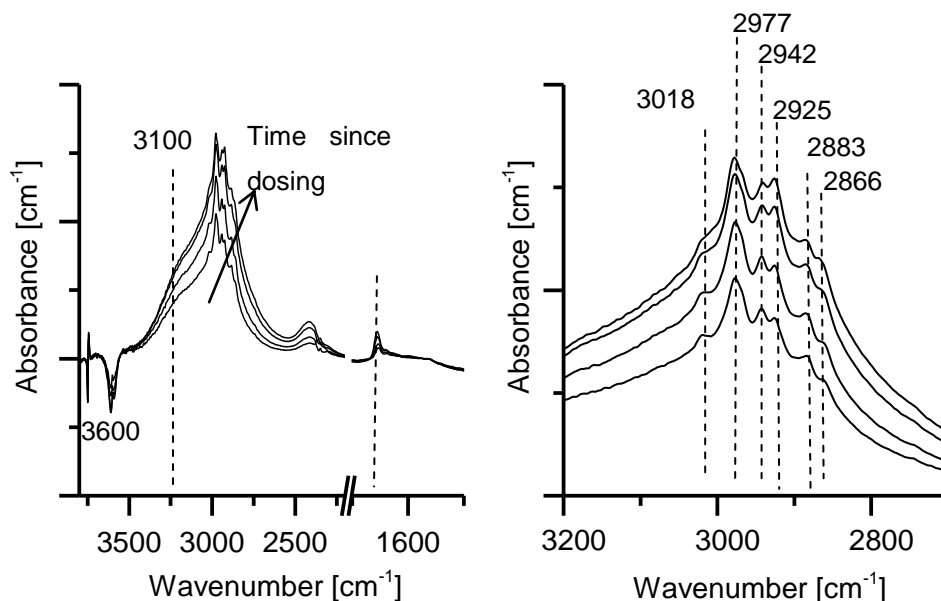


Figure 3.5: Difference spectra following adsorption of 1-pentene on FER-25 at 323 K. Complete spectral range following adsorption during 1, 2, 3 and 9 min after introducing 0.05 mbar of 1-pentene (left) and zoom into CH stretching vibration (right).

The peak at 2400 cm^{-1} , which is also – although not being discussed – clearly visibly in the spectra for butene adsorption reported earlier^{10,18}, is assigned to combination IR bands of the double bond stretching vibration and bending vibrations of CH_2 groups which become visible upon formation of a π -complex.²⁵ Presence of this combination band was attributed to a strong polarization of the double bond, which indicates a partial transfer of the proton to the double bond.²⁵ This deformation of the molecule agrees well with the observed $\text{C}=\text{C}$ stretching vibration at 1654 cm^{-1} , which is absent for the gas 2-pentene adsorbed on silicalite (Figure S.2).

It is surprising to observe a stable π -bounded alkene at 323 K. No indications for formation of an alkoxide nor dimerization were found as observed for butenes on MOR and ZSM-5 already at room temperature.^{9,10} Dimerization was evidenced by liberation of initially covered BAS.^{9,10} Following the same experimental procedure, slow liberation of BAS was observed as soon as

outgassing was started. Careful evaluation of the corresponding CH stretching vibration revealed that (slow) desorption and not a surface reaction was monitored (Figure S.4). A stable (for 2 h) and reversible adsorption in the form of a π -bounded 2-pentene was also observed at 423 K (Figure S.5). Hence, the only reaction observed at these conditions was the double bond isomerization. It is therefore concluded that the rapid double bond isomerization follows the concerted mechanism – not involving a proton transfer – as already evidenced from H/D experiments by Kondo et al. at low temperatures.¹⁶

In a next experiment, stepwise dosing of 1-pentene was performed at 323 K and followed by IR spectroscopy. A plot of the area of the CH stretching vibrations (Figure 3.6) gives a linear correlation with the corresponding integral area of disappeared BAS up to a BAS coverage of about 80%. If the area of disappeared BAS is plotted as a function of the peak corresponding to C=C stretching vibrations, a linear correlation over the complete adsorption range is observed. Considering the fact, that for 2-pentene this peak is only visible for alkene molecules that are interacting with BAS, this indicates once more the stable and stoichiometric interaction of the linear pentenes with the BAS of FER. For higher pressures and higher alkene coverage the deviation from the linear correlation (Figure 3.6, left) points to a physisorption (adsorption in the pores without interacting with a Brønsted acid site).

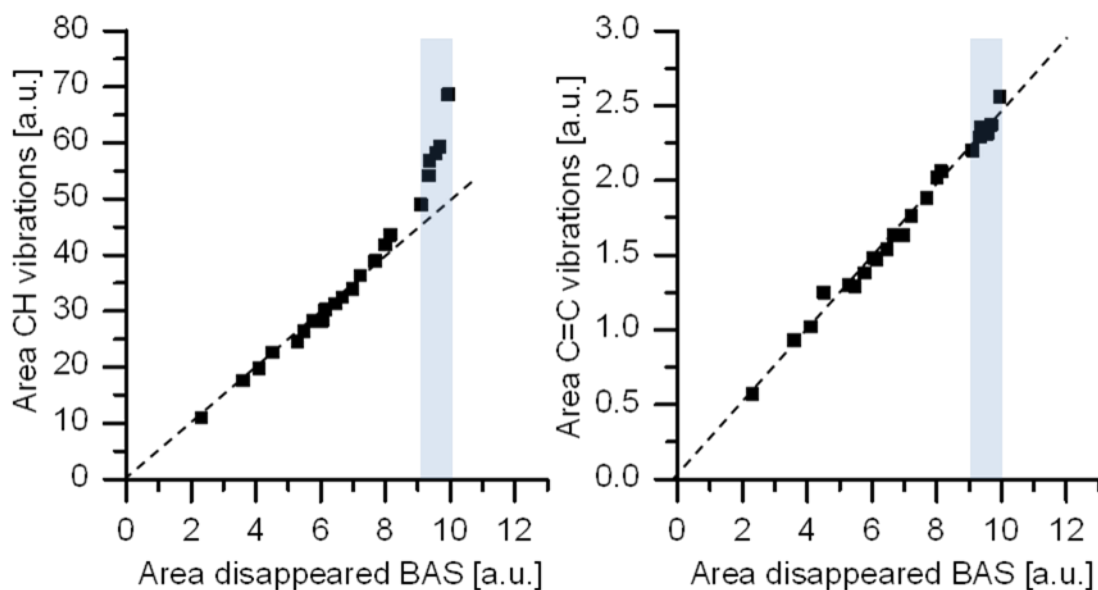


Figure 3.6: Stepwise adsorption of 1-pentene on FER-25 at 323 K (pressure range 0 - 5 mbar). The correlations between disappeared BAS (integrated from $3666 - 3540 \text{ cm}^{-1}$) and (left) CH stretching vibrations (integrated from $3040 - 2680 \text{ cm}^{-1}$) as well as (right) C=C stretching vibration (integrated from $1680 - 1590 \text{ cm}^{-1}$) are shown.

The sample FER-25 contains BAS at four different positions within the framework. These BAS in different environments within the pore system of the zeolite might interact differently with the olefin molecule. Therefore, a closer look at the OH and C=C stretching region (Figure S.6) will help to answer that question. The difference spectra indicate, that in the OH stretching region first the OH groups with a stretching frequency of 3609 and 3587 cm^{-1} disappear. In order to quantitatively evaluate this, deconvolution of spectra was done using 4 Gaussian functions (compare with Figure 3.3). The result is shown in Figure 3.7. Up to a pentene coverage of about 0.2 mmol/g , mainly OH groups located in easily accessible 10 and 8 MR pores (Figure S.7, 3609 cm^{-1} and 3587 cm^{-1}) are selectively covered. For higher pentene partial pressures also the acid sites located within the 8 MR cages (3600 cm^{-1}) and to less extent also those assigned to be in 6 MR pores (3563) start to interact with the linear alkenes. This implies that in ferrierite 2-pentene adsorbs preferentially in the 10 and 8 MR pores.

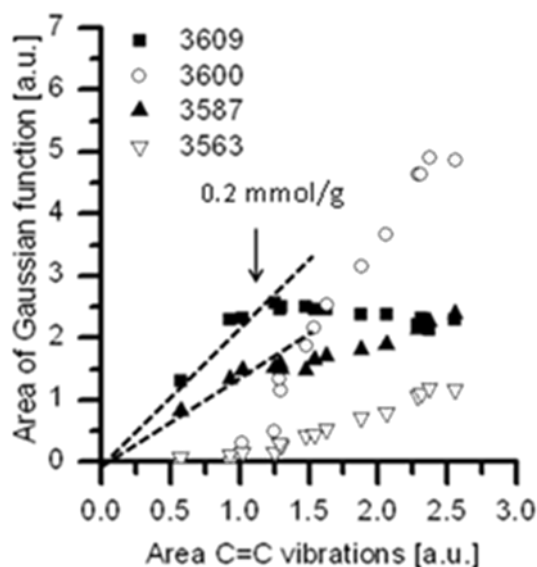


Figure 3.7: Results of deconvolution of OH stretching region using four Gaussian functions centered at 3609, 3600, 3587 and 3563 cm^{-1} shown as function of integrated C=C stretching vibration ($T = 323 \text{ K}$, 0 – 5 mbar 1-pentene).

A similar behavior has been reported for n-pentane in ferrierite.^{26,27} While propane and n-butane show no preferential adsorption, a critical chain length seems to be reached with n-pentane.²⁷ At low n-pentane partial pressure, 10 MR pores are preferentially occupied. Higher pressures are necessary in order to fill the 8 MR cages.²⁷ Due to the restricted space that is available in this 8 MR cage, n-pentane molecules adsorbed in this environment are expected to be highly coiled, and therefore adsorption is energetically disfavored in comparison to 8 and 10 MR pores.^{26,27}

Our experimental finding for adsorption of 1-pentene shows hence a comparable behavior as found for n-pentane. The distortion by coiling of the alkene molecule can be also evidenced in the C=C stretching region where for higher coverages a second contribution around 1638 cm^{-1} becomes clearly visible (Figure S.6).

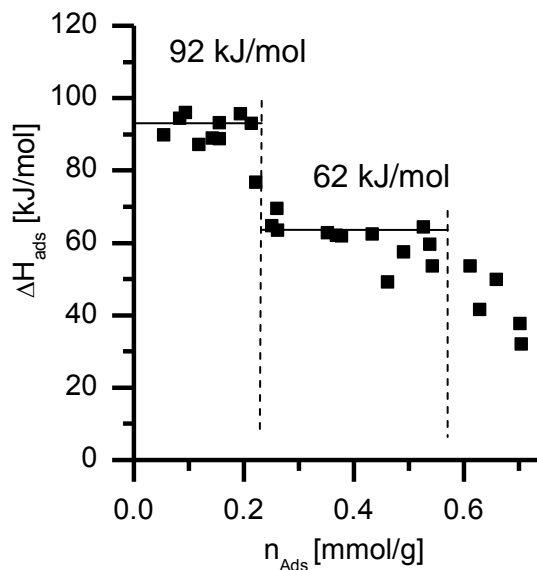


Figure 3.8: Differential heat of adsorption determined at 323 K (2-pentene on FER-25). Lines indicate zones of different adsorption behavior. (Data of three independent experiments is shown).

Having established the absence of any substantial reaction at 323 K (besides double bond isomerization) enables meaningful determination of heats of adsorption by calorimetry. At 323 K, 2-pentene (cis and trans) is the most abundant double bond isomer (90 %, calculated with HSC Chemistry 6.0) according to thermodynamics. As it was shown before, double bond isomerization occurs readily and therefore the isomers are expected to be found in the thermodynamic equilibrium. Therefore experiments were performed with 2-pentene, making enthalpic contributions from double bond isomerization negligible. Figure 3.8 shows the differential heat of adsorption (ΔH_{ads}) determined for 2-pentene. Three regions can be discerned. For coverages of up to 0.2 mmol/g a value of 92 kJ/mol was determined. ΔH_{ads} decrease to 62 kJ/mol in the second region. If the adsorbed amount was higher than 0.6 mmol/g heat of adsorption decreased further. For n-pentane in H-FER a comparable maximum adsorption capacity of 0.56 mmol/g ($T = 333$ K) was determined earlier.²⁸

It is striking that the step in the differential heat of adsorption plot (Figure 3.8) coincides with the starting coverage of BAS located in the 8 MR cages

(Figure 3.7). Hence, the value of 92 kJ/mol is assigned to interaction of 2-pentene with easily accessible BAS located in 10 and 8 MR ring pores. The second value, 62 kJ/mol corresponds therefore to interaction of 2-pentene with BAS located in 8 MR cages.

Using this assignment, the contribution from the π -interaction can be estimated. A heat of adsorption of -69 kJ/mol were reported earlier for the adsorption of n-pentane on FER.²⁸ This reveals the additional contribution of the π -interaction of the double bond with the BAS to be 23 kJ/mol. The contribution of the proton to the alkane sorption is estimated to be 10 kJ/mol (as determined for MFI/silicalite)⁶, and hence 33 kJ/mol correspond to the overall contribution from the π -complex. It shall be noted that this refers to adsorption in the easily accessible 10 MR pores and BAS that are located in the 8 MR pores but have access to the 10 MR pore system. In a next step, adsorption of 1-pentene on MFI type zeolites which consist of intersecting 10 MR channels, will be investigated.

3.3.4. Study of adsorption and surface reaction of 1-pentene on MFI-90

Surface reaction of 1-pentene at 323 K

In contrast to FER, π -bound pentenes are not stable on MFI-90 at a temperature of 323 K.

Figure 3.9 shows the time resolved surface reaction of 1-pentene. It shall be noted that the reaction, upon dosing of 1-pentene, was followed under vacuum conditions. Initially, the linear pentenes form the π -bounded complex as can be derived from the initial ($t = 0.5$ min) presence of the characteristic H-C=C stretching vibration (3020 cm^{-1}) as well as the presence of C=C stretching vibration (1654 cm^{-1} , not shown). Additionally, a broad contribution from the hydrogen-bonding shifted OH groups around 3100 cm^{-1} is clearly visible. Since the spectrum is showing the characteristics of 2-pentene, the double bond isomerization seems to be completely equilibrated at this initial stage of the surface reaction. This is in good agreement with the findings for FER.

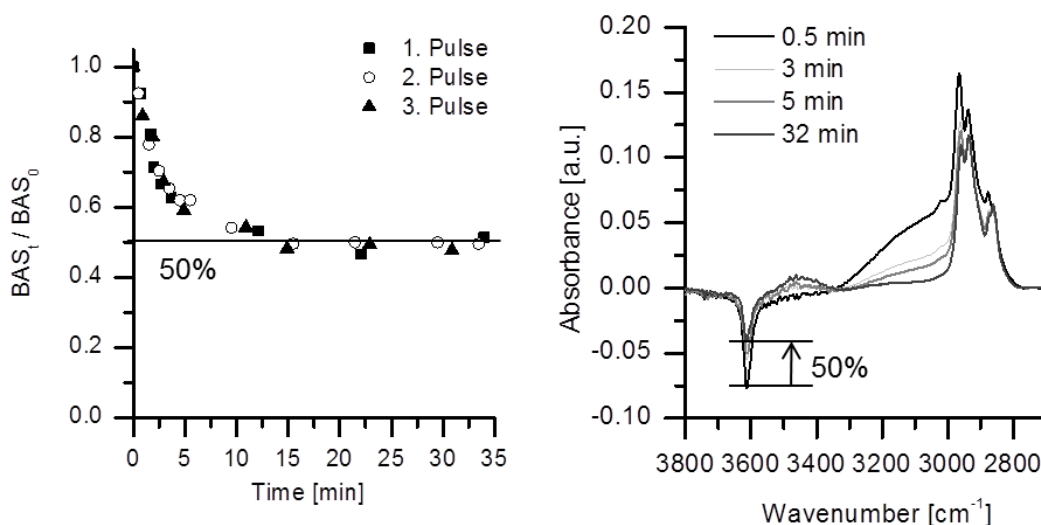


Figure 3.9: Time course of surface reaction on MFI-90 upon pulsing of 1-pentene followed by IR spectroscopy ($T = 323$ K). Liberation of BAS (shown for three sequent pulses; 1st pulse – 13 % of all BAS initially covered, 2nd Pulse – 31 %, 3rd pulse – 68 %) plotted as function of time. BAS_0 signifies the number of (additional) initially covered BAS (left). Difference spectra for different times after pulsing 1-pentene are shown on the right.

Starting from this initial π -bound alkene a surface reaction is clearly observed. With increasing reaction time ($t = 3$ - 32 min), the broad peak attributed to hydrogen bonded OH groups disappears and the initially interacting BAS are restored which is evidenced by a decrease (difference spectra) of the band centered at 3610 cm^{-1} . It is interesting to note, that in this case surface coverage of the alkene does not decrease concomitantly (Figure S.8). The area (integrated HC stretching vibration) increases with increasing reaction time and decreasing BAS coverage. This is attributed to a change in the extinction coefficient upon reaction of the linear pentene.

At the end of the reaction about 50 % of all initially covered BAS remain so. This finding points towards dimerization of pentene. The reaction can be also evidenced in the change of the characteristic peaks of the CH stretching vibration. Dimerization of 1-butene at room temperature was also described by Domen et al. for MOR and MFI.^{9,10} They also report that 50% of the BAS

initially interacting with the olefin monomer become accessible after surface reaction.

At 3450 cm^{-1} a minor contribution becomes visible. Kondo et al. attributed this to a shifted OH group caused by the interaction with the aliphatic chain of the formed dimer. In this case, especially when considering that the extinction coefficient of the shifted BAS increases upon polarization by an alkane, only a minority species seems to be coordinated in that way.²⁹ The absence of an additional bathochromic shift correlated with the BAS that remain disappeared even after prolonged reaction time, implies a chemical reaction of these OH groups – most likely chemisorption of the dimer. Formation of such an alkoxy species upon dimerization was described earlier for 2-methylpropene for MOR.⁹

Figure 3.9 shows also the time course of BAS recovery for a sequence of three pulses. The reaction followed, despite of different surface coverage in pentene and the additional presence of dimers, in all three cases the same kinetics. A simple exponential rate law can be used to describe the kinetics. It is therefore assumed that dimerization is first order with respect to physisorbed pentene (initially disappeared BAS represent physisorbed pentene molecules). Activation of a physisorbed pentene seems to be the rate determining step (RDS). As soon as the activated complex is formed it is scavenged by reaction with a second pentene molecule. This implies a high surface mobility of physisorbed alkenes at this temperature, which was already evidenced by others for butenes.^{16,18,19}

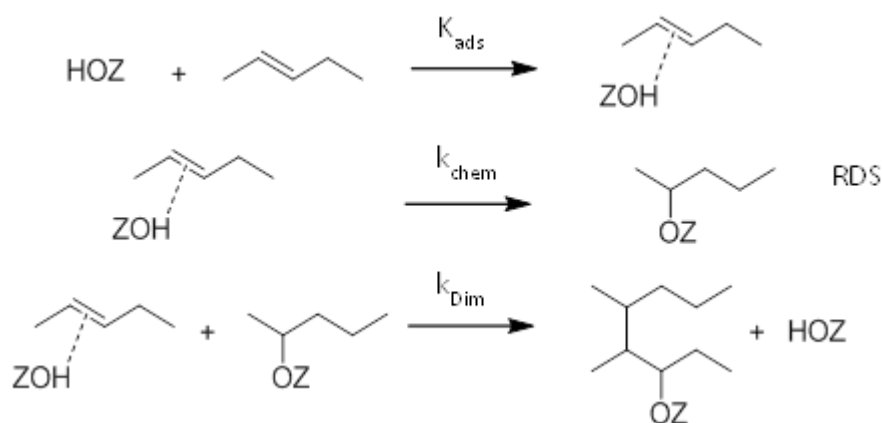


Figure 3.10: Reaction scheme for dimerization reaction of 2-pentene on a zeolite. HOZ symbolize BAS.

The dimerization reaction is depicted in Figure 3.10. Adsorption and formation of the π -bound pentene is very fast and irreversible. Hence, the adsorption step must not be considered for the surface reaction. Reaction starts from the π -bound alkene and the RDS is formation of the chemisorbed intermediate. At this point it shall be noted that it cannot be differentiated whether the alkoxide is formed or rather the carbenium ion is the reactive intermediate. This intermediate reacts readily with another physisorbed and highly mobile pentene molecule which results in formation of a chemisorbed dimer and liberation of a BAS. Therefore, the coverage with the chemisorbed pentene is expected to be very low. The liberation of the BAS can be easily followed by IR spectroscopy. This observable can be used for fitting of a rate law. Θ^* is defined as the ratio of liberated BAS and initially ($t = 0$) covered BAS. Equation 1 is derived by using the aforementioned assumptions (see Scheme 1, Supporting Information).

$$1 - 2\Theta^* = \exp(-2 \cdot k_{\text{chem}} \cdot t) \quad (\text{Eq. 1})$$

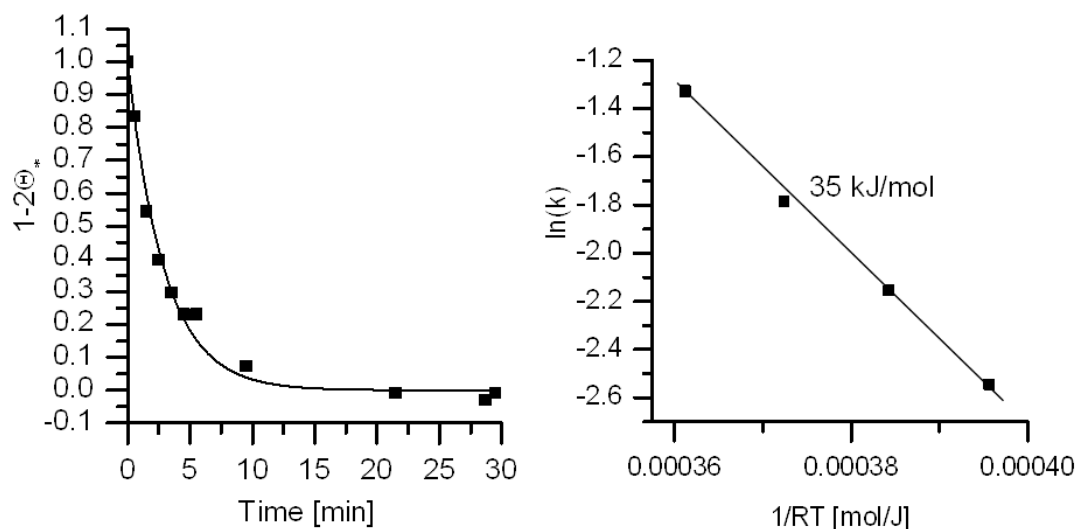


Figure 3.11: Kinetics of surface reaction at 323 K fitted by using Eq. 1 (left) and corresponding Arrhenius plot (right). Symbols signify experimentally determined values, line show results of fitting. The results for 304, 313, and 333 K are shown in Figure S.9.

Figure 3.11 shows the results of this fit for 323 K. By determining k_{chem} for different temperatures (304 – 333 K) an activation energy for the transition between the physisorbed alkene and the alkoxide can be determined. The resulting value of 35 kJ/mol is close to experimentally determined values for H/D exchange reaction mediated by butenes on zeolite ZSM-5 (31 ± 8 kJ/mol).^{9,21} The rate constant for the H/D exchange reaction are also comparable (if extrapolated to 323 K)⁹ to the values determined by this fitting method ($k_{\text{chem}} = 0.335 \text{ min}^{-1}$, $T = 323 \text{ K}$). This observation points strongly to the fact that indeed chemisorption is monitored by this kind of analysis and that dimerization and H/D exchange reactions have a similar transition state. Most likely this transition involves formation of the carbenium ion, which reacts then readily with a second pentene. The similarity between the activation energies and rate constant for H/D exchange reactions and dimerization implies in our opinion that the alkoxide is not formed. During the slow H/D exchange with butene the alkoxide was not observed.¹⁸

Hence, the likewise obtained activation energy obtained in our case describes the transition from the physisorbed to the chemisorbed alkene. If the alkoxide was formed, activation of the chemisorbed species is expected to be the RDS

for the dimerization reaction. It is likely that the activated complex resembles a carbenium ion. Hence, a higher barrier than that observed for the exothermic alkoxide formation (see below) would be observed, if the alkoxide was actually formed.

In addition it shall be noted that double bond isomerization was faster than dimerization. Already 1 min after dosing of 1-pentene, 2-pentene was the dominant species on the zeolite surface (Figure 3.11). If double bond isomerization involved a carbenium ion like transition state, the rate should be comparable to that of dimerization. Hence double bond isomerization can proceed via a pathway which does not involve a carbenium ion. This points to a concerted mechanism as evidenced earlier.

Estimation of the enthalpic contribution from chemisorption

Having established from IR experiments, that upon dimerization the chemisorbed dimer is the dominant species formed enables one to deduce the heat of chemisorption of the dimer. The overall released heat of reaction can be followed by calorimetric measurements and was determined to be 285 ± 7 kJ for each mol of formed dimer. 2-pentene was dosed for these experiments. Therefore enthalpic contributions from double bond isomerization can be neglected. Figure 3.12 shows the steps that need to be considered when trying to dissect the overall dimerization reaction. For this analysis, we start first from the gas phase without considering the zeolite confinement. The gas phase reaction, that is the C-C bond formation between two pentene molecules was estimated to be 88 kJ/mol (see Supporting Information S.2 for details). If this formed gas phase dimer is transferred into the zeolite confinement an additional 120 kJ/mol need to be considered for the physisorption of the dimer, not considering interaction with BAS.⁶ The contribution from the π -interaction of the double bond was determined in the previous section for FER. This value of 33 kJ/mol can be used, for the purpose of an estimate, for the π -bound dimer in MFI. Adding up all these contributions results in a theoretical value of 241 kJ/mol for formation of the π -bound dimer, which is experimentally not observed. The enthalpic

contribution from formation of the alkoxide is not considered yet and should equal the difference between 241 kJ/mol and the experimental value of 285 kJ/mol. Hence, enthalpic contributions from chemisorption are estimated to be 44 kJ/mol.

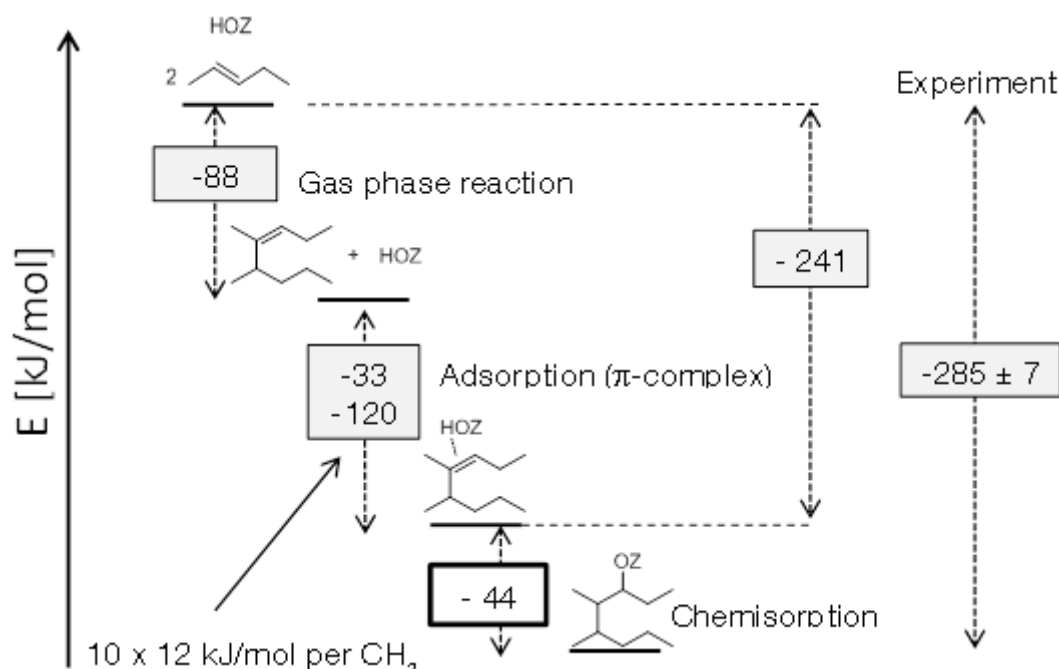


Figure 3.12: Schematic illustration of enthalpic dissection of the dimerization reaction of 2-pentene within a zeolite confinement.

This allows one to complete the enthalpic picture of the adsorption of linear pentenes in MFI type zeolites. For n-pentane in MFI the heat of adsorption is 62 kJ/mol.⁵ Adding 23 kJ/mol for the additional interaction of the BAS with the double bond, as determined from adsorption in FER, gives an estimate of 85 kJ/mol for formation of the π -complex in MFI. In the case of MFI, this intermediate is not stable and formation of the alkoxide species is expected to proceed via an activated step which involves most likely formation of the carbenium ion. The overall heat of chemisorption is, based on a careful analysis of the dimerization reaction, estimated to be 129 kJ/mol.

The remarkable difference in the adsorption behavior between the two framework types needs to be explained. As can be seen in Table 3.2, the d_{\max} (maximum free sphere diameter) is quite comparable for MFI and FER. It has

to be noted that for FER this is located in the 8 MR cage (see illustration in Figure S.7), whereas for MFI this is located in the highly accessible intersection of the 10 MR pore channels.^{23,30}

Table 3.2: Pore dimensions of zeolites MFI and FER.³⁰

	d_{\max}^a [nm]	Crystallographic entrance pore diameter [nm]	
FER	0.463	0.54 x 0.42 (10 MR)	0.48 x 0.35 (8 MR)
MFI	0.464	0.56 x 0.53 (10 MR)	0.56 x 0.51 (10 MR)

^a Maximum free sphere diameter

Formation of the alkoxide or carbenium ion from the π -complex involves rehybridization of at least one sp^2 carbon atom to a sp^3 carbon atom. Therefore, the transition state from the planar (along C=C bond) pentene molecule to the carbenium ion/alkoxide will involve a transition state complex which occupies more space within the zeolite confinement.^{1,11} In MFI type zeolites, the larger channel size (0.56 x 0.53 nm - straight channel) seems to enable this slow transformation whereas for FER the tighter channel nature (0.54 x 0.42 nm) increases the enthalpic barrier for formation of the voluminous carbenium ion. This might explain why a stable π -complex is observed for adsorption of olefin on FER.

3.4. Conclusions

This work focuses on adsorption phenomena on three different zeolites. In the absence of BAS (silicalite) double bond isomerization does not occur ($T = 323\text{ K}$), which leads to the conclusion that acid sites are a prerequisite for this type of reaction. It is on the other hand interesting to note, that for FER rapid double bond isomerization is observed despite of sole formation of a π -complex (no indications for formation of an alkoxide were observed). This points clearly to the fact that a chemisorbed alkoxide is not a prerequisite for double bond isomerization and is in good agreement with findings by others for sub ambient temperatures.^{10,18-20} Stable and reversible formation of the π -complex was even observed for 423 K.

In FER adsorption of the pentene molecules takes place preferentially in the highly accessible 10 and 8 MR pores of the FER framework. Only for higher 1-pentene partial pressures was adsorption into the 8 MR cage observed, which is accompanied by a deformation of the 2-pentene molecule due to the restricted space that is available within this pore confinement. A similar behavior was reported for n-pentane in FER.²⁷ Heats of adsorption on FER were determined by using 2-pentene. The differential heat of adsorption (Figure 3.8) shows a step at a pentene coverage of 0.2 mmol/g. This coincides with the preferential adsorption in the 10 and 8 MR for coverages below 0.2 mmol/g as evidenced by deconvolution of the OH stretching region (Figure 3.7).

The corresponding heat of 92 kJ/mol allows one to deduce the enthalpic contribution from formation of the π -complex. For adsorption of n-pentane in FER a ΔH_{ads} of -69 kJ/mol was reported on the same type of zeolite at approximately the same coverage.²⁸ Consequently, overall enthalpic contribution from formation of the π -complex is -33 kJ/mol. Please note in passing, that one has to account for 10 kJ/mol for the interaction of the alkane

with BAS.⁶ The second region ($\Delta H_{\text{ads}} = -62 \text{ kJ/mol}$) corresponds to adsorption of 2-pentene in the 8 MR cage.

The situation is different for the MFI type zeolite. In good agreement with the results for butene adsorption, slow dimerization is observed above room temperature.^{9,10} The chemisorbed dimer is clearly formed. This allows one to deduce the contribution from chemisorption (ΔH_{chem}) by considering dimerization and the formation of the alkoxide. Doing so, ΔH_{chem} was estimated to be -44 kJ/mol .

Moreover, the kinetics of this surface reaction was explored by following the reappearance of BAS upon formation of the dimer. Activation of the physisorbed pentene is the rate determining step. The transition state involves most likely formation of a carbenium ion. The corresponding activation energy for formation of the transition state was determined to be 35 kJ/mol .

ACKNOWLEDGMENTS

The authors thank Franz X. Hecht for N_2 physisorption measurements, Martin Neukamm for conducting elemental analysis and Prof. Andreas Jentys for helpful discussions concerning interpretation of the IR spectra. We also thank BU Catalysts, Clariant Produkte (Deutschland) GmbH (former Sued-Chemie AG) for the financial support and fruitful discussions in the framework of MuniCat.

3.5. References

- (1) Nguyen, C. M.; De Moor, B. A.; Reyniers, M.-F.; Marin, G. B. *The Journal of Physical Chemistry C* **2011**, *115*, 23831.
- (2) Corma, A. *Chemical reviews* **1995**, *95*, 559.
- (3) Buchanan, J. S.; Santiesteban, J. G.; Haag, W. O. *Journal of Catalysis* **1996**, *158*, 279.
- (4) Rahimi, N.; Karimzadeh, R. *Applied Catalysis A: General* **2011**, *398*, 1.
- (5) De Moor, B. A.; Reyniers, M. F.; Gobin, O. C.; Lercher, J. A.; Marin, G. B. *J. Phys. Chem. C* **2011**, *115*, 1204.
- (6) Eder, F.; Lercher, J. A. *Zeolites* **1997**, *18*, 75.
- (7) Eder, F.; Stockenhuber, M.; Lercher, J. A. *The Journal of Physical Chemistry B* **1997**, *101*, 5414.
- (8) Nieminen, V.; Sierka, M.; Murzin, D. Y.; Sauer, J. *Journal of Catalysis* **2005**, *231*, 393.
- (9) Ishikawa, H.; Yoda, E.; Kondo, J. N.; Wakabayashi, F.; Domen, K. *The Journal of Physical Chemistry B* **1999**, *103*, 5681.
- (10) Kondo, J. N.; Liqun, S.; Wakabayashi, F.; Domen, K. *Catalysis Letters* **1997**, *47*, 129.
- (11) Bhan, A.; Joshi, Y. V.; Delgass, W. N.; Thomson, K. T. *The Journal of Physical Chemistry B* **2003**, *107*, 10476.
- (12) Boronat, M.; Viruela, P. M.; Corma, A. *Journal of the American Chemical Society* **2004**, *126*, 3300.
- (13) Kondo, J. N.; Wakabayashi, F.; Domen, K. *The Journal of Physical Chemistry B* **1998**, *102*, 2259.
- (14) Pascual, P.; Ungerer, P.; Tavitian, B.; Pernot, P.; Boutin, A. *Physical Chemistry Chemical Physics* **2003**, *5*, 3684.
- (15) Haw, J. F.; Richardson, B. R.; Oshiro, I. S.; Lazo, N. D.; Speed, J. A. *Journal of the American Chemical Society* **1989**, *111*, 2052.
- (16) Kondo, J. N.; Domen, K.; Wakabayashi, F. *Microporous and Mesoporous Materials* **1998**, *21*, 429.
- (17) Yoda, E.; Kondo, J. N.; Domen, K. *The Journal of Physical Chemistry B* **2005**, *109*, 1464.
- (18) Kondo, J. N.; Shao, L.; Wakabayashi, F.; Domen, K. *The Journal of Physical Chemistry B* **1997**, *101*, 9314.
- (19) Stepanov, A. G.; Arzumanov, S. S.; Luzgin, M. V.; Ernst, H.; Freude, D. *Journal of Catalysis* **2005**, *229*, 243.
- (20) Boronat, M.; Viruela, P.; Corma, A. *The Journal of Physical Chemistry A* **1998**, *102*, 982.
- (21) Stepanov, A. G.; Luzgin, M. V.; Arzumanov, S. S.; Ernst, H.; Freude, D. *Journal of Catalysis* **2002**, *211*, 165.
- (22) Subbotina, I. R.; Shelimov, B. N.; Kazanskii, V. B. *Kinetics and Catalysis* **2002**, *43*, 412.
- (23) Zholobenko, V. L.; Lukyanov, D. B.; Dwyer, J.; Smith, W. J. *The Journal of Physical Chemistry B* **1998**, *102*, 2715.
- (24) Armaroli, T.; Finocchio, E.; Busca, G.; Rossini, S. *Vibrational Spectroscopy* **1999**, *20*, 85.

- (25) Kazansky, V. B.; Subbotina, I. R.; Jentoft, F. *Journal of Catalysis* **2006**, *240*, 66.
- (26) Pascual, P.; Boutin, A. *Physical Chemistry Chemical Physics* **2004**, *6*, 2015.
- (27) van Well, W. J. M.; Cottin, X.; de Haan, J. W.; Smit, B.; Nivarthi, G.; Lercher, J. A.; van Hooff, J. H. C.; van Santen, R. A. *The Journal of Physical Chemistry B* **1998**, *102*, 3945.
- (28) Eder, F.; Lercher, J. A. *The Journal of Physical Chemistry B* **1997**, *101*, 1273.
- (29) Makarova, M. A.; Ojo, A. F.; Karim, K.; Hunger, M.; Dwyer, J. *The Journal of Physical Chemistry* **1994**, *98*, 3619.
- (30) Miyaji, A.; Sakamoto, Y.; Iwase, Y.; Yashima, T.; Koide, R.; Motokura, K.; Baba, T. *Journal of Catalysis* **2013**, *302*, 101.

3.6. Supporting Information

S.1 Deconvolution of acid sites in FER

Starting from the peak positions reported by Zholoblenko et al.¹ deconvolution was further optimized. For doing so, peak positions were allowed to be shifted by $\pm 4 \text{ cm}^{-1}$ while intensity and width was not fixed. A set of optimized fitting parameters (Table S.1) was likewise obtained by fitting the OH stretching region ($3655 - 3522 \text{ cm}^{-1}$) of the activated sample, the first and last difference spectrum upon 1-pentene adsorption (see Figure S.5).

All spectra were then fitted by using Grams Version 7.02 and the values presented in Table S.1. Peak center and width were fixed and only the peak intensities were allowed to be adjusted freely.

Table S.1 Position and width of Gaussian functions employed for deconvolution of OH stretching vibration.

	Center [cm^{-1}]	Width [cm^{-1}]
Peak 1	3609	31.9
Peak 2	3600	30.2
Peak 3	3587	31.8
Peak 4	3563	38.2

(1) Zholobenko, V. L.; Lukyanov, D. B.; Dwyer, J.; Smith, W. J. *The Journal of Physical Chemistry B* **1998**, *102*, 2715.

S.2 Reaction enthalpy of dimerization reaction

The dimerization reaction of two 2-pentene molecules will result inter alia in formation of 4,5-dimethyl-3-octene. As thermodynamic data was not available for these branched olefinic C_{10} isomers, the analogue reaction with two butene molecules was used in order to estimate the reaction enthalpy for this dimerization reaction: e.g. $\Delta H_r = -88 \text{ kJ/mol}$ ($2 \times 2\text{-butene} \rightarrow 3,4\text{-dimethyl-2-hexene}$). HSC Chemistry 6.0 was used.

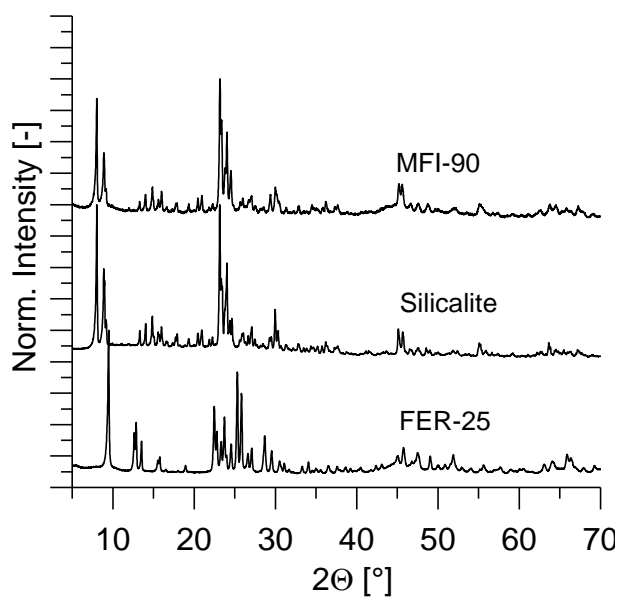


Figure S.1. XRD of samples MFI-90, silicalite and FER-25.

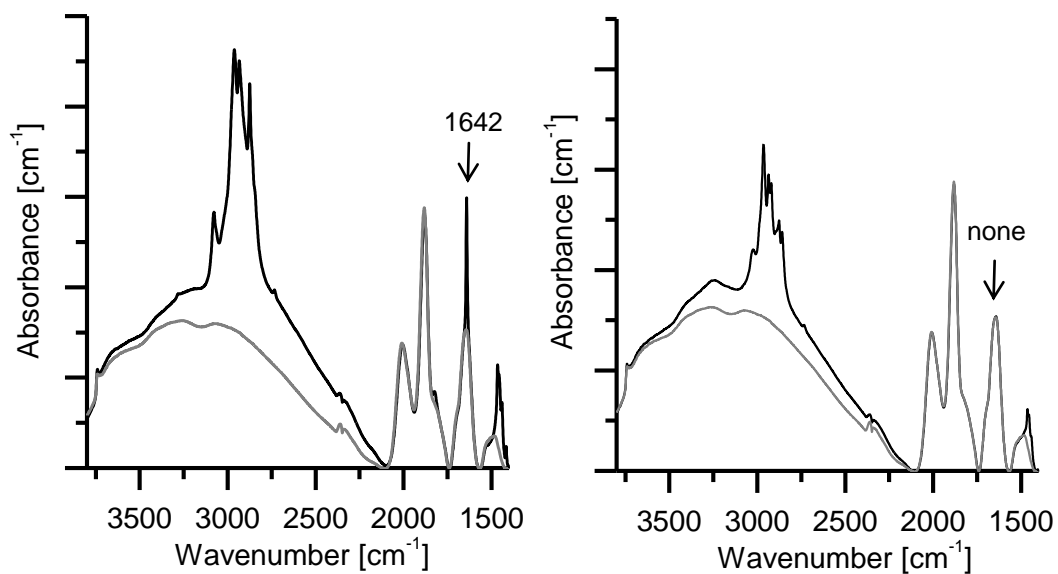


Figure S.2. Adsorption of 1-pentene (left, 0.600 mbar) and 2-pentene (right, 0.400 mbar) on Silicalite. Grey = activated spectrum of Silicalite, black = adsorbed pentene. ($T = 323\text{ K}$).

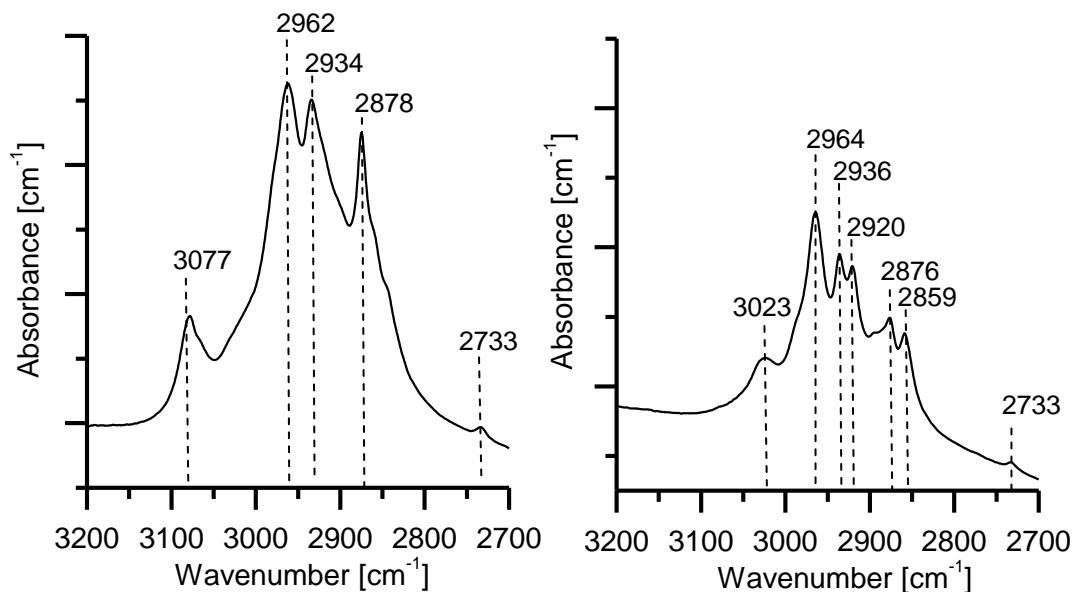


Figure S.3. Zoom into CH stretching region of 1-pentene (left) and 2-pentene (right) adsorbed onto Silicalite ($T = 323 \text{ K}$). Lines indicate frequencies of characteristic vibrations.

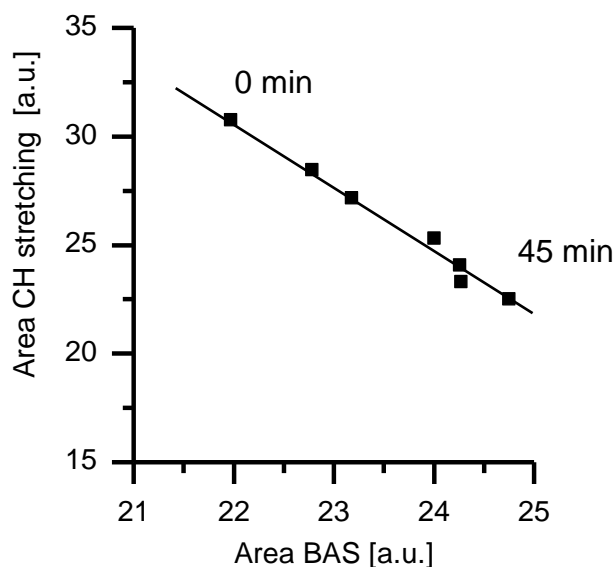


Figure S.4: Correlation of integral area of BAS (3670 – 3490 cm^{-1}) and integral area of CH stretching vibration (3060 – 2680 cm^{-1}) during outgassing. Initially 0.05 mbar of 1-pentene had been introduced into the IR cell. (FER-25, $T = 323 \text{ K}$, 45 min of outgassing lie between the first and the last point)

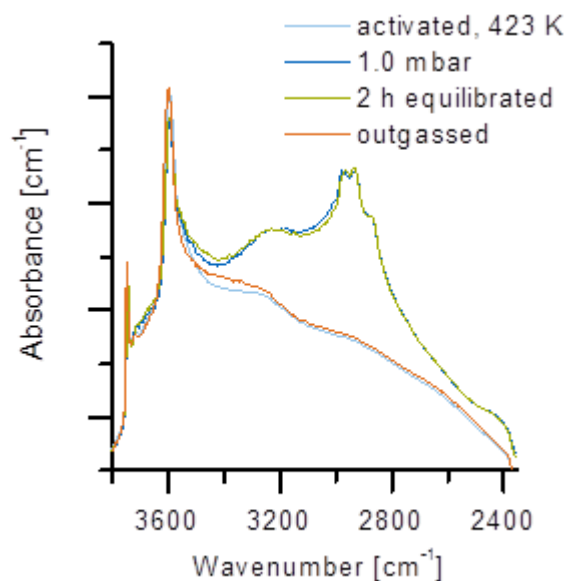


Figure S.5: IR spectra of 1-pentene adsorbed onto FER-25 at 423

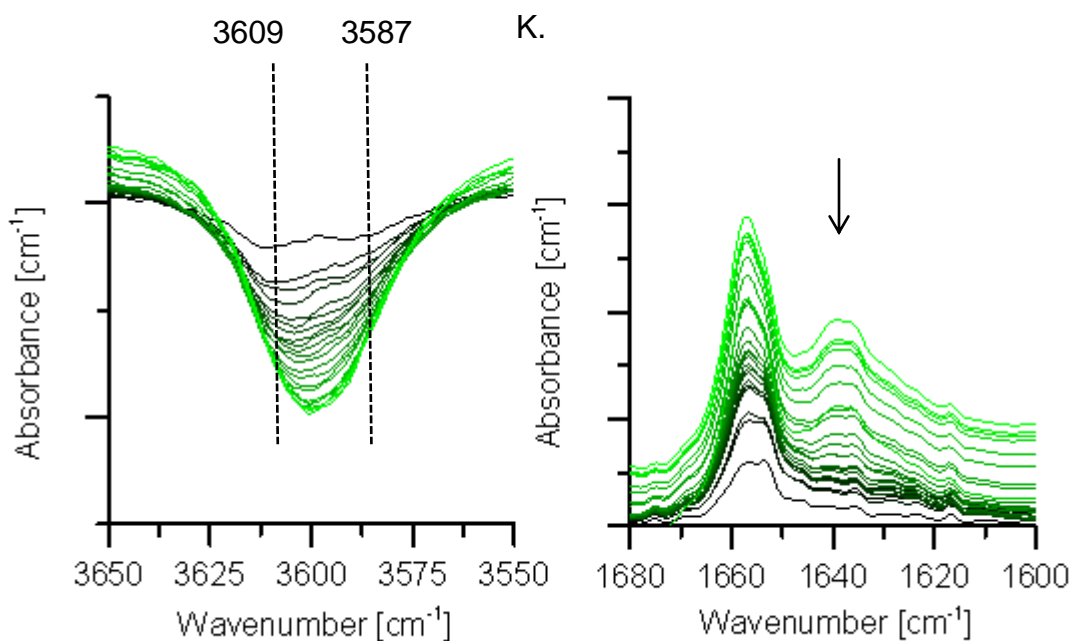


Figure S.6: Difference spectra shown for the OH stretching region (left) and C=C stretching region (right) for the pressure range of 0 – 5 mbar 1-pentene for FER-25 at 323 K. The color gradient from dark green to light green indicates the increasing 1-pentene partial pressure during adsorption.

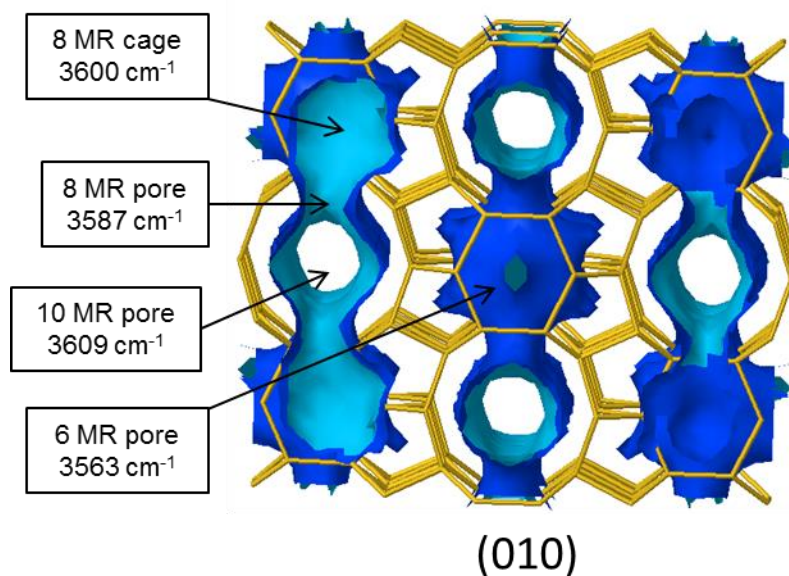


Figure S.7: Location of acid sites within the framework of FER (3D drawing taken from: Ch. Baerlocher and L.B. McCusker, Database of Zeolite Structures: <http://www.iza-structure.org/databases/>)

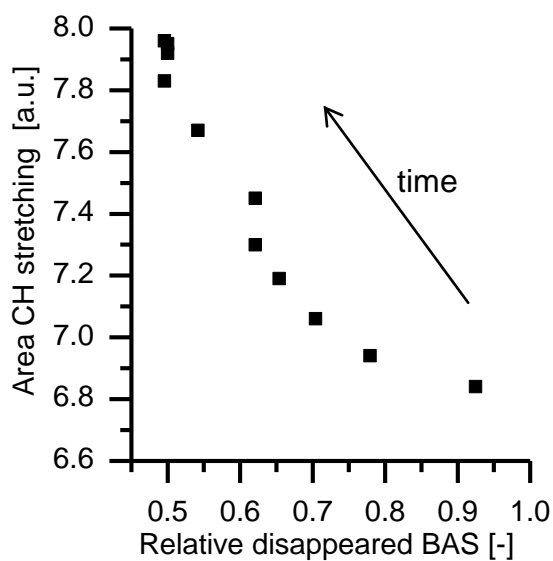


Figure S.8: Correlation of disappeared BAS ($3680 - 3555 \text{ cm}^{-1}$) and integral area of CH stretching vibration ($2990 - 2815 \text{ cm}^{-1}$) during outgassing. Initially 0.05 mbar of 1-pentene had been introduced into the IR cell. ($T = 323 \text{ K}$, 30 min of outgassing lie between the first and the last point).

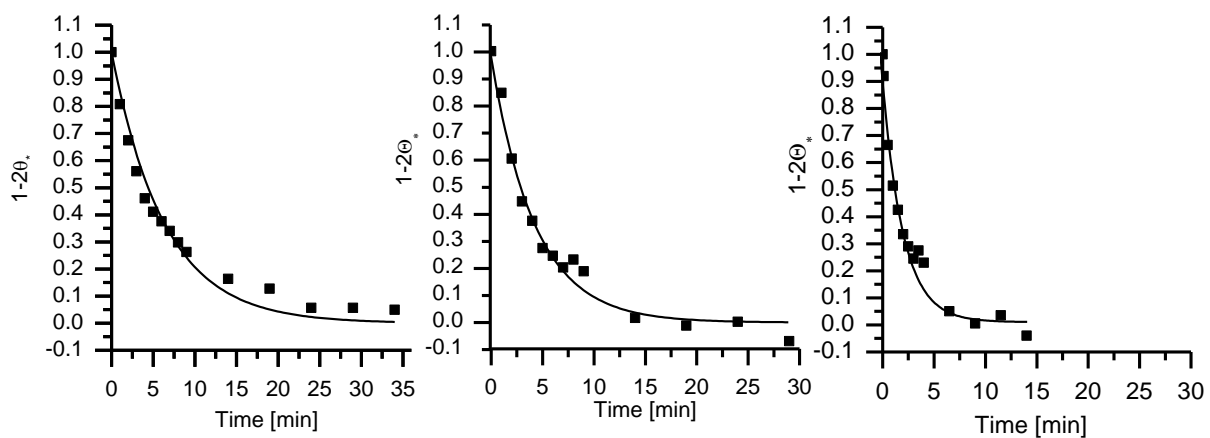


Figure S.9. Fitting results for dimerization for 304 K (left), 313 K (center) and 333 K (right).

Scheme 1 – Kinetics of dimerization

$$(Eq. S1) \quad \frac{d\Theta_{phys}}{dt} = -k_{chem} \cdot \Theta_{phys} - k_{Dim} \Theta_{chem} \Theta_{phys}$$

$$(Eq. S2) \quad \frac{d\Theta_{chem}}{dt} = k_{chem} \cdot \Theta_{phys} - k_{Dim} \Theta_{chem} \Theta_{phys}$$

$$(Eq. S3) \quad \frac{d\Theta_{Dim}}{dt} = k_{Dim} \Theta_{chem} \Theta_{phys}$$

$$(Eq. S4) \quad \frac{d\Theta_{*}}{dt} = k_{Dim} \Theta_{chem} \Theta_{phys}$$

Θ_{*} = recovered BAS ; Θ_{phys} = physisorbed pentene; Θ_{chem} = chemisorbed pentene;

Θ_{Dim} = chemisorbed pentene; k_{dim} = rate constant for dimerization, k_{chem} = rate constant for chemisorption

Site balance:

$$1 = \Theta_{*} + \Theta_{phys} + \Theta_{chem} + \Theta_{Dim}$$

Assumption 1: $k_{dim} \gg k_{chem}$ $\Theta_{chem} \approx 0$; Chemisorption is RDS

$$1 = \Theta_{*} + \Theta_{phys} + \Theta_{Dim} \quad \text{with } \Theta_{*} = \Theta_{Dim} \quad (\text{stoichiometry})$$

$$\Theta_{phys} = 1 - 2\Theta_{*}$$

If $\Theta_{chem} \approx 0$ $\frac{d\Theta_{chem}}{dt} \approx 0$ (coverage is always close to zero)

$$(Eq. S5) \quad k_{chem} \cdot \Theta_{phys} = k_{Dim} \Theta_{chem} \Theta_{phys}$$

$$(Eq. S6) \quad \frac{d\Theta_{*}}{dt} = k_{chem} \cdot \Theta_{phys} = k_{chem} \cdot (1 - 2\Theta_{*})$$

$$(Eq. S7) \quad \left(\frac{d\Theta_{*}}{dt}\right) = k_{chem} (1 - 2\Theta_{*}) \quad \text{Solve integrals with initial conditions: } \Theta_{*,0} = 0; t_0 = 0$$

$$(Eq. S8) \quad -0.5 \ln(1 - 2\Theta_{*}) - \ln(1) = k_{chem} t \quad \text{With } \ln(1) = 0$$

$$(Eq. S9) \quad 1 - 2\Theta_{*} = \exp(-2 \cdot k_{chem} \cdot t)$$

Chapter 4

4. Towards quantitative understanding of light alkene cracking on zeolites - case of 1-pentene on HZSM5

This chapter is based on:

S. Schallmoser, M. Sanchez-Sanchez, A.C. van Veen, J.A. Lercher, “*Elementary steps in light olefin cracking on ZSM-5*”, paper ready for submission.

Abstract: The elementary steps of 1-pentene cracking on MFI type zeolites are exemplarily explored as a model for cracking of light alkenes via carbenium ions. Pathways for monomolecular cracking and for dimerization followed by cracking were qualitatively and quantitatively identified on a molecular level. The intrinsic activation barrier for monomolecular cracking for pentene varied between 208 and 219 kJ/mol, which is somewhat higher than the true activation energy for n-pentane cracking. The almost 40 times higher rate of cracking compared to pentane is attributed to the higher coverage of pentene resulting from its two-fold higher heat of chemisorption. In absence of extra-framework Al species all BAS are equally active for 1-pentene cracking. The presence of extra-framework Al in proximity of BAS leads to high initial activity, but lower catalyst stability with time on stream.

4.1. Introduction

The transformation of alkenes on acid catalysts involves a multitude of reactions including isomerization, hydride transfer, oligomerization and cracking.^{1,2} Despite the fact that these reactions are widely practiced, surprisingly little detailed kinetic information is available, linking the elementary steps of the reaction to properties of Brønsted acid sites and the reaction environment.³⁻¹⁰ This insight is, however, important to develop more active and selective catalysts for a large variety of reactions. A particular case is the rising global demand for propene, which has led to vivid interest in cracking of less valuable light alkenes over the last years.^{1,3,4,11}

H-ZSM-5 has been an industrially established additive to enhance propene production in fluid catalytic cracking.³ Its three dimensional pore structure consists of interconnecting sinusoidal and straight 10-membered ring channels.¹² The active sites for cracking in such a catalyst are Brønsted acid sites (BAS).^{2,4} Adsorption of short chain alkenes on these acid sites is described by two steps, (i) the interaction of the alkene double bond with the BAS forming a π -complex followed by (ii) the addition of the acidic proton to the double bond.¹³⁻¹⁵ The nature of the resulting chemisorbed species on the surface of the solid acid is debated. It has been proposed to be a covalently bound alkoxide (alkyl silyl ether) or an ion pair (carbenium ion).^{13,16-19} To date, the adsorption of alkenes in zeolites, with the exception of a series of NMR studies, has been predominantly theoretically addressed.^{13,15,19-21} In a very recent contribution we studied experimentally and theoretically the elementary steps of the adsorption of 1-pentene on H-ZSM-5 and determined the heat of chemisorption (-129 kJ/mol).²²

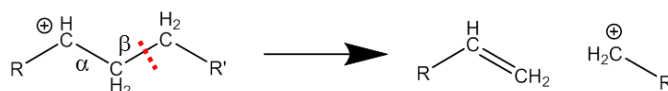


Figure 4.1: Illustration of protolytic alkene cracking (carbenium ion) following the empiric β -scission rule.

Because of the apparently well-established catalytic chemistry catalyzed cracking of alkenes were only infrequently studied during the last 20 years.³⁻¹⁰ Cracking of alkenes proceeds through scission of a C-C bond of the carbenium ion in the β -position relative to the positive charge (Figure 4.1).⁴ A free alkene and a chemisorbed carbenium ion are formed. The latter could either desorb producing a second alkene, crack further via β -scission or be alkylated by another alkene.⁴ Most of the studies have focused on the cracking of 1-butene, which proceeds via dimerization and subsequent cracking of the dimer.⁶⁻⁸

The most complete study on olefin cracking by Buchanan et al.⁴ discusses in detail the impact of cracking pathways of C₅ to C₈ olefins on the overall rate via analyzing the possibilities to crack from energetically favored isomers to energetically favored products without, however, considering the quantitative aspects (variations in the energies of activations) these pathways imply. It is interesting that similar strategies have been used to rationalize alkane hydrocracking (the rate determining step being considered to be olefin cracking) again without considering the implications for the energies and entropies of activation. Moreover, this study⁴ addresses the remarkable differences in activity of alkane (transition via carbonium ion) and alkene (carbenium ion) cracking, though not providing explanations for the observed higher activity of olefins.

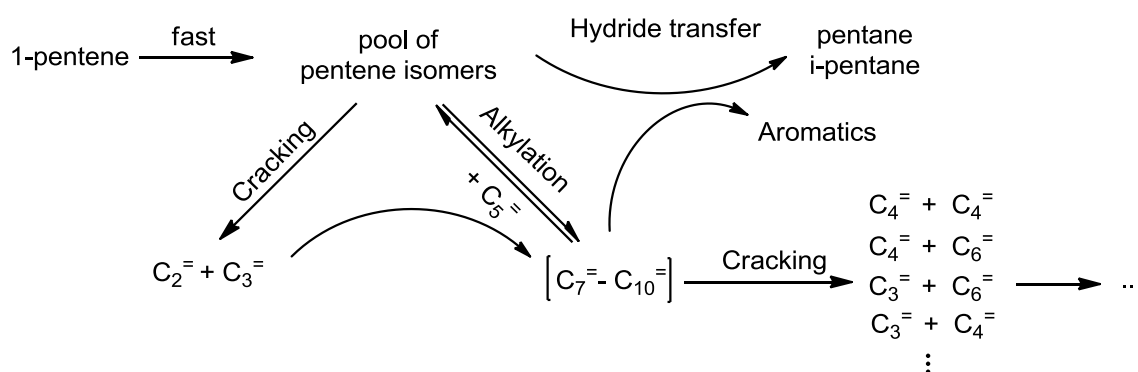
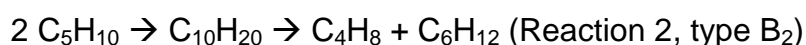
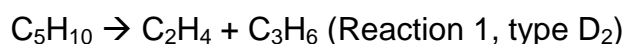


Figure 4.2: Simplified scheme of possible pathways in 1-pentene cracking on acidic catalysts (Adapted from refs. ^{3,23}).

Mechanistically, cracking of 1-pentene is interesting, because in contrast to butene, two principal pathways coexist. Reaction 1 exemplifies the monomolecular cracking pathway, Reaction 2 dimerization/oligomerization followed by cracking.^{3,4} Figure 4.2 illustrates further possible pathways and side reactions commonly observed for pentene cracking on acid catalysts/zeolites. Especially for higher conversions, also the primary products (ethene, propene, butenes) are subject to further alkylation and subsequent cracking of the formed larger alkenes.^{3,4}



Olefins can form several types of carbenium ions with differing relative stabilities (primary, secondary and tertiary). Buchanan et al.⁴ introduced a refined nomenclature for the various types of β -scission that can be observed in olefin cracking reflecting the different reactivities of carbenium ions involved throughout cracking. We adopt this nomenclature. Hence, Reaction 1 can be classified as type D₂ (cracking of a secondary carbenium ion to a primary carbenium ion, Figure 4.3). A special case for this type of reaction is the type D₃ which results in formation of a CH₃-carbenium ion (Figure 4.3). For reaction 2 (dimerization cracking) a large number of C₁₀ olefins that are formed from six different pentene isomers need to be considered. Nevertheless, the dominant transitions will involve cracking from a tertiary carbenium ion to a secondary, assuming that dimethyl substitution is due to pore restrictions within the zeolite improbable. Therefore we classify this reaction as type B₂.

Please note that observed reactivity of the different pathways follows generally the order: B > D.⁴ Buchanan et al.⁴ attribute this to a difference in population of the different carbenium ions (e.g. tertiary carbenium ions are more stable than secondary), without further analyzing the intrinsic energetic barriers of these pathways.

Parallel acid catalyzed isomerization of the alkenes must be also considered in zeolites. At the reaction temperatures used for cracking ($T > 673$ K) isomerization (of 1-pentene) will occur faster than cracking; above 553 K both double bond and skeletal isomerization are equilibrated.²⁴ Therefore, the presence of six pentene isomers has to be included in mechanistic considerations. The different pentene isomers react differently with BAS (Figure 4.3). Upon protonation, primary carbenium ions are not formed under the reaction conditions used.⁴ While the skeletal isomers of 1-pentene are able to form (more stable) tertiary carbenium ions, cracking of these intermediates via β -scission results for all cases in the energetically unstable CH_3^+ fragment (type D₃).⁴ In view of these considerations, we hypothesize that only linear isomers of 1-pentene undergo direct monomolecular cracking.

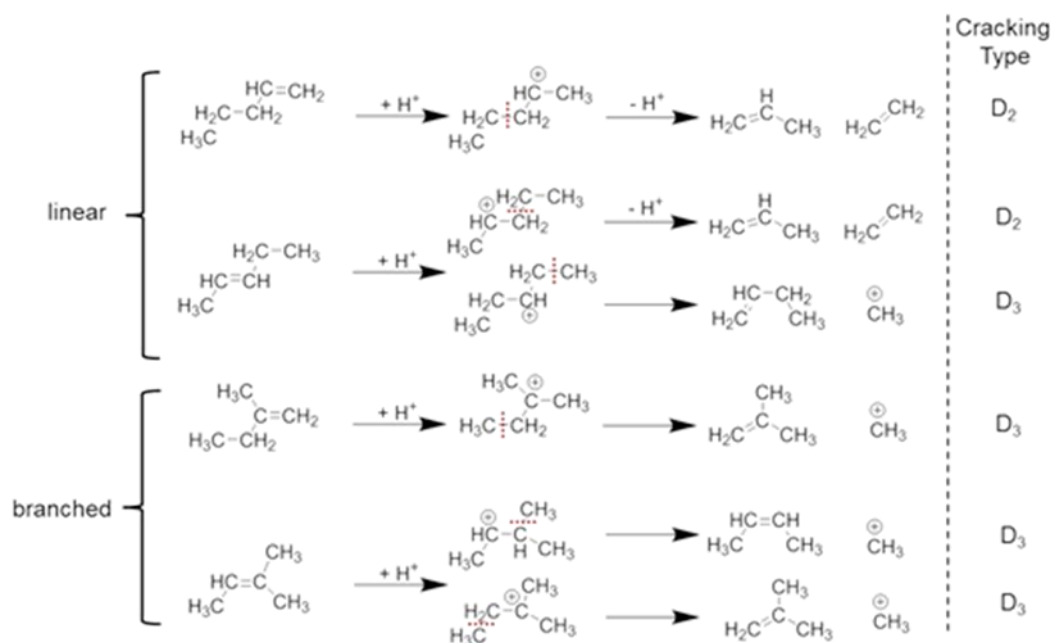


Figure 4.3: Possible cracking paths of pentene isomers via direct β -scission.

Understanding alkene cracking encompasses, however, not only the analysis of the cracking pathways, but also the elucidation of the impact of the zeolite characteristics on the activity and selectivity. For alkane cracking, the intrinsic activity of acid sites seems to depend markedly on the overall concentration of these sites as well as on the local environment of the catalytically active BAS.²⁵⁻²⁸ Recently, we have shown that extra-framework Al (EFAI, Al_xO_y

species which is not incorporated into the zeolite framework), sites in the proximity of BAS causes a drastic increase in catalytic activity of MFI with higher Al concentrations.²⁸ Here, we use this series of MFI type zeolites with varying acid site concentration to study catalytic cracking of pentene, which is one of the simplest examples of alkenes.

The high reactivity of olefins and the associated difficulty of measuring detailed adsorption energies and structures have so far prevented a microscopic analysis of individual reaction steps in alkene cracking. In turn, this has led to an unusually high degree of speculation with respect to the importance of these adsorption structures, the steric constraints in which the reaction takes place and the associated enthalpic and entropic factors determining the reactivity of a particular alkene. Using recently derived insight about the nature of adsorbed pentene and the associated thermodynamic parameters, pentene cracking has been qualitatively and quantitatively analyzed as a case study for the conversion of light alkenes on medium pore zeolites.

4.2. Experimental

Catalysts

Ten MFI zeolites were studied, the samples being designated as MFI-X, with “X” relating to their overall atomic Si/Al ratio. Five commercial H-ZSM-5 samples were provided by *Zeolyst International* (MFI-15 = CBV3024E, MFI-25 = CBV5524G and MFI-40 = CBV8014) and Clariant AG (MFI-60 and MFI-90). In addition, two H-ZSM-5 catalysts with a low Al content (MFI-470 and MFI-230) were synthesized following a procedure described earlier.²⁸

Samples

MFI-15 and MFI-25 were additionally chemically modified in order to reduce the concentration of EFAI using ammonium hexafluorosilicate (AHFS).²⁸ These samples were denoted as MFI-15-AHFS and MFI-25-AHFS. Static calcination (self-steaming) of MFI-15 was used to increase the concentration

of EFAI with respect to the total BAS.²⁸ This sample was denoted as MFI-15-ST.

Kinetic measurements of 1-pentene cracking

Cracking of 1-pentene at atmospheric pressure was studied over H-ZSM-5 (250 – 315 μm pellets, 10 mg – 150 mg) charged with SiC dilution (250 – 315 μm fraction, 290 mg – 150 mg) into a quartz tube ($\varnothing = 6$ mm). The temperature was measured at the wall of the quartz tube. Prior to the kinetic measurements, the catalysts were activated in synthetic air (30 mL/min) at 843 K for 2 h. After flushing for 30 min with N_2 , evaporated 1-pentene (>99.3% purity) was introduced in a mixture with N_2 (total flow 100 – 400 mL/min, 1-pentene concentration 0.05 – 12 vol.%) at atmospheric pressure. The product stream was analyzed online with a gas chromatograph (Agilent 7890A) with DB-1, HayeSepQ and Molecular Sieve 13X columns separating the product stream. The gas chromatograph was equipped with FID and TCD detectors for analysis of all products including non-carbonaceous compounds. In the first step, deactivation was investigated for MFI-90. After 6 h time on stream (TOS), the pentene consumption rate decreased by 15 % of its initial value, and deactivation was found to be in quasi steady state (Figure S1, less than 5 % activity loss in the following 10 h TOS). Therefore, the catalyst was allowed to run for 6 h prior to all measurements determining kinetic parameters.

Isomerization among the six pentene isomers is expected to be faster than cracking, implying that the ratio between the six isomers should approach thermodynamic equilibrium values. This assumption was verified analyzing the cracking effluent at 763 K: For conversions larger than 2 %, linear and branched pentene isomers were equilibrated (Figure S2) and even for conversions below 2 %, only a small deviation from the equilibrium towards linear isomers was observed. Consequently, all pentene isomers are treated as one indistinguishable pentene pool for further kinetic analysis. Conversion X is reported according to equation 1, lumping the pentene isomers.

$$X = 1 - \frac{\sum C(\text{pentene isomers})}{C_0(1 - \text{pentene})} \quad (\text{Equ. 4.1})$$

Activation energies and reaction orders were determined after 6 h time on stream (TOS) for MFI-90 in the range of 707 K – 843 K. Impact of catalyst deactivation on the measurements was ruled out by randomly changing the reaction temperature for determining activation energies. Blank reactor experiments were performed to exclude contributions of gas phase reactions. Absence of internal mass transport limitations was confirmed evaluating the Weisz-Prater criterion (see Supporting Information S.1).²⁹

For the highly active samples (MFI-15, MFI-25 and MFI-15-ST) dilution with silica (Aerosil 300) was necessary in order to assure a homogeneous distribution in the reactor bed. For doing so, 250 mg of silica were mixed carefully in a mortar with 25 mg of zeolite. The resulting powder was used for pelletizing. Blank tests showed that pure silica was inactive for 1-pentene cracking at 763 K. Due to the strong deactivation, temperature dependence of the rate constants was determined for the MFI-15 series by reactivation at 550 °C in a flow of synthetic air (30 ml/min; 10 K/min, 1h) before each temperature step. Rates for each temperature were then extrapolated to initial TOS. These extrapolated values were used for the Arrhenius evaluation to determine the corresponding activation energies.

In order to compare the activity of samples with varying Al concentration in the lattice and after chemical modifications to vary the extra-framework Al, reaction rates were determined at a conversion of 4 – 5 % at 763 K. Also in this case the rates were extrapolated to 0 min TOS in order to avoid differences induced by different rates of deactivation.

IR spectroscopy

The nature and concentration of acid sites was analyzed by IR spectroscopy of adsorbed pyridine following the procedure described earlier.³⁰ Briefly, Brønsted acid sites (BAS) and Lewis acid sites (LAS) are determined upon

adsorption of pyridine at 423 K and subsequent outgassing for 1 h. Strong Brønsted acid sites (SBAS) and strong Lewis acid sites (SLAS) were determined by heating the sample to 723 K (10 K/min) for 30 minutes and quantifying the remaining adsorbed pyridine after subsequent cooling to 423 K.

Elemental analysis

The elemental composition of the samples was determined by atomic absorption spectroscopy in a Unicam M Series Flame-AAS equipped with an FS 95 autosampler and a GF 95 graphite furnace.

XRD

X-Ray powder diffraction determined the crystal structure for all samples. The Philips X'Pert Pro instrument used Cu-K α radiation of 0.154056nm (45 kV and 40 mA) and a rotating powder sample holder applying a step size of 0.019° /s in the 2 θ range of 5° to 70°.

4.3. Results and discussion

4.3.1. Analysis of the reaction network of 1-pentene cracking

To derive the complex reaction network, 1-pentene cracking was studied on MFI-90. Physicochemical properties of the zeolite sample are summarized in Table S1. Ethene, propene, butenes and hexenes comprised about 95% of all products (Figure 4.4). Cyclopentane was observed as a further significant product (~3 %). Additionally, traces of pentanes, methane, higher alkenes and aromatics were detected, as well as molecular H₂. For the study of the cracking reaction pathways, only the main products will be considered.

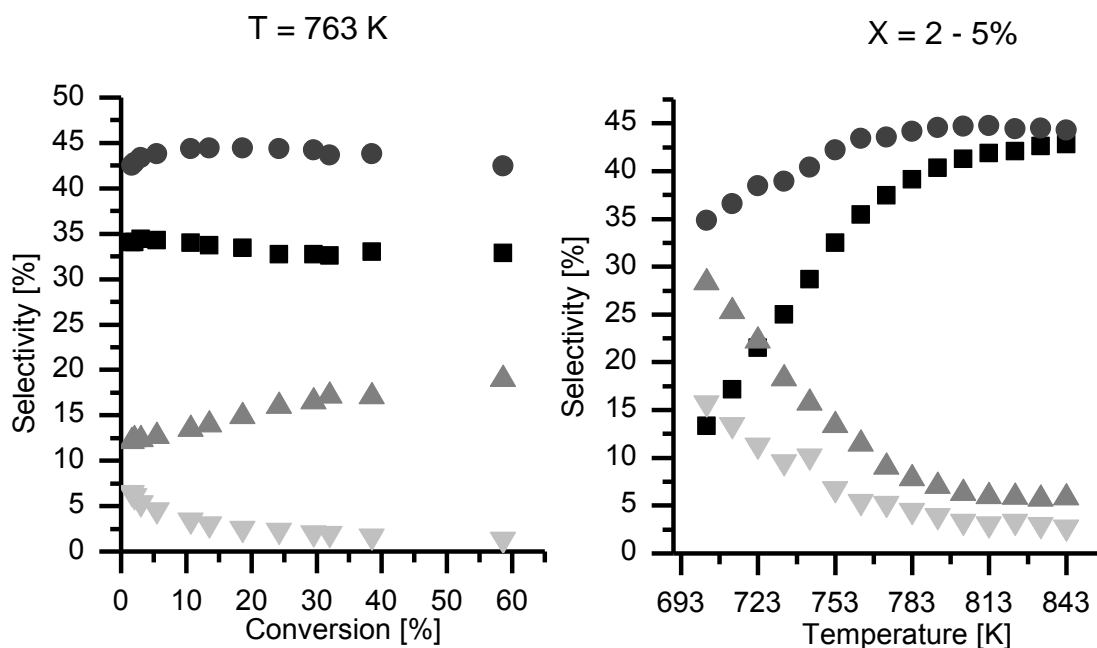


Figure 4.4: Product distribution of the main products as a function of pentene conversion (a) and temperature dependence of product distribution at low conversions (b). (●= propene, ■= ethene, ▲ = butenes, ▼= hexenes)

Figure 4.4 (a) depicts the dependence of the selectivities towards main products as a function of pentene conversion. Selectivity to butenes increased from initially 12 % to almost 20 % at 60% conversion, while in parallel the concentration of hexenes in the products decreased from initially 7 % to a value close to zero. The selectivity to ethene declined slightly from initially 34.5% to 32.5% over the conversion range studied. Propene selectivity passed a broad maximum ($S = 44.5\%$) at 15% conversion.

The shift of product distribution at high conversions, especially in the case of butene selectivity, is attributed to the alkylation of pentene isomers with initially formed light alkenes (especially ethene and propene), as indicated in Figure 4.2. The formed higher alkene intermediates ($C_7^=$ to $C_9^=$) crack subsequently to form butenes at the expense of short chain alkenes. It has to be noted that alkenes with more than six carbon atom were not observed in significant concentrations. It is generally expected that cracking activity increases with increasing chain length.⁴ Therefore, long chain alkenes crack

readily into shorter fragments in this temperature range preventing them from existing at considerable concentrations in the zeolite framework.

Temperature variation at low initial conversions (Figure 4.4b) showed a preferential formation of propene and ethene over butenes and hexenes at temperatures higher than 723 K. At temperatures above 773 K more than 81 % of all formed products were ethene and propene. Selectivity to products stemming from the dimerization cracking pathway dropped drastically with increasing temperature, i.e., selectivity to butenes (hexenes) dropped from 28% (16%) at 703 K to 6% (3%) at 843 K, as bimolecular dimerization reaction is thermodynamically disfavored at higher temperatures.⁴ Selectivities towards the main products reached constant values at temperatures above 798 K.

Considering reactions (1) and (2) as the only pathways for the formation of the main products, selectivities towards butenes and hexenes must vary in parallel, as should selectivities to propene and ethene. The product distributions (Figure 4.4) do not correspond to the stoichiometry of (1) and (2) for a wide range of temperatures and conversions. For instance, at 763 K and low conversions, selectivity to propene was 8.5 % higher than the selectivity to ethene (S_{ethene}), and S_{butene} was 5 % higher than S_{hexene} . The ratio between these differences was very close to 2:1. At low conversions the selectivity difference of the two products from the same pathway (ethene/propene for monomolecular cracking; butene/hexene for dimerization cracking) are satisfactorily explained by cracking of hexene to propene, consuming hexene (at the expense of butane) and adding propene but not ethene.⁴



In the temperature range of 703 K – 843 K, a kinetic regime with a reaction order close to one was observed for ethene formation via monomolecular pentene cracking (Type D₂). This implies that not desorption of the products

but cracking itself is the rate determining step. The apparent activation energy calculated was 79 kJ/mol (Figure S3, Table 4.1). For comparison, the kinetic analysis of the protolytic cracking of n-pentane was taken from ref. ²⁸ and the results are summarized in Table 4.1.

Table 4.1: Overview of apparent and intrinsic activation energies, reaction order (RO) and rate constants determined for the different pathways in 1-pentene cracking (upper section) and protolytic n-pentane cracking (lower section).

Pathway	T [K]	E _{a,meas} ^a [kJ/mol]	E _{a,int} [kJ/mol]	RO [-]	k _{meas} [mol/mol _{BAS} s bar] ⁽²⁾
Monomolecular Cracking					
Type D ₂	703 – 843	79	208	1	1.1 ^b
Dimerization cracking					
Type B ₂	703 – 733	-71	214	2	13.2 ^c
Monomolecular Cracking					
Type D ₃	813 – 843	90	219	1.2	0.60 ^d
n-Pentane cracking^e	753 – 793	129	192	1	0.03 ^b

^aError ± 4 kJ/mol; ^b at 773 K; ^c at 733 K; ^d at 813 K; ^e sum of all cracking pathways as determined for n-pentane cracking.

In the case of the butene formation rate two different cracking pathways (B₂ and D₃) are monitored depending on the temperature range studied. The reaction order for dimerization cracking is two between 703 K and 733 K. For monomolecular cracking (type D₃) a reaction order of close to one is observed between 813 K and 843 K (Table 4.1). The Arrhenius type plot for butene formation (Figure 4.5) reflects also the transition between dimerization cracking (type B₂) and monomolecular cracking (Type D₃). Dimerization cracking (703 K – 733 K) gives a negative apparent activation energy of -71 kJ/mol whereas monomolecular cracking (Type D₃, 813 K – 843 K) shows a positive apparent activation energy of 90 kJ/mol.

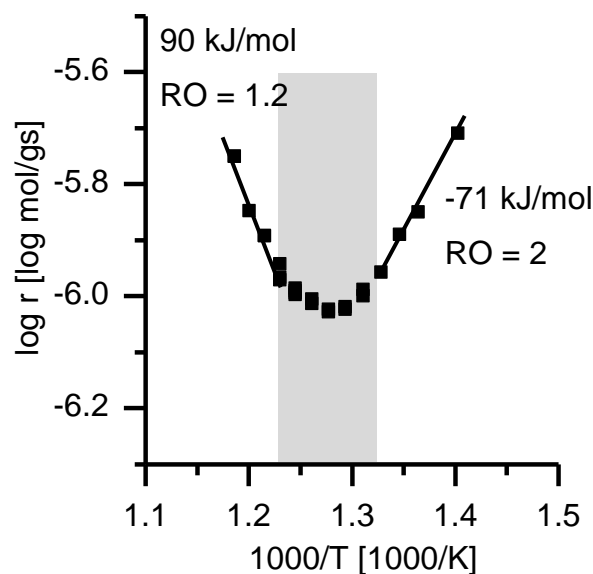


Figure 4.5: Arrhenius type plot for dimerization cracking of 1-pentene (butene formation rate) in the temperature range of 703 K – 843 K.

In order to understand the negative apparent activation energy observed for dimerization cracking, Figure 4.6 illustrates one possible pathway in the bimolecular cracking of pentene. All pathways must have three common sequential steps prior to cracking. First, one pentene molecule is chemisorbed and the second is presumably physisorbed close by and mainly interacting with the zeolite wall. The second step is the dimerization. Finally,

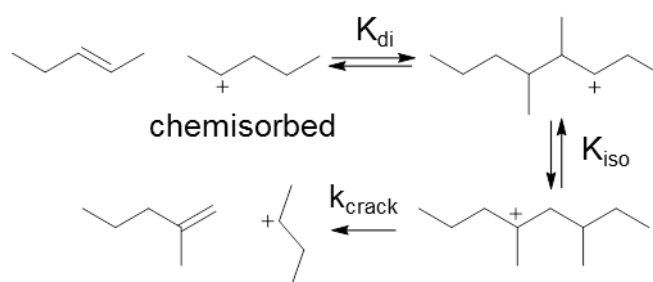


Figure 4.1: Illustration of a possible dimerization cracking pathway resulting in butene and hexene starting with 2-pentene as formed in the preceding rapid isomerization.

an isomerization (H-shift or methyl-shift) is required as cracking via β -scission would otherwise result in reconstitution of pentene and would hence not be reflected in the observed rate. The isomerized C₁₀ species cracks

preferentially into hexene and butenes. The cracking step of the isomerized decene molecule can be assumed to be rate determining. Considering the second pentene molecule as physisorbed, cracking rates for the suggested bimolecular mechanism can be described by Equ. 4.2 (for details Supplementary Information S.2). Accordingly, the measured activation energy encompassed, besides the actual intrinsic barrier, also the enthalpic contributions from chemisorption, physisorption, dimerization and isomerization (Equ. 4.3).

$$r_{\text{crack}} = K_{\text{chem}}K_{\text{phy}}K_{\text{Di}}K_{\text{iso}}k_{\text{crack}} (p_{\text{C5=}})^2 \quad (\text{Equ. 4.2})$$

$$\Delta E_{\text{a,meas}} = \Delta H_{\text{chem}} + \Delta H_{\text{phy}} + \Delta H_{\text{Di}} + \Delta H_{\text{iso}} + H_{\text{crack}} \quad (\text{Equ. 4.3})$$

It has been shown earlier that the overall enthalpy for dimerization of linear pentene (including chemisorption, dimerization and isomerization) is 285 ± 7 kJ/mol.²² With a ground state of the cracking intermediate of about 285 kJ/mol below the 1-pentene gas phase state and a measured activation energy of -71 kJ/mol, the true intrinsic barrier of bimolecular cracking amounts roughly to 214 kJ/mol (Table 4.1).

4.3.2. Intrinsic barriers in alkene cracking

With the heat of chemisorption for 2-pentene established (129 kJ/mol) we are now in the position to gain insight into intrinsic enthalpic barriers ($E_{\text{a,int}}$) of monomolecular alkene cracking according to β -scission mechanism (Table 1). Similar to the analysis for alkane cracking, the coverage of 1-pentene is low at the high reaction temperatures as shown by the perfect first order in cracking. Therefore equation 4.4 can be used to calculate the intrinsic energetic barrier.³¹

$$E_{\text{a,int}} = -\Delta H_{\text{ads}} + E_{\text{a,meas}} \quad (\text{Equ. 4.4})$$

This leads to a value of $E_{\text{a,int}} = 208$ kJ/mol, which is 16 kJ/mol higher than that reported previously for n-pentane cracking and confirmed experimentally with

the same catalyst ($E_{a,int} = 192 \text{ kJ/mol}$).²⁸ The slightly higher energy of activation for alkene than for alkane is attributed to differences in the carbocations formed in the transition state. For alkane cracking, addition of the proton to the C-C bond (non-classical pentacoordinated carbonium ion) affects directly the α -bond to be cleaved.^{2,32} In contrast, upon addition of the proton to an alkene, the C-C bond in direct vicinity of the positive charge is shortened (*i.e.*, strengthened) and concomitantly the bond in the β -position to the positive charge is weakened.³³ However, the latter effect is expected to be less pronounced than the weakening of C-C bond in the carbonium ion. Theoretical studies predict values in the range of 185 - 289 kJ/mol for alkenes cracking via β -scission³³⁻³⁵, which is in the range of our findings.

On the other hand, the rate constant obtained for monomolecular pentene cracking was approximately 40 times higher compared to n-pentane cracking (adding up all cracking pathways) over the same catalyst (Table 4.1). This is in good agreement with the paper of Buchanan et al. ($k_{\text{pentene}}/k_{\text{pentane}} = 32$).⁴ As the intrinsic enthalpic barrier is higher for pentene compared to n-pentane cracking, the higher rate of the former is attributed to a higher population of the reacting species in the ground state. The heat of chemisorption of pentene ($\Delta H_{ads} = -129 \text{ kJ/mol}$) is more than twice that of n-pentane ($\Delta H_{ads} = -62 \text{ kJ/mol}$) leading to a much higher equilibrium constant for pentenes³⁶

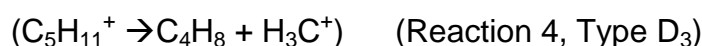
$$K_{ads} = \exp\left(\frac{\Delta H_{ads}}{RT} + \frac{\Delta S_{ads}}{R}\right) \quad \text{(Equ. 4.5)}$$

Using the theoretical and experimental values from de Moor et al. for n-pentane, one obtains for the adsorption constants^{15,36} $K_{\text{pentane}} = 0.01$ and $K_{\text{pentene}} = 13.0$ at 773 K. Considering the intrinsic activation energies (Table 4.1) for 1-pentene and n-pentane cracking an expected rate ratio can be calculated according to Equ. 4.6. If preexponential factors are assumed to be of the same order of magnitude, alkene cracking rate is expected to be 94 times (at 773 K) faster than alkane cracking. This fits with the experimentally observed rate ratio of about 40.

$$\frac{k_{alkene}}{k_{alkane}} = \frac{K_{alkene} \cdot A_{0,alkene} \cdot \exp\left(\frac{-E_{alkene,int}}{RT}\right)}{K_{alkane} \cdot A_{0,alkane} \cdot \exp\left(\frac{-E_{alkane,int}}{RT}\right)} \quad (\text{Equ. 4.6})$$

It is moreover interesting that the intrinsic barrier of the dimerization cracking pathway which involves cracking of branched decene isomers (dominated by type B₂ - cracking from tertiary to secondary carbenium ions, E_{a,int} = 214 kJ/mol) is comparable to that of linear pentene molecules (type D₂, cracking from secondary to primary carbenium ion, E_{a,int} = 208 kJ/mol). We assume that in both cases cracking of the carbenium ion is the rate determining step. In order to explain the observed reactivity differences of the different pathways (type B > type D) as described by Buchanan et al.⁴ a difference in the intrinsic enthalpic barrier cannot be used as argument. Our results point simply to the fact that a difference in surface coverage or population of the different carbenium ions or alkoxides is mostly responsible for the difference in activity. As reaction order is in both cases positive, an increased surface population affects the rate directly.

Monomolecular cracking (type D₃) accounts to butene formation in the high temperature regime (813 K – 843 K). Selectivities of ethene and propene were almost equal accounting for 81 % - 90 % of all products formed. The bimolecular cracking is concluded to be highly disfavored at high temperatures as the entropy loss (ΔS°) upon dimerization becomes dominant in the free energy term (ΔG° = ΔH° - TΔS°), being replaced to a low extent by a monomolecular pathway comprising of cracking of a C₅ carbenium ion into butene and a methoxy group.



The intrinsic energy barrier for this pathway was 11 kJ/mol larger than the barrier for Reaction 1 (Table 4.1). This is attributed to the formation of the energetically disfavored CH₃⁺. The methoxy species reacts with pentene, present in large excess in the zeolite pores, forming hexene.

4.3.3. Impact of Al content and presence of EFAI on 1-pentene cracking

At this point the question arises, whether or not the concentration of aluminum in the zeolite lattice leads to differences in the rate of cracking. The impact of the Al density was studied at 763 K. Figure 4.7 shows a linear activity/SBAS concentration correlation for samples with relatively low SBAS content ($< 400 \mu\text{mol/g}$) which passes through the origin. This is in good agreement with our previous observations for n-pentane cracking,²⁸ and clearly indicates that all SBAS are active and equally active in catalytic cracking of alkenes. It is also interesting to note, that the pathway selectivity (monomolecular cracking – dimerization cracking) seems to be independent of BAS concentration as can be deduced from Figure 4.7.

Deviations from the linearity observed in Figure 4.7 for samples with higher Al content are attributed to the presence of EFAI species in proximity of SBAS (SBAS-AIOH). Detailed information on the characteristics of the zeolite samples employed in Figure 4.7 and Figure 4.8 can be found in ref.²⁸ and Table S1. Briefly, the samples MFI-15, MFI-25 and MFI-15-ST contain EFAI species which give rise to a characteristic O-H band at 3656 cm^{-1} in the IR spectra. By IR spectroscopy of the adsorbed base molecules pyridine and NH_3 it was evidenced that a certain fraction of these sites was in close proximity of SBAS. Such species was found responsible for an enhanced activity in n-pentane cracking by either stabilizing a later transition state or by inducing a higher proton mobility of the zeolitic proton.²⁸

Interestingly, the same rate enhancement effect is also observed for alkene cracking, which proceeds via a completely different transition state (carbenium ion). Further evidence is that the selective removal of EFAI species by ammonium hexafluorosilicate treatment (AHFS) produced samples with identical pentene cracking rate per SBAS than MFI samples with SBAS $< 400 \mu\text{mol/g}$.

Figure 4.8 shows the rate normalized to the concentration of overall SBAS as determined by adsorption of pyridine. The sample MFI-15-ST is about 9 times

more active per SBAS than MFI-15-AHFS. This proves, in good agreement with the results observed for n-pentane cracking, that SBAS-AIOH sites possess a much higher catalytic activity than isolated Brønsted acid sites. Figure S4 shows that the rate enhancement effect is a function of SBAS-AIOH concentration. A comparison with n-pentane cracking indicates that for comparable reaction conditions the relative higher rate of SBAS-AIOH compared to SBAS is slightly higher for alkene cracking (Figure S4).

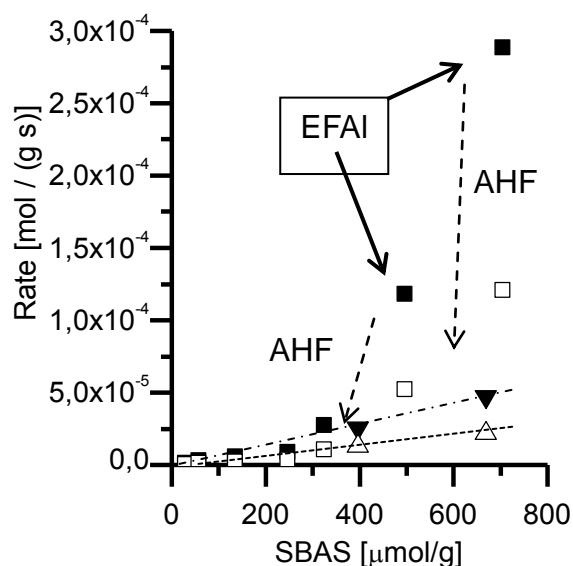


Figure 4.7: Rate of ethene (closed symbols) and butene formation (open symbols) plotted as function of SBAS concentration. Triangles were used to represent the rate determined for AHFS modified samples and dashed arrows indicate the impact of the AHFS modification ($T = 763 \text{ K}$).

Table 4.2 provides an overview of the experimentally determined activation energies for the monomolecular cracking pathway. In good agreement with our previous findings for n-pentane cracking, the more active sites also have a slightly higher apparent energy of activation.²⁸ This is overcompensated by a remarkable increase of the preexponential factor (Equ. 4.7). Hence, the rate enhancement caused by the interplay of SBAS and EFAI sites must be related to an entropic effect (increased A_{meas}) for alkene cracking.

$$r_{\text{meas}} = A_{\text{meas}} \exp(-E_a/RT) \quad (\text{Equ. 4.7})$$

Table 4.2: Overview of apparent activation energies determined for the MFI-15 series

	$E_{a,\text{ethene}}^a$ [kJ/mol]	A_{meas} [mol/(mol _{SBAS} bar s)]
MFI-15-ST	91	$2.7 \cdot 10^7$
MFI-15	86	$6.9 \cdot 10^6$
MFI-15-AHFS	81	$6.6 \cdot 10^5$

^aError \pm 3 kJ/mol

Moreover, the relative butene and ethene selectivities, which are proxies for the bimolecular and monomolecular pathways respectively, were found to be the same in the wide range of SBAS concentrations examined here (Figure 4.7). As seen in Figures 4.7 and 4.8, the presence of EFAl sites did not significantly influence the relative pathway selectivities, i.e., both pathways are accelerated equally by the presence of EFAl. This is especially interesting, as both pathways share a common intermediate – a chemisorbed pentene. This surface species could either crack directly (Reaction 1) or reacts with a second pentene molecule which is physisorbed in the zeolite pore (Reaction 2).

Hence any increase in coverage of the chemisorbed or physisorbed pentene induced by the presence of EFAl sites in proximity of SBAS would explain the rate enhancement for both pathways. A direct evaluation of the coverage of 1-pentene and its isomers is not possible due to the high reactivity of alkenes under the current experimental conditions. For n-pentane cracking, however, adsorption parameters are easily accessible and were found to be comparable within the MFI-15 series.²⁸ While we would presently refrain from postulating the existence of a significantly higher concentration of reacting olefins at the sterically constrained Brønsted acid site (SBAS-AIOH), it should be noted that chemisorption is an activated process and is formed by the reaction of a π -bonded pentene with a BAS.^{37,38} Hence, observations from alkane adsorption have to be transferred with caution to alkene adsorption.

EFAI in the proximity of a SBAS polarizes the zeolite framework resulting in a more delocalized proton in these highly active zeolites, as suggested earlier by us.²⁸ The probability of a successful protonation and hence alkoxide formation (activated transition from the π -complex to the alkoxide) is expected to be increased by the presence of a more delocalized proton, as more modes resulting in proton addition to the hydrocarbon become available. Alternatively we speculate that stabilizing a later, and hence more loose transition state at SBAS-EFAI sites leads to a higher transition entropy and in turn to a higher pre-exponential factor.²⁸

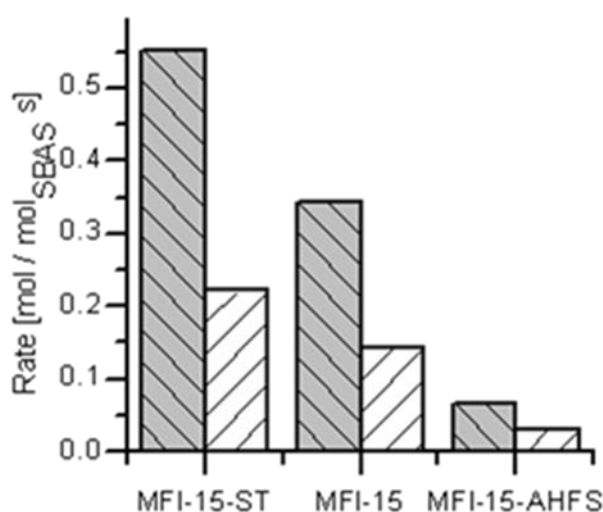


Figure 4.8: Rate normalized to SBAS concentration for the MFI-15 series. Ethene formation rate is represented in grey columns, butene formation rate in white columns. (T = 763 K)

Figure 4.9 illustrates the presumable transition state in alkene cracking. Theoretical calculations point towards formation of a six-ring structure, where two oxygen atoms next to Al are involved.^{33,35} Charge analysis revealed that there is a positive charge located at the hydrocarbon fragment.³⁵ An EFAI species which is located in proximity of a SBAS, and hence in proximity of the transition state complex, could stabilize formation of this transition state and could shift it, in analogy to n-pentane cracking, towards a later transition state pushing further apart the two product-like fragments (ethene and propene).²⁸ This induces more rotational and vibrational degrees of freedom of the fragments and hence transition entropy is expected to increase.

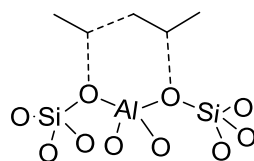


Figure 4.9: Presumable transition state for cracking of a linear pentene molecule catalyzed by a zeolitic BAS.

Taking into account that mono- and bimolecular cracking pathways are equally influenced by the presence of EFAl, this would imply in addition that the impact of EFAl on the nature of the transition state is the same for a C₅ carbenium ion (reaction 1, type D₂) and a C₁₀ carbenium ion (reaction 2, type B₂). Therefore, we prefer currently the model of a more delocalized proton, which affects the common intermediate of both pathways, i.e., the chemisorbed pentene molecule. On the basis of our assumption that for both pathways cracking is the rate determining step, the presence of EFAl might increase the value of K for the alkene chemisorption, which is an activated process, and hence population of the species in the ground state of olefin cracking.

At this point it has to be noted that the phenomenon of rate enhancement is clearly observed for 1-pentene cracking but is not stable with TOS. All samples which contain a clearly detectable concentration of EFAl sites in proximity of SBAS showed a strong deactivation with TOS (Figure S6). This shows clearly that the unique combination of EFAl sites in proximity of SBAS does not only enhance the cracking pathways but also secondary pathways that lead to deactivation. It is interesting to note that such deactivation behavior was not observed for the same samples in n-pentane cracking.²⁸ Hence, deactivation is not associated with thermal instability of these highly active sites.

4.4. Conclusions

The present study provides a qualitative and quantitative description of olefin cracking based on the model olefin 1-pentene. Monomolecular cracking (type D₂, secondary to primary carbenium ion) was followed by studying the ethene formation rate. The reaction order was 1 and the intrinsic activation energy was found to be 208 kJ/mol. Comparison of pentene cracking with pentane cracking shows that the intrinsic activation energy for monomolecular cracking of pentene is 16 kJ/mol higher than that of n-pentane cracking. This implies that carbenium ions are not simply energetically easier to cleave. Consequently, the remarkable differences in the activity of ZSM-5 in protolytic cracking of alkanes and alkenes ($k_{\text{pentene}}/k_{\text{pentane}} = 36$) must be attributed to the higher coverage of the alkene compared to the alkane. The coverage difference is a direct consequence of the higher heat of chemisorption for the alkene (more than twice the heat of adsorption of the alkane).

Our model alkene enables further analysis of a cracking pathway involving carbenium ions with differing stabilities: Dimerization cracking (type B₂, tertiary to secondary carbenium ion) and monomolecular olefin cracking of type D₃ which involves formation of a methoxy species. Both pathways are characterized by butene as key product. Dimerization cracking (type B₂) was observed as the dominant pathway at low temperatures (703 – 733 K) and the reaction order was determined to be two and the apparent activation energy was found to be negative (-71 kJ/mol). The cracking mechanism follows a bimolecular mechanism involving an oligomer intermediate which is not observed in the product spectrum. Cracking of the oligomer (probably a dimer) is the rate determining step. The intrinsic activation energy (214 kJ/mol) of this pathway is somewhat comparable to that of monomolecular cracking (type D₂). This is surprising in the light of the observed rate differences⁴ for these two cracking pathways (B type and D type). Based on our insight we are in the position to attribute this to differences in the population of the ground states (tertiary carbenium ions are more likely to be formed). For higher temperatures (813 – 843 K) butene formation is

dominated by a monomolecular cracking pathway (RO was close to one, $E_{a,int} = 219$ kJ/mol).

Besides the intrinsic properties of the multitude of alkenes observed in 1-pentene cracking, the study covers also the impact of main zeolite characteristics on catalytic activity in alkene cracking. In the absence of EFAl species in proximity of SBAS, all SBAS were found to be active and equally active in alkene cracking for a broad range of framework Al concentrations. When such EFAl species were present, a remarkable rate enhancement was observed which was slightly more pronounced than that observed for n-pentane cracking earlier.²⁸ Besides the cracking pathways, also deactivation pathways were observed to be enhanced by the presence of these sites.

Two possible explanations for the rate enhancement by EFAl in proximity of SBAS are presented: 1) EFAl species stabilizes the charged transition state complex, in analogy to alkane cracking or 2) the presence of more delocalized protons causes an increased coverage of the chemisorbed pentene isomers. The latter possibility offers a straight forward explanation of the equal increase in both monomolecular and bimolecular cracking rates.

Acknowledgements

The authors thank BU Catalysts, Clariant Produkte (Deutschland) GmbH (former Sued-Chemie AG) for the financial support and fruitful discussions in the framework of MuniCat, Martin Neukamm for AAS measurements and Xaver Hecht for N₂ physisorption measurements.

4.5. References

- (1) Rahimi, N.; Karimzadeh, R. *Applied Catalysis A: General* **2011**, 398, 1.
- (2) Kissin, Y. V. *Catalysis Reviews* **2001**, 43, 85.
- (3) Bortnovsky, O.; Sazama, P.; Wichterlova, B. *Applied Catalysis A: General* **2005**, 287, 203.
- (4) Buchanan, J. S.; Santiesteban, J. G.; Haag, W. O. *Journal of Catalysis* **1996**, 158, 279.
- (5) Koyama, T.-r.; Hayashi, Y.; Horie, H.; Kawauchi, S.; Matsumoto, A.; Iwase, Y.; Sakamoto, Y.; Miyaji, A.; Motokura, K.; Baba, T. *Physical Chemistry Chemical Physics* **2010**, 12, 2541.
- (6) Sazama, P.; Dědeček, J.; Gábová, V.; Wichterlová, B.; Spoto, G.; Bordiga, S. *Journal of Catalysis* **2008**, 254, 180.
- (7) Xu, G.; Zhu, X.; Xie, S.; Li, X.; Liu, S.; Xu, L. *Catalysis Letters* **2009**, 130, 204.
- (8) Zhao, G.; Teng, J.; Xie, Z.; Jin, W.; Yang, W.; Chen, Q.; Tang, Y. *Journal of Catalysis* **2007**, 248, 29.
- (9) Zhu, X.; Liu, S.; Song, Y.; Xu, L. *Applied Catalysis A: General* **2005**, 288, 134.
- (10) Miyaji, A.; Sakamoto, Y.; Iwase, Y.; Yashima, T.; Koide, R.; Motokura, K.; Baba, T. *Journal of Catalysis* **2013**, 302, 101.
- (11) Hsu C. S. , R. P. R. *Practical Advances in Petroleum Processing*; Springer; Vol. 1.
- (12) Holm, M. S.; Svelle, S.; Joensen, F.; Beato, P.; Christensen, C. H.; Bordiga, S.; Bjorgen, M. *Applied Catalysis a-General* **2009**, 356, 23.
- (13) Nieminen, V.; Sierka, M.; Murzin, D. Y.; Sauer, J. *Journal of Catalysis* **2005**, 231, 393.
- (14) Sauer, J.; Ugliengo, P.; Garrone, E.; Saunders, V. R. *Chemical Reviews* **1994**, 94, 2095.
- (15) Nguyen, C. M.; De Moor, B. A.; Reyniers, M.-F.; Marin, G. B. *The Journal of Physical Chemistry C* **2011**, 115, 23831.
- (16) Boronat, M.; Viruela, P. M.; Corma, A. *Journal of the American Chemical Society* **2004**, 126, 3300.
- (17) Ishikawa, H.; Yoda, E.; Kondo, J. N.; Wakabayashi, F.; Domen, K. *The Journal of Physical Chemistry B* **1999**, 103, 5681.
- (18) Kondo, J. N.; Wakabayashi, F.; Domen, K. *The Journal of Physical Chemistry B* **1998**, 102, 2259.
- (19) Bhan, A.; Joshi, Y. V.; Delgass, W. N.; Thomson, K. T. *The Journal of Physical Chemistry B* **2003**, 107, 10476.
- (20) Pascual, P.; Ungerer, P.; Tavitian, B.; Pernot, P.; Boutin, A. *Physical Chemistry Chemical Physics* **2003**, 5, 3684.
- (21) Haw, J. F.; Richardson, B. R.; Oshiro, I. S.; Lazo, N. D.; Speed, J. A. *Journal of the American Chemical Society* **1989**, 111, 2052.
- (22) Schallmoser, S.; Sanchez-Sanchez, M.; Lercher, J. A. *Pentene Adsorption* **2014**.
- (23) Höchtel, M.; Jentys, A.; Vinek, H. *Applied Catalysis A: General* **2001**, 207, 397.
- (24) Mäurer, T.; Kraushaar-Czarnetzki, B. *Journal of Catalysis* **1999**, 187, 202.

- (25) Janda, A.; Bell, A. T. *Journal of the American Chemical Society* **2013**, *135*, 19193.
- (26) Yu, Z. W.; Li, S. H.; Wang, Q.; Zheng, A. M.; Jun, X.; Chen, L.; Deng, F. *J. Phys. Chem. C* **2011**, *115*, 22320.
- (27) Xu, B.; Sievers, C.; Hong, S. B.; Prins, R.; van Bokhoven, J. A. *Journal of Catalysis* **2006**, *244*, 163.
- (28) Schallmoser, S.; Ikuno, T.; Wagenhofer, M. F.; Kolvenbach, R.; Haller, G. L.; Sanchez-Sanchez, M.; Lercher, J. A. *Journal of Catalysis* **2014**, *316*, 93
- (29) Weisz, P. B.; Prater, C. D. In *Advances in Catalysis*; W.G. Frankenburg, V. I. K., Rideal, E. K., Eds.; Academic Press: 1954; Vol. Volume 6, p 143.
- (30) Maier, S. M.; Jentys, A.; Lercher, J. A. *The Journal of Physical Chemistry C* **2011**, *115*, 8005.
- (31) Gounder, R.; Iglesia, E. *Journal of the American Chemical Society* **2009**, *131*, 1958.
- (32) Hunter, K. C.; East, A. L. L. *The Journal of Physical Chemistry A* **2002**, *106*, 1346.
- (33) Jeffrey Hay, P.; Redondo, A.; Guo, Y. *Catalysis Today* **1999**, *50*, 517.
- (34) Guo, Y.-H.; Pu, M.; Wu, J.-Y.; Zhang, J.-Y.; Chen, B.-H. *Applied Surface Science* **2007**, *254*, 604.
- (35) Rigby, A. M.; Kramer, G. J.; van Santen, R. A. *Journal of Catalysis* **1997**, *170*, 1.
- (36) De Moor, B. A.; Reyniers, M. F.; Gobin, O. C.; Lercher, J. A.; Marin, G. B. *Journal of Physical Chemistry C* **2011**, *115*, 1204.
- (37) Boronat, M.; Viruela, P.; Corma, A. *The Journal of Physical Chemistry A* **1998**, *102*, 982.
- (38) Kondo, J. N.; Liqun, S.; Wakabayashi, F.; Domen, K. *Catalysis Letters* **1997**, *47*, 129.

4.6. Supporting Information

S.1 – Prater-Weisz criterion for estimation of internal mass transport limitations

$$Wz = \frac{L_c^2}{D_{eff}} \frac{r_{meas} \cdot \rho_{Cat}}{c_{i,0} \cdot \frac{(m+1)}{2}}$$

The Prater-Weisz criterion can be used to estimate presence of internal transport limitations.¹ For $Wz \ll 1$, mass transport limitations can be excluded. In a conservative estimate, the highest rate at 843 K is employed. Moreover, length of the primary zeolite crystals (1 μm) is used as L_c . For D_{eff} a value of $1 \times 10^{-4} \text{ cm}^2/\text{s}$ is employed, which was reported for the large olefin 1-hexene.² Using the catalyst density of $1.8 \times 10^6 \text{ g/m}^3$ and an reactant concentration of 1.2 mol/m^3 we obtain a Wz of 0.003. Internal transport limitations can therefore be excluded.

Symbols:

Wz = Weisz number

L_c = characteristic length [m]

D_{eff} = effective Diffusion coefficient [m^2/s]

r_{meas} = measured apparent rate [mol/g s]

ρ_{Cat} = catalyst density [g/m^3]

m = reaction order (assumed to be one)

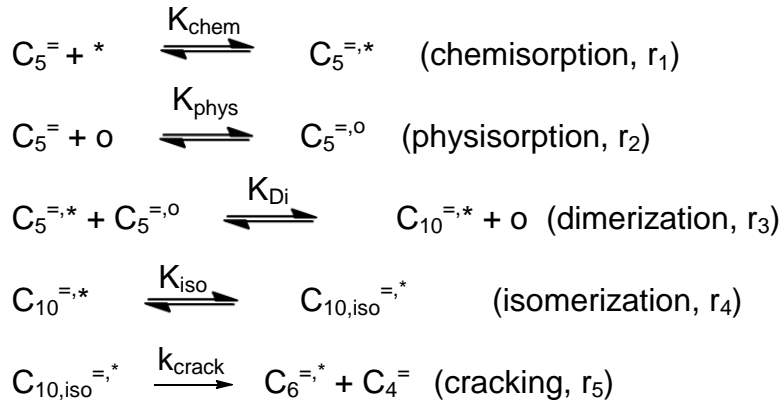
$c_{i,0}$ = reactant concentration [mol/m^3]

(1) Weisz, P. B.; Prater, C. D. In *Advances in Catalysis*; W.G. Frankenburg, V. I. K., Rideal, E. K., Eds.; Academic Press: 1954; Vol. Volume 6, p 143.

(2) Haag, W. O.; Lago, R. M.; Weisz, P. B. *Faraday Discussions of the Chemical Society* **1981**, 72, 317.

S.2 – Derivation of rate expressions for dimerization cracking

Reaction scheme



We tentatively assume that a chemisorbed pentene isomer is alkylated by another adjacent physisorbed pentene molecule. Furthermore, cracking of the formed and isomerized dimer is presumably the rate determining step. All other steps are in quasi equilibrium. Consequently, the net forward rate (r_{crack}) is solely determined by r_5 .

$$r_1 = r_2 = r_3 = r_4 = 0$$

$$r_{\text{crack}} = r_5$$

Considering the high reaction temperature ($T > 703$ K) adsorption can be estimated to be within the linear range of the adsorption isotherm (physisorption and chemisorption) and at low coverages of the pentene isomers. Therefore, a Henry type behavior for adsorption can be assumed.

$$\Theta(C_5^{=,*}) = K_{\text{Chem}} \cdot p_{C_5^=}$$

$$\Theta(C_5^{=,o}) = K_{\text{Phys}} \cdot p_{C_5^=}$$

Deriving the individual rate equation for each reaction step gives:

$$r_3 = k_{\text{di}} \cdot \Theta(C_5^{=,o}) \cdot \Theta(C_5^{=,*}) - k_{\text{di-1}} \cdot \Theta(C_{10}^{=,*}) = 0$$

$$r_4 = k_{iso} \cdot \theta(C_{10}^{=,*}) - k_{iso-1} \cdot \theta(C_{10,iso}^{=,*}) = 0$$

$$r_{crack} = r_5 = k_{crack} \cdot \theta(C_{10,iso}^{=,*}) \neq 0$$

With $K_{Di} = \frac{k_{Di}}{k_{Di-1}}$ and $K_{Iso} = \frac{k_{iso}}{k_{iso-1}}$ we derive the following expression for the

overall rate of cracking:

$$r_{crack} = k_{crack} \cdot K_{Di} \cdot K_{Iso} \cdot K_{chem} \cdot K_{phys} \cdot (pC_{5=})^2$$

All rate and equilibrium constants can be written in an Arrhenius type form:

$$K_i = k_0 \cdot \exp(-\Delta H_i / RT)$$

With the measured rate being defined as

$$r_{meas} = k_{meas} \cdot (pC_{5=})^2 = r_{crack}$$

we get

$$k_{meas} = k_{crack} \cdot K_{Di} \cdot K_{Iso} \cdot K_{chem} \cdot K_{phys}$$

Therefore, using the Arrhenius type form of the rate and equilibrium constants, we obtain

$$E_{a,meas} = \Delta H_{chem} + \Delta H_{phys} + \Delta H_{Di} + \Delta H_{Iso} + E_{a,crack}$$

Symbols:

$\theta(i)$ = surface coverage of species i

K = equilibrium constant

k_i = forward rate constant of step i

k_{i-1} = backward rate constant of step i

H_i = enthalpy of step i

p_{C_5} = partial pressure of 1-pentene

S.3 Reaction enthalpy of dimerization reaction

The dimerization reaction of two 2-pentene molecules will result inter alia in formation of 4,5-dimethyl-3-octene. As thermodynamic data was not available for these branched olefinic C_{10} isomers, the analogue reaction with two butene molecules was used in order to estimate the reaction enthalpy for this dimerization reaction: e.g. $\Delta H_r = -88$ kJ/mol (2 x 2-butene \rightarrow 3,4-dimethyl-2-hexene). HSC Chemistry 6.0 was used.

Table S1: Physiochemical properties of investigated catalysts. Note MFI-15-ST was a different batch with slightly different characteristics when compared to Chapter 2.

Name ^a	S _{BET} [m ² /g]	Si:Al ^a	BAS ^b	SBAS ^b	[μmol/g]		
					LAS ^b	SLAS ^b	BAS ^c
MFI-15	405	15	843	705	213	168	820
MFI-15-AHFS	409	27	717	669	51	36	691
MFI-15-ST	415	17	443	340	245	168	398
MFI-25	425	25	564	496	137	94	538
MFI-25-AHFS	446	26	425	396	31	21	449
MFI-40	425	39	374	324	78	66	353
MFI-60	512	58	286	257	59	39	238
MFI-90	454	88	141	135	33	29	158
MFI-240	431	240	62	57	11	10	68
MFI-470	400	470	30	29	7	3	36

^a Molar ratio of Si and Al determined with AAS.

^b Determined by IR spectroscopy of adsorbed pyridine.

^c Determined by NH₃ TPD.

Figures

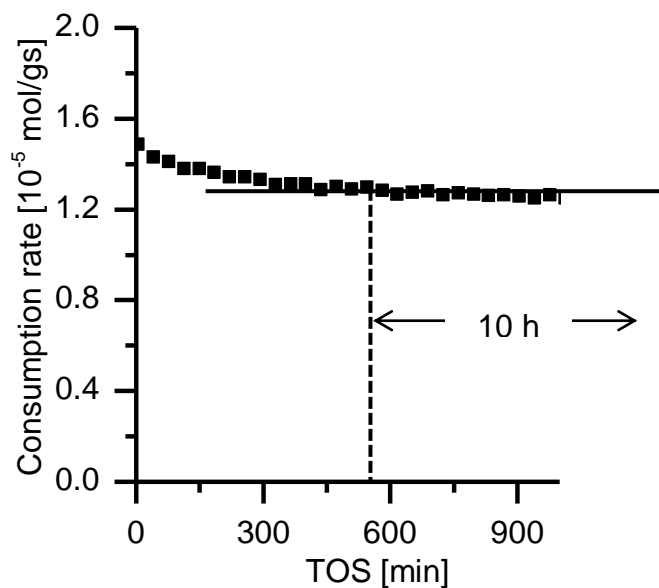


Figure S1: Consumption rate of 1-pentene at 763 K as function of TOS (shown for sample MFI-90).

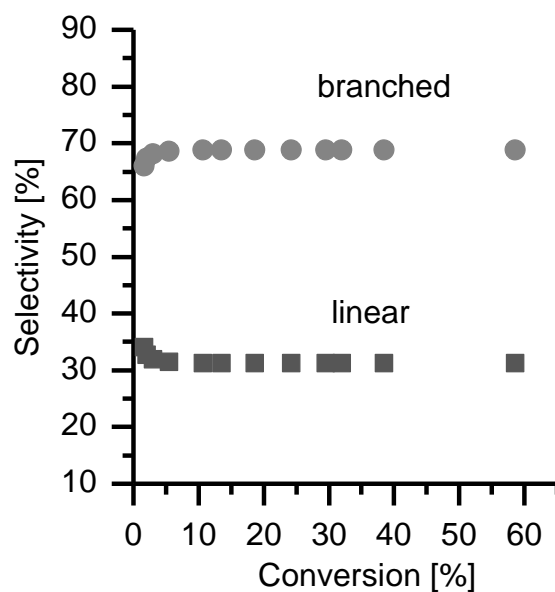


Figure S2: Relative selectivity of branched and linear pentene isomers as function of conversion ($T = 763$ K).

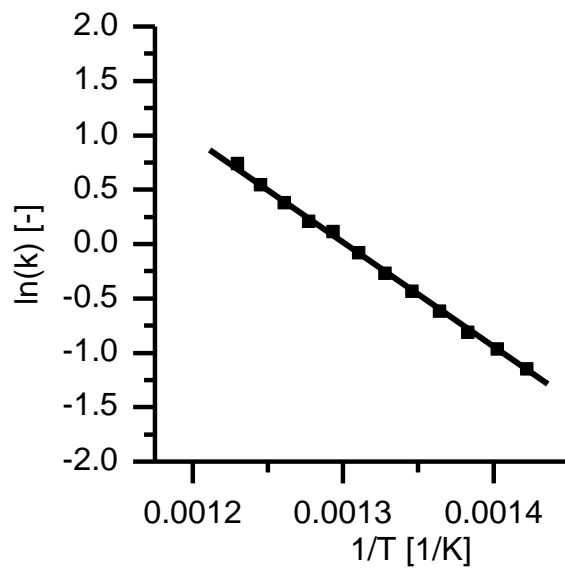


Figure S3: Arrhenius type plot for ethene formation (monomolecular cracking).

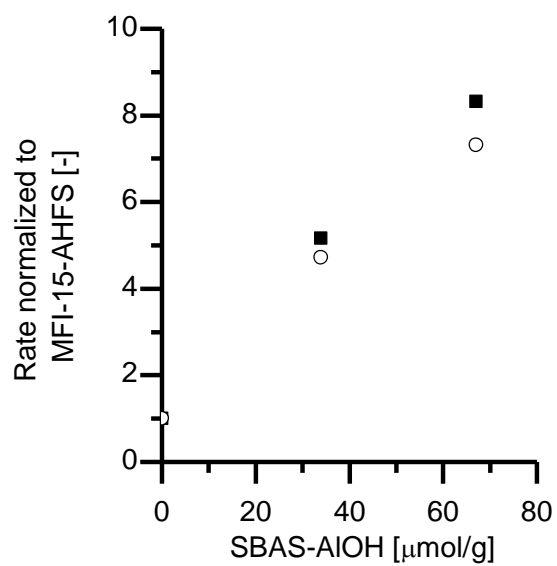


Figure S4: Overall n-pentane cracking (o) and 1-pentene cracking (■) rate normalized to MFI-15-AHFS for MFI-15-series (T =763 K).

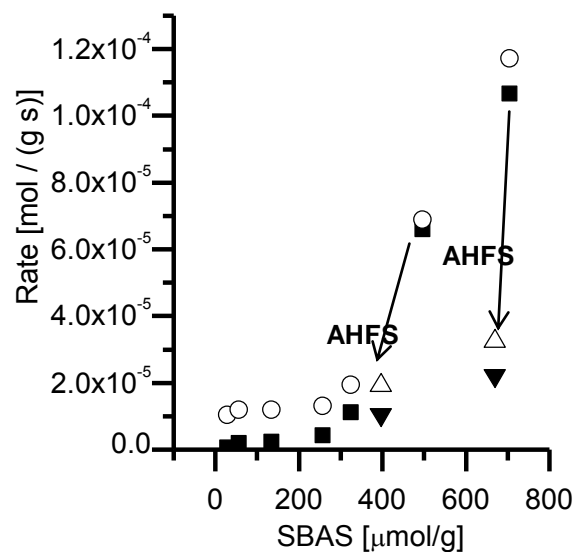


Figure S5: Rate of ethene (closed symbols) and butene formation (open symbols) plotted as function of SBAS concentration. Triangles were used to represent the rate determined for AHFS modified samples and arrows indicate the impact of the AHFS modification ($T = 733 \text{ K}$). Please note that for the sake of readability rate values of butene formation have been shifted by $1.0 \times 10^{-5} \text{ mol / (g s)}$.

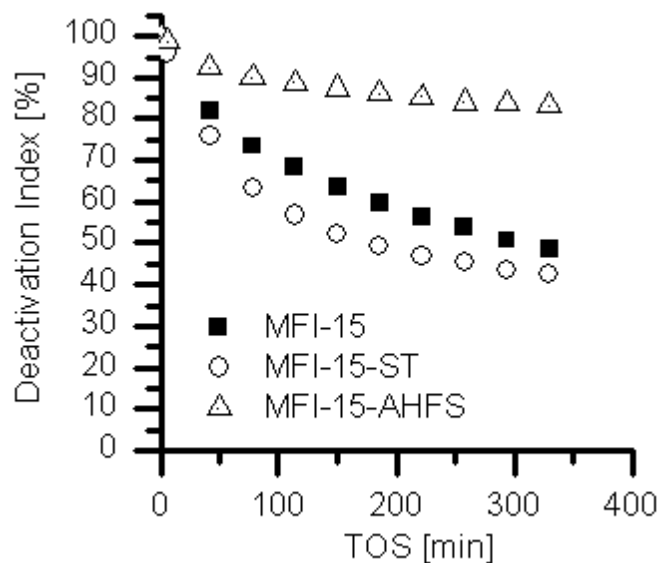


Figure S6: Deactivation behavior of the MFI-15 series ($T=763 \text{ K}$) shown as function of TOS. Deactivation Index represents the rate normalized by the initial activity. Initial conversion was about 5 % for all three samples.

Chapter 5

5. Summary and conclusions

Catalytic transformations of hydrocarbons were investigated over MFI-type zeolites. In the first part of this work (Chapter 2) it was shown that Al defects, which show a characteristic band at 3656 cm^{-1} in the IR spectra, play a crucial role in n-pentane cracking. The concentration of these defect sites could be tuned by chemical modification (AHFS treatment, static calcination). The proximity of those EFAl sites to SBAS was proofed with basic probe molecules (pyridine, ammonia). Zeolite samples which contained those Al-defects showed an overall (per BAS) higher activity. A detailed kinetic analysis of the cracking pathways showed an increased preexponential factor if those EFAl sites were present. It has to be noted that no indication for a change in intrinsic acid strength of the BAS could be observed.

Based on these observations, two models for explaining the rate enhancement effect of this unique interplay of sites have been proposed: A) a stabilization of a later and hence more loose transition state could increase the transition state entropy B) a more delocalized proton would increase protonation probability of the alkane molecule.

The second part (Chapter 3) focuses on understanding of adsorption of olefins on zeolites. Besides MFI, which is industrially very relevant, also FER was investigated. Those two framework types differ with respect to their pore dimensions with FER having the smaller pore diameters. Adsorption of 1-pentene in the 8 and 10 MR pores of FER results in formation of a stable π -complex which is reversibly formed in the temperature range of 323 – 423 K. It is remarkable that the double isomerization occurs rapidly at these

temperatures although there is no evidence for formation of a chemisorbed species.

In the larger 10 MR pores of MFI a different adsorption behavior is observed. Upon initial formation of the π -complex slow dimerization is observed. This surface reaction is characterized by liberation of 50% of the initially covered BAS. A temperature dependent study of this slow surface reaction enabled determination of the activation energy of the dimerization reaction. This observed barrier of 35 kJ/mol corresponds most likely to the carbenium ion formation. Hence, chemisorption itself is an activated process. Theory further supports this assumption. A carbenium ion is the transition state when going from the π -complex to the alkoxide.

A careful analysis of the heats of adsorption in FER and for the overall dimerization reaction in MFI allowed us to deduce adsorption parameters for MFI. For the π -complex values of 85 kJ/mol are estimated, for alkoxide formation 129 kJ/mol. These values will be the basis for the kinetic analysis in 1-pentene cracking.

A detailed kinetic analysis of 1-pentene cracking is presented in the last part of this thesis (Chapter 4). The six isomers of 1-pentene were found to be in thermodynamic equilibrium for the studied temperature range (693 K – 833 K). Hence all pentene isomers could be treated as one pentene pool. Ethene and butenes were identified as key intermediates for monomolecular cracking and bimolecular cracking respectively. For ethene formation one kinetic regime with a reaction order of one and an apparent activation energy of 78 kJ/mol was observed for the entire temperature range.

Butene formation showed clearly two kinetic regimes. For lower temperature a reaction order of two and a negative apparent activation energy of -69 kJ/mol was observed. The negative apparent barrier can be understood in the light of the exothermic dimerization step which precedes the actual rate determining step (cracking). For higher temperatures ($T > 793$ K) a reaction order of one and an $E_{a,meas}$ of 90 kJ/mol is found. Under these conditions

dimerization cracking is disfavored. Direct monomolecular cracking of pentene resulting in a butene molecule and a methyl fragment is an additional pathway which becomes favorable for these conditions.

1-Pentene cracking is found to be 36 times more active than n-pentane cracking. Despite the fact that two different transition states are postulated for n-pentane (carbonium ion) and 1-pentene (carbenium ion) cracking, intrinsic barriers were found to be comparable. Hence, the higher activity of alkenes in the cracking reaction can be mainly attributed to a higher coverage of the alkenes. This is also reflected in the almost double heat of chemisorption.

In good agreement with the findings for n-pentane cracking a similar rate enhancement effect is observed for 1-pentene cracking if EFAl sites are present in close proximity to SBAS. Both cracking pathways (monomolecular and bimolecular cracking) seem to be accelerated equally. Hence it is speculated that the activated formation of a chemisorbed C₅ species, which is a common intermediate of both cracking pathways, is due to the presence of a more delocalized proton favored. Hence an overall higher number of this surface species is expected to be formed if those highly active sites are present.

Chapter 6

6. Zusammenfassung

Die katalytische Umsetzung von Kohlenwasserstoffen wurde an Zeolithen des Typs MFI untersucht. Im ersten Teil dieser Arbeit (Kapitel 2) wird gezeigt, dass Al Defekte – welche im IR Spektrum eine charakteristische Bande bei 3656 cm^{-1} aufweisen - eine entscheidende Rolle im katalytischen Cracken von n-Pentan aufweisen. Die Konzentration dieser Defektzentren konnte durch chemische Modifizierung entscheidend beeinflusst werden. Eine Behandlung mit AHFS erniedrigte die Konzentration dieser Zentren wohingegen statische Kalzinierung zu einer deutlichen Konzentrationserhöhung dieser Defekte führte.

Die lokale Nähe dieser Al-Defekte zu BAS konnte mittels basischer Probenmoleküle (Ammoniak, Pyridin) eindeutig gezeigt werden. In Anwesenheit dieser Al-Defekte wurde eine deutlich erhöhte katalytische Aktivität beim n-Pentan Cracken festgestellt. Eine detaillierte kinetische Auswertung der katalytischen Ergebnisse zeigt, dass bei Anwesenheit dieser Defektzentren vor allem der Präexponentielle Faktor zunimmt. Eine Veränderung der intrinsischen Säurestärke von BAS in Anwesenheit dieser Al-Defekte konnte dabei nicht festgestellt werden.

Basierend auf diesen Beobachtungen wurden zwei Modelle zur Erklärung dieses Phänomens entwickelt: A) ein späterer und damit entropisch begünstigter Übergangszustand wird durch das Zusammenspiel von BAS und Al-Defekt stabilisiert; B) der Al-Defekt begünstigt eine stärkere Delokalisierung des Protons (BAS) und erhöht dadurch die Wahrscheinlichkeit einer erfolgreichen Protonierung und damit einhergehend der Bildung des Übergangszustandes.

Im zweiten Teil (Kapitel 3) wird die Adsorption von Olefinen auf Zeolithen untersucht. Neben MFI, einem industriell sehr relevanten Material, wurden auch die Adsorptionseigenschaften von FER untersucht. Diese beiden Gittertypen unterscheiden sich in ihren Porendimensionen, wobei FER die kleineren Porendurchmesser aufweist. Adsorption von 1-Penten in den 8 und 10 MR Poren von FER führt zur Bildung von stabilen π -Komplexen welche reversibel im Temperaturbereich von 323 – 423 K gebildet werden. Es ist bemerkenswert, dass bereits bei diesen Temperaturen die Doppelbindungsisomerisierung quasi instantan zu beobachten ist obwohl keine Beweise für das Vorliegen eines chemisorbierten Intermediates zu finden waren.

In den größeren 10 MR Poren des Zeoliths MFI wurde ein anderes Adsorptionsverhalten von 1-Penten beobachtet. Nach der anfänglichen Bildung des π -Komplexes setzt eine langsame Dimerisierung ein. Diese Oberflächenreaktion ist durch Freisetzung von 50% der ursprünglich bedeckten BAS gekennzeichnet. Eine Studie der Temperaturabhängigkeit dieser Reaktion ermöglichte es die Aktivierungsenergie dieser Oberflächenreaktion zu bestimmen. Die dabei beobachtete Barriere von 35 kJ/mol entspricht dabei wahrscheinlich der Bildung des Carbeniumions. Folglich ist die Bildung des Alkoxides aus dem π -Komplex ein aktivierter Vorgang. Theoretische Berechnungen bestätigen diese Annahme.

Die sorgfältige Analyse der Adsorptionswärmern in FER sowie der gesamten freigesetzten Reaktionswärme der Dimerisierung in MFI ermöglichte dabei eine Abschätzung der Adsorptionsparameter in MFI. Für die Bildung des π -Komplex von 1-Penten mit dem BAS wird ein Wert von 85 kJ/mol abgeschätzt, für die Alkoxidbildung 129 kJ/mol.

Eine detaillierte kinetische Auswertung des 1-Penten Crackings wird im letzten Teil (Kapitel 4) dieser Arbeit gezeigt. Im untersuchten Temperaturbereich (693 K – 833 K) lagen die sechs Pentenisomere untereinander im thermodynamischen Gleichgewicht. Daher wurden für die kinetische Auswertung alle Isomere als ein Penten-Pool behandelt. Ethen

und die drei Butenisomere wurden als Schlüsselintermediate für das monomolekulare beziehungsweise bimolekulare Cracken identifiziert. Für die Ethenbildung wurde dabei ein kinetisches Regime ($E_a = 78 \text{ kJ/mol}$, Reaktionsordnung 1) für den gesamten Temperaturbereich gefunden.

Bei der Butenbildung hingegen konnten zwei kinetische Regime identifiziert werden. Bei niedrigeren Temperaturen wird eine Reaktionsordnung von zwei sowie eine negative scheinbare Aktivierungsenergie ($E_a = -69 \text{ kJ/mol}$) beobachtet. Diese scheinbare negative energetische Barriere kann unter Berücksichtigung der exothermen Dimerisierung, welche dem ratenlimitierenden Schritt (Cracken) vorangeht verstanden werden. Für höhere Temperaturen ($T > 793 \text{ K}$) wird auch für die Butenbildung eine Reaktionsordnung von eins sowie eine positive apparente Barriere von 90 kJ/mol beobachtet. Bei diesen Bedingungen ist die Dimerisierung thermodynamisch ungünstig. Direktes monomolekulares Cracken wird bei diesen hohen Temperaturen ein zusätzlicher Reaktionspfad. Dabei wird pro Pentenmolekül ein Butenmolekül sowie ein Methylfragment gebildet.

Insgesamt ist das katalytische Cracken von 1-Penten circa 36mal aktiver als n-Pentan Cracken. Trotz der Tatsache, dass für beide Substrate zwei verschiedene Übergangszustände definiert sind die gefundenen intrinsischen energetischen Barrieren sehr vergleichbar. Daher kann die höhere Aktivität von Alkenen beim katalytischen Cracken hauptsächlich auf eine höhere Bedeckung zurückgeführt werden. Dies spiegelt sich auch in der fast doppelt so hohen Chemisorptionswärme von Alkenen wider.

In guter Übereinstimmung mit den Beobachtungen beim n-Pentan Cracken wird auch beim Olefincracken eine vergleichbare Beschleunigung der katalytischen Aktivität in Anwesenheit von EFAI Zentren in lokaler Nähe zu SBAS beobachtet. Die beiden dominanten Reaktionspfade (monomolekulares / bimolekulares Cracken) werden dabei gleichermaßen beschleunigt. Es wird daher spekuliert, dass die Anwesenheit eines delokalisierten Protons die Alkoxidbildung erleichtert. Das Alkoxid ist ein gemeinsames Intermediat beider Reaktionspfade, wodurch beide Reaktionen

gleichermaßen beschleunigt werden wenn sich die Bedeckung dieser Spezies erhöht.

7. List of publications

Journal contributions

S. Schallmoser, T. Ikuno, M.F. Wagenhofer, R. Kolvenbach, M. Sanchez-Sanchez, J.A. Lercher, „*Impact of the local environment of BAS in ZSM-5 on the catalytic activity in n-pentane cracking*” *J. Catal* (2014), 316 93 – 102.

F. Schüssler, S. Schallmoser, H. Shi, G.L. Haller, E. Ember, J.A. Lercher, “*Enhancement of dehydrogenation and hydride transfer by La³⁺ cations in zeolites during acid catalyzed alkane reactions*”, *ACS Catalysis* (2014), 4 1743 – 1752.

M. Zabeti, S. Sai, B. Karthick, G. Raman, L. Lefferts, S. Schallmoser, J.A. Lercher, K. Seshan, “*Aliphatic hydrocarbons from lignocellulose via pyrolysis over cesium modified amorphous silica alumina catalyst*”, submitted to *ACS Catalysis*.

S. Schallmoser, M. Sanchez-Sanchez, A.C. van Veen, J.A. Lercher, “*Towards quantitative understanding of light alkene cracking on zeolites - case of 1-pentene on HZSM5*”, paper ready for submission.

S. Schallmoser, J. Van der Mynsbrugge, K. De Wispelaere, M. Sanchez-Sanchez, M. Waroquier, V. Van Speybroeck, J.A. Lercher, “*Study of adsorption and reaction of 1-pentene over MFI and FER at intermediate temperatures*”, paper in preparation.

Oral presentations

S. Schallmoser, M. Sanchez-Sanchez, J.A. Lercher, “*Impact of the local environment of BAS on the catalytic activity of ZSM-5 in n-pentane cracking*”, 47. Jahrestreffen Deutscher Katalytiker, 2014, Weimar.

S. Schallmoser, A.C. van Veen, J.A. Lercher, “*Elementary steps of light olefin cracking on MFI type zeolites*”, 23rd North American Catalysis Society Meeting, 2013, Louisville.

S. Schallmoser, A.C. van Veen, J.A. Lercher, “*Elementary steps of light olefin cracking on MFI type zeolites*”, 25. Deutsche Zeolith Tagung, 2013, Hamburg.

Selected poster presentations

S. Schallmoser, A.C. van Veen, J.A. Lercher, “*Elementary steps of light olefin cracking on MFI type zeolites*”, 17th International Zeolite Conference, 2013, Moskau.

S. Schallmoser, L. Lin, J.A. Lercher, “*Impact of enthalpic and entropic contributions on the selectivity of alkane cracking*”, 46. Jahrestreffen Deutscher Katalytiker, 2013, Weimar.

8. Lebenslauf

Name	Stefan Schallmoser (geb. Meier)
Staatsangehörigkeit	Deutsch
Geburtsdatum	27.02.1986 in Simbach am Inn
Ausbildung	
Seit 11/2010	Promotion am Lehrstuhl für Technische Chemie 2 bei Prof. Johannes A. Lercher (TU München)
03/2010 – 10/2010	Master's Thesis: „Kinetische Ausprüfung von Acrolein-Katalysatoren mit Highthroughput-Reaktoren“ in der Forschungsabteilung (Heufeld) der Süd-Chemie AG (heute Clariant AG)
08/2009 – 12/2009	Auslandssemester an der McGill University (Montreal, Kanada)
2008 – 2010	Master of Science in Chemistry <ul style="list-style-type: none">• Hauptfach Technische Chemie• Nebenfach Katalyse und Reaktionstechnik
2005 – 2008	Bachelor of Science in Chemistry
03/2008 – 04/2008	Bachelor's Thesis: „Funktionalisierung von Carbon Nanotubes“ am WACKER-Lehrstuhl für Makromolekulare Chemie
1996 - 2005	Abitur am Tassilo-Gymnasium, Simbach am Inn